

Εγγραφή μεσοσκοπικών δομών σε διαλύματα
πολυμερών με ακτίνες **LASER**: Συνθήκες και
Μηχανισμός του φαινομένου

Εμμανουήλ Γ. Ανυφαντάκης



Πανεπιστήμιο Κρήτης

Σχολή Θετικών και Τεχνολογικών Επιστημών

Τμήμα Χημείας



Ίδρυμα Τεχνολογίας & Έρευνας-Ινστιτούτο Ηλεκτρονικής

Δομής & Λείζερ



Max Planck Institute for Polymer Research

Ηράκλειο, Δεκέμβριος 2009

Writing mesoscopic structures in polymer solutions using LASER beams: Conditions and mechanism of the phenomenon

Emmanouil G. Anyfantakis



University of Crete

School of Science and Technology

Department of Chemistry



Foundation for Research & Technology – Hellas - Institute
of Electronic Structure & LASER



Max Planck Institute for Polymer Research

Heraklion, December 2009

Η παρούσα Διδακτορική Διατριβή εκπονήθηκε με την υποστήριξη του έργου ΠΕΝΕΔ 2003, υποέργο 03ΕΔ581. Το έργο υλοποιείται στο πλαίσιο του Μέτρου 8.3 του Ε.Π. Ανταγωνιστικότητα – Γ' Κοινοτικό Πλαίσιο Στήριξης και συγχρηματοδοτείται:

- κατά 75% της Δημόσιας Δαπάνης από την Ευρωπαϊκή Ένωση – Ευρωπαϊκό Κοινωνικό Ταμείο
- κατά 25% της Δημόσιας Δαπάνης από το Ελληνικό Δημόσιο – Υπουργείο Ανάπτυξης – Γενική Γραμματεία Έρευνας και Τεχνολογίας
- από τον ιδιωτικό τομέα (S&B Βιομηχανικά Ορυκτά ΑΕ και Αναλυτικές Συσκευές ΑΕ)

*«Ἐὰν μὴ ἔλπηται, ἀνέλπιστον οὐκ ἐξευρήσει, ἀνεξερεύνητον ἐὼν
καὶ ἄπορον»*

Ἡράκλειτος ὁ Ἐφέσιος [544 πΧ (ἢ 535 πΧ)-484 πΧ (ἢ 475 πΧ)]

*« If you do not expect the unexpected, you will not find it; for
it is hard to be sought out and difficult »*

Heraclitus of Ephesus [544 BC (or 535 BC)-484 BC (or 475 BC)]

Περίληψη

Το θέμα της παρούσας διατριβής είναι η μελέτη της απρόσμενης απόκρισης διαυγών ημιαραιών πολυμερικών διαλυμάτων σε ασθενή ακτινοβολία LASER στο ορατό. Στα πλαίσια της διατριβής, διεξήχθη λεπτομερής πειραματική εξέταση με σκοπό τη δημιουργία ξεκάθαρης φαινομενολογίας, την προσπάθεια απόκτησης γνώσης σχετικά με το μηχανισμό αλληλεπίδρασης φωτός-ύλης και την εύρεση μεθόδων μικρο-εγγραφής στα υλικά αυτά.

Στα πλαίσια της παραπάνω διερεύνησης, μια απεικονιστική μέθοδος βασισμένη στην Ποσοτική Μικροσκοπία Αντίθεσης Φάσης αποδείχτηκε ότι είναι ένα ισχυρό πειραματικό εργαλείο για τη διερεύνηση του φαινομένου, και συγκεκριμένα για τη μελέτη της κινητικής του.

Μια πληθώρα νέων σημαντικών αποτελεσμάτων συλλέχθηκε:

- Απροσδόκητα, ανάλογα με το διαλύτη που χρησιμοποιείται, τα διαλύματα πολυ-διενίων αποκρίνονται στο οπτικό πεδίο είτε αυξάνοντας είτε μειώνοντας τη συγκέντρωση πολυμερούς μέσα στον ακτινοβολούμενο όγκο.
- Η αντιστρεψιμότητα του φαινομένου της εγγραφής εξαρτάται από το χρόνο ακτινοβολήσης, και αναπάντεχα, εκτεταμένοι χρόνοι ακτινοβολήσης έχουν ως αποτέλεσμα δομές με μεγάλους χρόνους ζωής οι οποίες δεν επαναδιαλύονται σε καλούς για τα συγκεκριμένα πολυμερή διαλύτες. Για σύντομους χρόνους έκθεσης, οι φωτοεπαγόμενες δομές είναι αντιστρεπτές.
- Η σαφής αναλογία του φαινομένου με μη-γραμμικά οπτικά φαινόμενα που λαμβάνουν χώρα σε άλλα συστήματα Χαλαρής Ύλης, όπως Οπτικά Χωρικά Σολιτόνια (Optical Spatial Solitons) και Ρυθμιστικές Αστάθειες (Modulation Instabilities) καταδείχθηκε.
- Εντυπωσιακά φαινόμενα με την εγγραφή με LASER, όπως για παράδειγμα ο σχηματισμός επιμηκών ινωδών δομών και η επίδειξη Αυτοεπαγόμενης Διαφάνειας επετεύχθη.
- Αιτιολογήσεις βασισμένες σε αναμενόμενες αλληλεπιδράσεις φωτός-ύλης αδυνατούν να εξηγήσουν τα φαινόμενα που παρατηρήθηκαν.

Παρόλο που ο μηχανισμός του φαινομένου παραμένει ασαφής, η αποκτηθείσα γνώση σχετικά με τις διάφορες δυνατότητες εγγραφής που προσφέρονται από διαφορετικά διαλύματα πολυ-διενίων μπορεί να ανοίξει το δρόμο για τη δημιουργία επιθυμητών 3D εγγραφών σε μικροσκοπικό επίπεδο.

Abstract

The subject of the present thesis is the study of the unexpected response of transparent semidilute polydiene solutions to weak visible LASER irradiation. A detailed experimental investigation was carried in order to establish a clear phenomenology of the observed effect and try to gain insight into the underlying coupling mechanism and to establish micropatterning routes in these materials.

An imaging method based on Quantitative Phase Contrast Microscopy was established as a powerful experimental tool allowing detailed study, in particular of the kinetics of the process.

A number of new important facts have been established:

- Surprisingly, depending on the solvent used, the polydiene solutions can respond to the optical field either by increasing or lowering the polymer concentration inside the irradiated volume.
- The reversibility of the writing process was found to depend on the irradiation time and unexpectedly, prolonged irradiations led to long-lived structures that could not be redissolved in good solvents for the polymers. For short exposures, the LASER-induced patterns are reversible.
- A clear analogy to non linear optical phenomena occurring in other Soft Matter systems, such as Optical Spatial Solitons and Modulation Instabilities was recognized.
- It has been shown that LASER writing can be successfully used to create impressive effects, such as the formation of very long fibrillar structures and the demonstration of Self Induced transparency.
- Rationalizations based on expected light-matter couplings cannot account for the observed phenomenology

Though the responsible mechanism still remains unclear, the obtained knowledge concerning the various patterning possibilities offered by the different polydiene solutions can open an avenue for much needed 3D micropatterning.

Foreword

The present thesis is organized as follows: **Chapter 1** starts with a brief discussion of the interactions between light and soft matter. Accordingly, the subject of the present study, which is the unexpected phenomenon of LASER-induced pattern formation in transparent polydiene solutions, is described. In **Chapter 2**, the characteristics of the polydiene solutions used during this study and the experimental techniques employed, are presented. In **Chapter 3**, the study of the early stage of fiber formation kinetics, as followed by real-time phase contrast microscopy, is reported. The decoupling of the sign of the optical contrast between polymer and solvent and the refractive index difference between the LASER-induced structures and the surrounding solution is reported in **Chapter 4**. In **Chapter 5**, a brief discussion concerning possible rationalizations of the observed effect is given and the conclusions of this study are presented.

Table of contents

<u>Chapter 1: Introduction</u>	1
1.1 Light - Matter Interactions	2
1.1.1 Light propagation in Matter	2
1.1.2 Non linear optical materials	5
1.2 Non linear optical phenomena in Soft Matter	6
1.2.1 Soft non linear optical materials	6
1.2.2 Type of nonlinearities in soft materials	6
1.2.3 Examples of non linear optical effects in Soft Matter	7
1.2.3.1 Self-guiding in colloidal dispersions	7
1.2.3.2 Optical Kerr effect in liquid crystals	8
1.2.3.3 Thermally induced non linear optical effects in binary mixtures	8
1.3 LASER-writing in polydiene solutions	10
1.4 Motivation and goals	13
1.5 State of the art at the start of this work	13
1.6 Related anomalous effects	17
1.6.1. Polymer solutions affected by electric fields	18
1.6.2 LASER-induced association in polymer and micellar solutions	21
References	33
<u>Chapter 2: Materials and Methods</u>	36
2.1 Polydiene Solutions	37
2.1.1 General properties of polydienes	37
2.1.2 Polymer solutions	38
2.1.3 Light scattering from polymer solutions	41
2.2 Sample preparation and characterization	44
2.2.1 Characterization of the linear and branched homopolymers	44
2.2.2 Characterization of the copolymer solutions	47
2.2.3 General semidilute solution preparation route	49
2.2.4 Characterization of the semidilute homopolymer solutions	50
2.3 Real time Phase Contrast Microscopy	51
2.3.1 Experimental Setup	52
2.3.2 Quantitative Phase Contrast Microscopy	53
2.4 Raman Scattering	61

References	65
<u>Chapter 3: LASER-induced fiber formation</u>	66
3.1 Introduction	67
3.2 Pattern formation kinetics	67
3.2.1 Quantitative Phase Contrast Microscopy	69
3.2.2 LASER power dependence	72
3.2.3 Polymer concentration dependence	73
3.2.4 Influence of solvent refractive index	75
3.2.5 Microstructure and molecular weight dependence	77
3.2.6. Late stage	80
3.2.7. Discussion on the pattern formation kinetics	82
3.3 Fiber formation: Similarities to Optical Spatial Solitons and Modulational Instabilities	83
3.3.1 Optical Spatial Solitons and Modulation Instabilities	83
3.3.2 Relation of LASER writing in polydiene solutions to OSS and MI	87
3.4 Characterization of the fibers	90
3.4.1 Reversibility of the phenomenon	90
3.4.2 Micro-Raman scattering of the irradiated material	94
3.5 Summary	97
References	100
<u>Chapter 4: Sign of the induced concentration change in various solvents</u>	101
4.1 Introduction	102
4.2 The inverse case: Solvent-rich channel formation	103
4.2.1 Polydienes in bromonaphthalene ($\Delta n < 0$)	103
4.2.2 Polydienes in THF ($\Delta n > 0$)	106
4.2.3 Summary of the solvents examined	107
4.2 LASER patterning of diblock copolymer solutions	110
4.2.1 Diblock copolymers: Positive case	110
4.2.2 Diblock copolymers: Negative case	111
4.2.3 Self-Induced Transparency in turbid solutions	113
4.3 Discussion	117
References	119

<u>Chapter 5: Discussion-Conclusions</u>	120
5.1 On the origin of the light-concentration coupling	121
5.1.1 Optical forces	121
5.1.2 Optical Kerr effect	123
5.1.3 Thermal effects	123
5.1.4 Other possibilities	124
5.2 Conclusions	125
5.3 Further work	127
References	130
<u>Appendix: Static and Dynamic Light Scattering</u>	131
Static and Dynamic Light Scattering	132
References	136

CHAPTER 1

INTRODUCTION

Light-Soft Matter interactions and related phenomena are discussed in this Chapter. In particular, examples of non linear effects arising from the application of external fields to such materials are outlined. The subject of the present study, which is the unexpected phenomenon of LASER-induced pattern formation in transparent polydiene solutions, is described.

1.1 Light - Matter Interactions

1.1.1 Light propagation in Matter

Light propagation in vacuum is very well described by the well-known Maxwell's equations, which provide the basis of modern Optics. The propagation of light in a homogeneous medium can also be described by the Maxwell's equations¹, which in this case have the following general form:

$$\vec{\nabla} \times \vec{E} = -\frac{\partial \vec{B}}{\partial t} \quad (\text{Equation 1.1})$$

$$\vec{\nabla} \times \vec{H} = \vec{J} + \frac{\partial \vec{D}}{\partial t} \quad (\text{Equation 1.2})$$

$$\vec{\nabla} \cdot \vec{D} = \rho \quad (\text{Equation 1.3})$$

$$\vec{\nabla} \cdot \vec{B} = 0 \quad (\text{Equation 1.4})$$

In the above expressions, \vec{E} is the electric field, \vec{H} is the magnetic field, \vec{J} is the current density and ρ is the electric charge density. The electric displacement \vec{D} and the magnetic induction \vec{B} can be written as

$$\vec{D} = \epsilon_0 \vec{E} + \vec{P} \quad (\text{Equation 1.5})$$

$$\vec{B} = \mu_0 (\vec{H} + \vec{M}) \quad (\text{Equation 1.6})$$

where \vec{P} is the polarization and ϵ_0, μ_0 is the permittivity and the permeability of vacuum, respectively. For non-magnetic ($\vec{M} = 0$) and non-conducting materials ($\vec{J} = 0$), the general wave equation for the electric field is expressed as

$$\nabla^2 \vec{E} - \frac{1}{c^2} \frac{\partial^2 \vec{E}}{\partial t^2} = \frac{1}{\epsilon_0 c^2} \frac{\partial^2 \vec{P}}{\partial t^2} \quad (\text{Equation 1.7})$$

where c is the speed of light in vacuum, equal to $\frac{1}{\sqrt{\epsilon_0 \mu_0}}$. It can be clearly seen that the propagation of light (**Equation 1.7**) depends strongly on the polarization of the medium.

Therefore permittivity is a physical quantity that describes how an electric field affects and is affected by a medium, and is determined by the ability of a material to be polarized in response to the field (and thereby reduce the total electric field inside it). The linear permittivity and permeability of a homogeneous material are usually given relative to that of free space, as a relative permittivity ϵ_r , and a relative permeability μ_r , respectively. ϵ_r is directly related to the electric susceptibility, χ , through the relation

$$\epsilon = \epsilon_r \epsilon_0 = (1 + \chi) \epsilon_0 \quad (\text{Equation 1.8})$$

The permittivity ϵ and permeability μ of a medium together determine the phase velocity u of electromagnetic radiation inside the medium:

$$\epsilon \mu = \frac{1}{u^2} \quad (\text{Equation 1.9})$$

At optical frequencies, it is more common to use the refractive index, n , which is related to the relative permittivity as following:

$$n = \sqrt{\epsilon_r \mu_r} \approx \sqrt{\epsilon_r} \quad (\text{Equation 1.10})$$

since μ_r is very close to unity at this frequency region.

As opposed to the response of vacuum, the response of materials to external fields generally depends on the frequency of the field, ω . This frequency dependence reflects the fact that a material's polarization does not respond instantaneously to an applied field. The response of materials to alternating fields is characterized by a complex permittivity, $\hat{\varepsilon}(\omega)$:

$$\hat{\varepsilon}(\omega) = \varepsilon'(\omega) + i\varepsilon''(\omega) \quad (\text{Equation 1.11})$$

where ε'' is the imaginary part of the permittivity, which is related to the dissipation (or loss) of energy within the medium and ε' is the real part, which is related to the stored energy within the medium. The response of a medium to static electric fields is described by the low-frequency limit of permittivity, ε_s (static permittivity), while at the high-frequency limit, the complex permittivity is commonly referred to as ε_∞ .

In the regime of linear optics, \vec{P} is assumed to be proportional in a linear fashion to the electric field \vec{E} of the applied light,

$$\vec{P}_{lin} = \varepsilon_0 \chi(1) \vec{E} \quad (\text{Equation 1.12})$$

where ε_0 is the permittivity of free space and $\chi(1)$ is the electric susceptibility of the material. Based on this linear assumption, Maxwell's equations lead to a set of linear differential equations in which only the terms proportional to \vec{E} are involved.

The invention of the LASER allowed the thorough investigation of non linear Optics, even though discoveries of some non linear optical phenomena, such as the Kerr and the Pockels effect, date back to the 19th century. When the electric field is strong enough (i.e. in case of LASER light), it can modify the material properties. Non linear terms have to be included to describe correctly the electronic polarization in this case²

$$\vec{P} = \vec{P}_{lin} + \vec{P}_{nl} \quad (\text{Equation 1.13})$$

where the non linear polarization contribution can be expressed by the power series

$$\vec{P}_{nl} = \varepsilon_0 \chi(2) \vec{E}^2 + \varepsilon_0 \chi(3) \vec{E}^3 + \dots \quad (\text{Equation 1.14})$$

This series describes the progressive nonlinearity of the interaction with increasing power of the electric field. Here, $\chi(2)$ and $\chi(3)$ are the second and third order non linear susceptibilities, respectively. They are material coefficients and are in general described by tensors.

1.1.2 Non linear optical materials

The study of non linear optical effects is a very broad and extremely active field of research encompassing Atomic and Molecular Physics, Photonics and other scientific areas. A wide class of materials possesses considerable optical nonlinearities, that is, properties such as the index of refraction are modified by the presence of intense light. Obviously, when a nonlinearity is introduced, the propagation of light (in the space or time domain) in the non linear material is altered. Light-induced refractive index modification is the fundamental process involved in several non linear optical effects, such as the optical Kerr effect and self focusing that will be described later.

Condensed matter includes several examples of non linear optical materials. A prominent example is liquid CS_2 , where the index of refraction is altered due to molecular orientation of the anisotropic molecules of the liquid³. In this case, Δn is proportional to the square of the electric field, a phenomenon known as the optical Kerr effect. Other Kerr materials include several types of inorganic glasses¹, and a more recent example is that of photorefractive crystals⁴.

1.2 Non linear optical phenomena in Soft Matter

1.2.1 Soft non linear optical materials

A specific class of materials has emerged, known as Soft Matter or complex fluids. These materials are often made up of more than one constituent, and are characterized by their large response to even relatively small excitations. As a result, applying external fields give the possibility of tailoring their properties at will. Their quantitative description in terms of coarse grained models and theories have been very successful over the last decades and gave rise to the field. Their response can often be understood at a mesoscopic scale, independent of the precise chemical composition. Soft Matter encompasses a wide class of materials, with typical examples being polymer melts and solutions, colloidal dispersions, liquid crystals and biomaterials⁵.

The study of nonlinearities in soft materials has been focused to their mechanical non linear response. Optically triggered nonlinearities in these materials have only been considered recently and the application and subsequent non linear effect of optical fields to Soft Matter appears to be a rich playground. However, despite the vivid interest during the last years⁶, this field is essentially only a little explored.

1.2.2 Type of nonlinearities in soft materials

In this class of materials, the modification of the optical properties triggered by the application of optical fields will arise from the mesoscopic degrees of freedom of these systems in transparent and non-resonant media. The most studied examples are electrostriction (optical forces) in colloidal dispersions, the optical Kerr effect in nematic liquid crystals, and thermal effects (Soret effect) in binary mixtures.

1.2.3 Examples of non linear optical effects in Soft Matter

1.2.3.1 Self-guiding in colloidal dispersions

Colloidal dispersions and nematic liquid crystals are two well-known cases of soft materials that exhibit significant non-resonant nonlinearities. In the case of aqueous suspensions of dielectric spheres, whose first investigation dates back to the early 1980s by Ashkin and coworkers⁷, the leading mechanism is expected to be electrostriction. The isotropic particles are subject to forces induced by light intensity gradients, thus moving in the region with higher or lower intensity, depending on the refractive index difference between the particles, n_p , and the suspension medium, n_0 ¹. In the well-studied case, where $n_p > n_0$, the gradient force works against diffusion to concentrate the particles within the high intensity region of the LASER beam. This, in turn, allows for optical waveguiding due to the refractive index change Δn which can be described by a local Kerr law

$$\Delta n = n_2 I \quad (\text{Equation 1.15})$$

where I is the light intensity and n_2 a constant that depends on the material. An experimental image of self-focusing and self-trapping is shown in **Figure 1.1**:

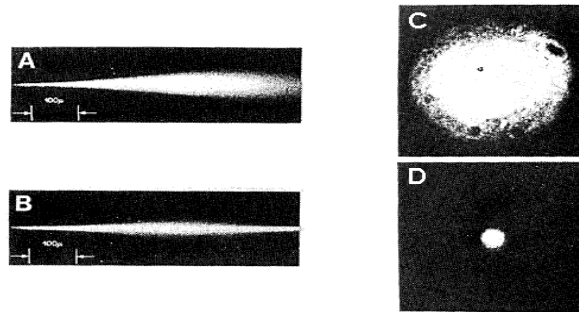


Figure 1.1: A, C: Beam trajectory and beam shape at the output face of the sample at low LASER power, where diffraction can be observed. B, D: The corresponding images above the critical power, where self-trapped filaments are formed. The non linear medium is an aqueous dispersion of poly (styrene) spheres.⁷

Below a critical power value, the expected diffraction and spreading of the beam can be observed (**Figure 1.1 A, C**). When the LASER power is increased above the critical value, the light is self-focused, as can be seen by the much narrower beam spot (**Figure 1.1 B, D**). The non linear medium in this case is an aqueous suspension of poly (styrene) spheres.

1.2.3.2 Optical Kerr effect in liquid crystals

Liquid crystals are another common class of soft non linear optical materials. They are transparent fluids consisting of elongated molecules. In both isotropic and ordered phases, liquid crystals possess extraordinarily large optical nonlinearities. Since liquid crystal molecules are anisotropic, a polarized LASER beam can induce an alignment or ordering in the isotropic phase, or a re-alignment of the molecules in the ordered phase, through the dipolar interaction in order to minimize the energy of the system. This ordering results in the modification of the index of refraction of the medium. This (re) orientational nonlinearity gives rise to a number of non linear optical effects, such as self-focusing and optical spatial solitons (discussed in **Chapter 3** of this thesis), in relatively low LASER power levels.⁸

1.2.3.3 Thermally induced non linear optical effects in binary mixtures

Non linear optical effects arising from thermal nonlinearities have been studied in several Soft Matter systems. Thermal diffusion, also known as the Soret effect, accounts for the mass transport in a multicomponent mixture which is driven by a temperature gradient. Thermodiffusion has been known for a long time, but its theoretical explanation for molecules in liquids is still under debate. Utilizing this effect, Voit et al.^{9, 10} employed a focused LASER beam ($\lambda = 515$ nm) to write spatial composition patterns in critical polymer blends of poly (dimethyl siloxane) / poly (ethyl methyl siloxane). Since these polymers are transparent, a minute amount of dye was added in the blends, which absorbs at the LASER wavelength and allows for optical heating. The patterns were formed in both the homogeneous and the two-phase region a few degrees above and below the critical temperature. A representative pattern demonstrated by these authors is shown in **Figure 1.2**:

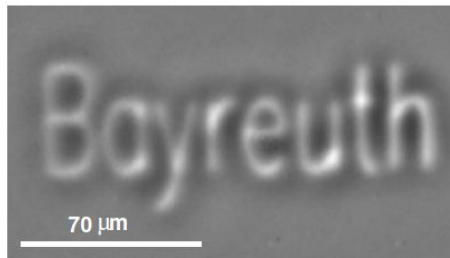


Figure 1.2: The word 'Bayreuth' as written by repeatedly scanning the LASER across the surface of the poly (dimethyl siloxane) / poly (ethyl methyl siloxane) critical polymer blend¹⁰.

Because of the critical divergence of the Soret coefficient, which is a measure for the stationary concentration change produced by a given temperature difference, moderate temperature gradients are sufficient to induce composition modulations of large amplitude.

Except for the case of polymer blends, the Soret effect can be used to produce spatial patterns in solutions. In such an experiment, Duhr et al.¹¹ utilized thermodiffusion to manipulate the DNA concentration in a thin water film. The temperature pattern 'DNA' was written into the solution film with an infrared LASER scanning microscope, as shown in **Fig 1.3:**

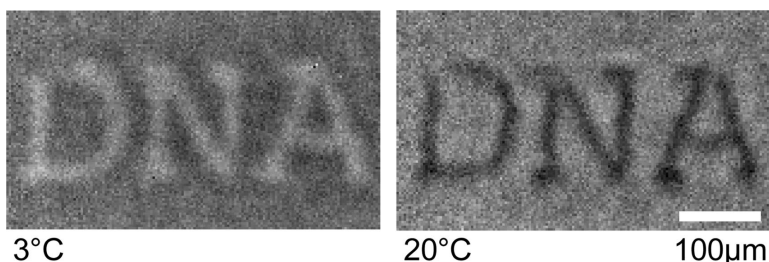


Figure 1.3: A thin water film is heated by 2K along the letters "DNA" with an infrared LASER. For a cooled chamber at 3°C, fluorescently tagged DNA accumulates at the warm letters. However, at room temperature, DNA moves into the cold, showing reduced fluorescence¹¹.

The temperature elevation due to absorption was 2K. Concentration of DNA molecules was imaged by using a fluorescent DNA tag. In an overall cooled chamber at 3 °C, DNA has a negative Soret coefficient, meaning that is thermophilic, thus it accumulates toward the heated letters 'DNA' during LASER irradiation. On the contrary, at room temperature DNA

is thermophobic, thus it moves to the cold regions. As a result, the local concentration of DNA molecules decreases and a spatial pattern consisting of lower-concentration (reduced fluorescence) letters is formed in the aqueous solution.

Delville et al¹² reported on the phase separation and droplet nucleation induced by LASER radiation ($\lambda = 514$ nm) in a quaternary mixture of water, n-dodecane, SDS and n-pentanol. This mixture, in the particular composition used, forms a micellar solution (water droplets in oil, with a diameter of 8 nm) at room temperature. The system is close to a demixing temperature (20 °C), such that a very small increase in micellar concentration induces a liquid-liquid phase separation towards a lower micellar concentration phase. The efficiency of the weakly focused LASER beam as an osmotic piston for driving a phase separation in this liquid mixture was shown. The nucleation droplets created, are trapped (due to electrostriction) in the light beam owing to their high positive polarizability. The droplets act like spherical lenses and in turn self-focus the beam¹³. The quench in composition in this case was confirmed to be due to thermodiffusion. The authors calculated the LASER-induced temperature variation for the particular system, given a beam waist of 5 μm and a power of $P = 100$ mW, to be about $4.4 \cdot 10^{-2}$ °C. This ΔT is enough to cause a concentration change of the order of 10^{-3} in the beam center, explaining the LASER-induced phase separation by the Soret effect. The electrostrictive contribution was calculated to be one order of magnitude less than the thermodiffusive contribution, due to the very small polarizability of the micelles.

1.3 LASER-writing in polydiene solutions

An unexpected phenomenon of Soft Matter response to the application of an external field was recently reported^{14, 15} in polydiene solutions, which does not seem to belong to the categories previously described.

The observed phenomenon is best described by a simple experiment: Light from a continuous wave LASER source, of wavelength $\lambda = 671$ nm, power $P = 100$ mW, is focused through a lens (focal length $f = 35$ mm) to the sample cell (**Figure 1.4**). The sample is a homogeneous, transparent solution of cis-1, 4 poly (isoprene) (molecular weight $M_w = 1090$ kg/mol) in decane, a good athermal solvent for this polymer. The polymer concentration is

$c = 6.64$ % wt. These solutions scatter weakly visible LASER light, as a result of the weak concentration fluctuations¹⁶.

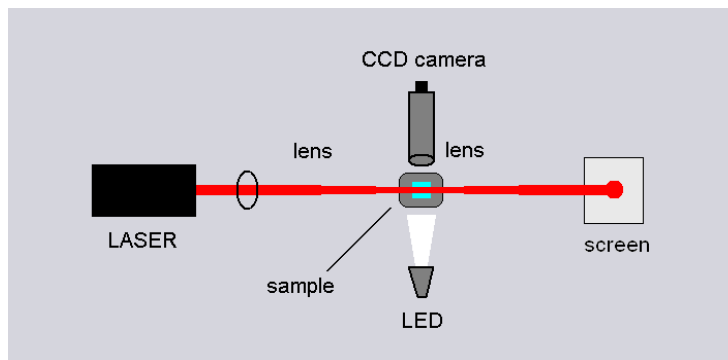


Figure 1.4: Schematic of the simple experimental setup: A LASER beam ($\lambda = 671$ nm, $P = 100$ mW) is focused by a spherical lens ($f = 35$ mm) to the sample cell. The scattered light at an angle $\theta = 90^\circ$ is monitored with a CCD camera. When the beam is switched off, illumination with white light from a LED allows for imaging the solution through the CCD camera. The transmitted beam spot is projected on a screen.

Contrarily to the standard cases of semidilute non-absorbing polymer solutions, this polymer-solvent system behaves in a dramatic way: Upon LASER irradiation, the initial Gaussian profile of the transmitted beam (**Figure 1.5 a**) changes continuously as time passes, showing constantly moving diffraction rings, and eventually widens up to a richly structured pattern (**Figure 1.5 b**):

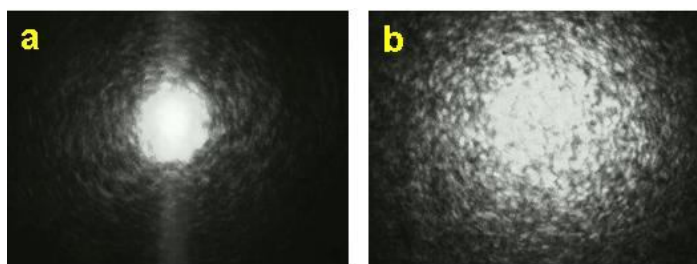


Figure 1.5: a) Image of the initially well-defined Gaussian spot of the transmitted LASER beam projected on the screen. b) The opening of the Gaussian beam spot to a speckle-like pattern.

This dynamic pattern initially evolves with a rapid rate, which progressively decreases for prolonged irradiation. Simultaneously with the opening of the beam spot, the initially weak

and smooth trace of the scattered light at a scattering angle $\theta = 90^\circ$ increases dramatically with time, as observed through the CCD camera (**Figure 1.6**):

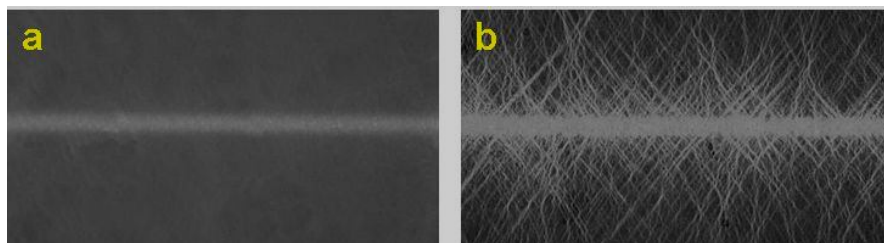


Figure 1.6: a) Image of the initially weak scattered intensity at a scattering angle $\theta = 90^\circ$ that is reaching the detector (CCD camera). b) Image of the increased scattered intensity as the phenomenon evolves.

Both the opening of the transmitted beam spot and the dramatical increase of the scattering intensity are indicative of a local alteration of the refractive index, which could give rise to such observations. By blocking the LASER beam and illuminating with white light from the LED, a string-like structure is imaged in the CCD camera, as shown in **Figure1.7**:

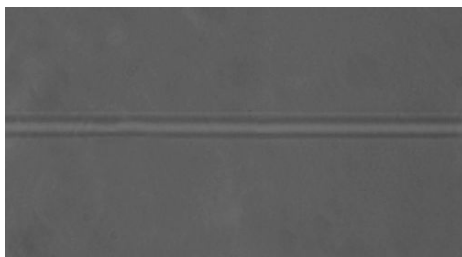


Figure 1.7: Microscope image of the string-like structure that is induced by the LASER light in the cis-1, 4 poly (isoprene)/decane solution. The diameter of the cylindrical structure is about $10 \mu\text{m}$.

A light-induced filament that is ‘written’ along the propagation direction of the LASER beam is optically detected due the existence of a refractive index contrast between the formed structure and the background solution. The diameter of the filament is about $10 \mu\text{m}$, while its length extends from the one wall of the cell to the other (\sim a few mm).

1.4 Motivation and goals

The anomalous case of optical pattern formation in the non absorbing polydiene solutions due to mild LASER light irradiation, described in **Section 1.3**, shows that these soft materials offer an unexpected and versatile materials for non linear Optics. However, despite the clear experimental observations, the nature and the physical origin of the underlying light-polymer / solvent coupling is unknown, since the common physical mechanisms responsible for analogous effects in other systems seem inadequate to give an explanation.

The main goal of this investigation is to establish a clear phenomenology for the observed effect, with the hope that it will provide key ingredients to elucidate its physical origin. Towards this direction, the systematic use of the writing process will be used in order to characterize the effect in detail, and explore its relation to the material properties and the irradiation conditions.

Shedding light to the microscopic mechanism of this light-matter interaction is of particular importance, as it could open new routes to 3D micropatterning in bulk polymer solutions. One step further, the richness of the polymer chemistry, in conjunction with the fundamental phenomena of Soft Matter manipulation and the potential applicability in optical and nanotechnology systems, could offer several perspectives.

1.5 State of the art at the start of this work

In this Section, the state of the art concerning the writing effect in semidilute polydiene solutions will be shortly discussed.

The distinct wave-medium coupling in the semidilute cis-1, 4 poly (isoprene) (PI) solutions probably relates to the polarizability anisotropy along the chain backbone, due to the presence of the double bond. This is supported by the similar behavior observed in semidilute solutions of cis-1, 4 poly (butadiene) (PB). The two macromolecules differ only in the presence of a methyl group (**Figure 1.8**). In contrast to these cases, solutions of 1, 2 poly (butadiene) (**Figure 1.8**), which has the double bond in the side group, behaves in a 'normal' neutral behavior, showing no unexpected effect¹⁵.

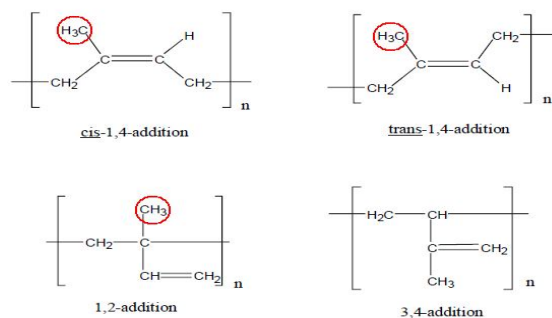


Figure 1.8: The different microstructures of poly (isoprene). The corresponding microstructures for poly (butadiene) (cis-1, 4, tans-1, 4, and 1, 2) can be visualized by substituting the methyl group (indicated by the red circles) with a hydrogen atom.

Sigel et al.¹⁵ reported the minimum critical concentration c_c above which the profile of the transmitted LASER beam definitely changes into a complex pattern on the screen, as a function of the degree of polymerization N (**Figure 1.9**). The value of this cutoff concentration appears to be insensitive to LASER power and displays the scaling $N^{0.8}$ validated for both PI and PB in hexane. This relationship resembles that of the overlap concentration c^* , and the absolute value is on the order of the entanglement concentration ($\sim 10 c^*$). Rheological measurements on these solutions revealed a rubberlike plateau in the dynamic shear modulus characteristic of a temporary entangled polymer network. Short chains dilute an entangled network, and consequently a symmetric (50:50) mixture of short ($N = 1910$) and long ($N = 17,060$) PI chains (PI mixture in **Figure 1.9**) exhibits a higher c_c value as compared to the c_c value expected for PI chains with the average N (~ 9500). It is not, therefore, the total polymer concentration but rather the chain connectivity that determines the critical value c_c . This notion is further corroborated by the behavior of the multiarm star PB, which has a lower overlap concentration c^* than the corresponding linear PB. Based on the scaling of **Figure 1.9**, no effect would be expected below a certain threshold N_c (~ 150), nearly equal to the chain length above which bulk PI becomes entangled. This prediction has been experimentally verified for a PI ($N = 70$)/ hexane solution at concentrations up to the bulk state. The location in the c_c - N plot also depends on the concentration of the C=C bonds in the chain. Partial ($\sim 55\%$) hydrogenation of PI to a block poly(isoprene-*r*-ethyl propylene) (PEP) increases c_c relative to the parent PI (**Figure**

1.9). Although a dot-like pattern is written in PI/toluene at 0.036 g/ml, no structure is formed in the PEP/toluene solution.

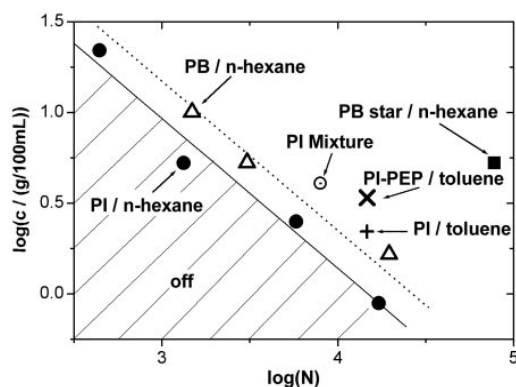


Figure 1.9: Critical minimum concentration c_c vs. the number of monomer units N necessary to observe changes in the transmitted beam through the indicated semidilute polymer solutions. The solid line represents a linear fit of the PI/hexane system. “PI mixture” stands for a symmetric mixture of a low ($N = 1910$) and high ($N = 17,060$) molar mass PI in hexane, and its c_c value falls well above the solid line because of the reduced number of entanglements. The dotted line indicates a linear fit of the PB/ hexane system.

Written patterns are polymer-rich stable regions. Their optical detection is based on the existence of an optical dielectric contrast ($n_p - n_s > 0$); at c_c no written pattern was detected and higher concentrations were needed. The evolution of the LASER beam trace in the solution (**Figure 1. 6**) and the dynamic pattern formation indicate that the LASER-induced enhancement of the polymer concentration exerts optical focusing and waveguiding actions on the LASER beam itself, thereby yielding autoamplification of the observed phenomena.

To determine whether chemical modification was an issue, a PI / hexane solution was irradiated for several hours, thus inducing extensive pattern formation. No detectable change in the narrow molecular weight distribution of PI was observed, independent of the amount of the added antioxidant (radical trap) used. ^1H and ^{13}C nuclear magnetic resonance analysis also excluded cis-trans chain isomerization. Furthermore, the effect induced by shorter wavelength light ($\lambda=532$ nm) was found to be weaker¹⁵.

Reversible optical recording of holographic gratings in solutions of 1, 4-PI ($M_w = 963$ kg/mol) in hexane at high concentrations ($c = 12.5 - 16.5$ % wt) was demonstrated by

Loppinet et. al¹⁴. The output of a LASER ($P = 150 \text{ mW}$, $\lambda = 647 \text{ nm}$) was divided into two beams of equal intensity. The beams were incident and fully overlapped into a glass cuvette containing the PI samples, forming 9 mm thick gratings with wavevectors along the vertical direction (**Figure 1.10, A**). Beam crossing (Bragg) angles were varied between 1.7° and 18.5° , respectively, resulting in interference gratings of spatial periods from 21 to $2 \mu\text{m}$.

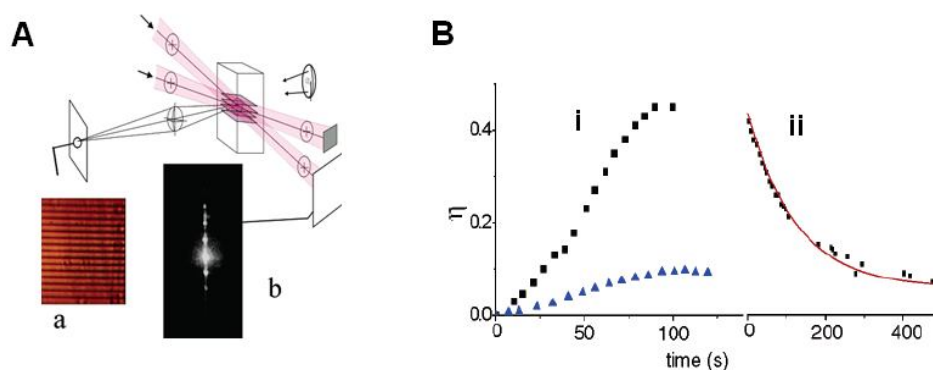


Figure 1.10: A) Schematic of the experimental configuration. The main beam of a red (647 nm) LASER is divided into two beams, which fully overlap in the sample forming the optical grating. A spatial periodic pattern corresponding to the grating planes is recorded by a microscope/CCD camera system (inset a). The projection of the diffracted beams on a screen is presented in inset (b). B) First-order diffraction efficiency recording (i) for spatial periods of $21 \mu\text{m}$ (squares) and $2 \mu\text{m}$ (triangles), and the dark decay (ii) for spatial periods of $21 \mu\text{m}$ (following the recording displayed in A (square)). The line is an exponential decay, and the polymer concentration is about 12.5 wt %.

By considering that grating formation is due to periodic polymer concentration variations in the illuminated region, the diffraction efficiency is $\eta \sim \sin^2(\pi d \Delta n / \lambda \cos \theta)$ for a refractive index modulation Δn , grating thickness d , wavelength λ and Bragg angle θ . In the mentioned experimental conditions $\theta = 1.7^\circ$, $d = 9 \text{ mm}$, and thus $\Delta n \sim 10^{-5}$, suggesting a concentration modulation of $\Delta c = (dn/dc)^{-1} \Delta n \sim 4 \cdot 10^{-3} \text{ wt \%}$. For comparison, the concentration fluctuations in the undisturbed semidilute polymer solution are approximately 5 orders of magnitude smaller.

The concentration (refractive index) gratings fade out (**Figure 1.10, B**) with a time scale depending on the spacing, the solution viscosity, and the exposure conditions and can, therefore, be controlled. When the recording is stopped in the early linear stage ($\eta < 0.05$),

the characteristic decay time appears to scale with the square of the spacing. For larger exposures, however, the decay mechanism appears to be more complex, in particular, with the occurrence of sedimentation.

The mechanism responsible for the observed non linear optical phenomenon seems to be unrelated to well-known cases. The increase of the refractive index in regions of large optical intensity from a first look points towards classical electrostriction. Nonetheless, due to the low polarizability and the small characteristic sizes of these Soft Matter systems, the exerted optical forces are minute compared to thermal energy.

Moreover, no evidence for optical trapping in polymer solutions under these conditions has been reported so far. Similarly, polarizability anisotropy along the chain backbone is found to be necessary but is not sufficient to provide a quantitative description of the phenomenon in terms of alignment mechanism. On the other hand, LASER-generated temperature gradients may cause concentration variations due to thermodiffusion¹¹. Likewise, the very weak absorption is not expected to initiate either any large concentration variations¹⁷, as solutions are in good solvents far from any demixing, or photopolymerization effects¹⁸. Obviously some more complex mechanisms are at work, which require the specific chemical structure of the polymer backbone.

The impressive new phenomenon was observed for first time during light scattering experiments in concentrated solutions of diblock copolymers of poly (isoprene-b-styrene) in toluene. After a number of separate experiments with homopolymer solutions of poly (styrene) and poly (isoprene) respectively, it was concluded that the latter was 'responsible' for this unexpected behavior.

1.6 Related anomalous effects

Some cases exhibiting an unexpected coupling between the external field and the Soft Matter system are presented in this part. Polymer solutions and liquid mixtures whose dynamics is affected by the application of an external electric field, and LASER-induced association in polymer and micellar solutions are briefly presented.

1.6.1. Polymer solutions affected by electric fields

Phase separation in binary solutions is mainly controlled by temperature and pressure, but it can also be influenced by subjecting these systems in external fields. In the vicinity of the coexistence curve, these solutions exhibit large concentration fluctuations. Such fluctuations can be anisotropically distorted through the application of an external field. Along these lines, Wirtz et al.^{19,20} demonstrated that an electric field can induce mixing of two-phase solutions, and this effect was shown to be universal to wide class of systems, including upper and lower critical point solutions (UCST and LCST, respectively). The studies were carried out conducting time dependent small-angle light scattering and dichroism experiments in semidilute solutions of PS in cyclohexane and poly (p-chlorostyrene) in ethyl carbitol, a UCST and a LCST case, respectively. The shift of the critical temperature was found to be quadratic in the electric-field strength. The experimental observations were in fairly good agreement with the trends predicted by a phenomenologically-based, mean-field theory. Gurovich²¹ later developed a theory considering an induced polarization and the change of the free energy of binary mixtures due to the electric field, which explained the above phenomena.

Mixing induced by uniform electric fields is detectable only at temperatures that are within a few hundredths of degree or less of the phase transition temperature of the system being studied. On the contrary, Tsori et al.²² demonstrated that electric fields can control the phase separation behavior of mixtures of simple liquids under more practical conditions, provided that the fields are non-uniform. More specifically, the authors managed to reversibly induce the demixing of paraffin and silicone oil at 1K above the phase transition temperature of the mixture. As long as the field gradients are turned off, the mixture becomes homogeneous again.

The effect of electric fields on the solution viscosity of atactic PS in THF and toluene was reported by Price et al.²³ These authors used rheology and dynamic light scattering (DLS) to study how the external field influences the molecular motion in the PS solution. The relaxation rate of the intensity autocorrelation function and the solution viscosity were found to increase with increasing amplitude of the electric field. Speeding-up of the dynamics was reported to depend on the polymer concentration, PS molecular weight, solvent, and frequency of the field. Follow-up studies were done by Wang et al.^{24, 25} in

solutions of PS in THF, in 1, 4-dioxane, and mixtures of these two solvents as well (**Figure 1.11**). DLS experiments on polymer solutions near the overlap concentration c^* , showed that while the decay rate of the correlation function increases with increasing the field strength in THF, in dioxane solutions a negligible effect of the external field in the solution dynamics can be observed.

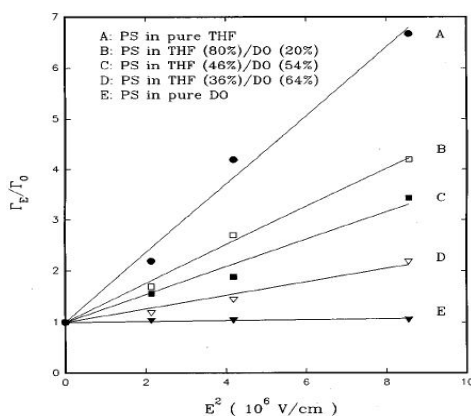


Figure 1.11: Field induced enhancement (through the ratio of the relaxation rates with and without the application of the electric field, Γ_E and Γ_0 respectively), for PS solutions in THF/1,4- dioxane mixed solvents at scattering angle $\theta = 90^\circ$: Solid lines are linear fits to the data²⁴.

The case of the mixed solvent exhibited an intermediate effect, depending on the THF content. A hydrodynamic theory was formulated to account for the electric field effect. The comparison of the calculations with experiments had shown that the polymer-solvent interaction plays an important role²⁴. In order to provide additional experimental data, a detailed study in a concentration range from the dilute to the concentrated regime was carried out²⁵. Under the application of the electric field, the translational diffusion coefficient of the PS chains dissolved in THF was found to be nearly constant in the dilute regime, but it increased rapidly as the solution approached the semidilute regime. As the polymer concentration was increased much beyond the semidilute to concentrated regimes, the effect of the electric field was greatly decreased. A rational picture to account for the observed effect was provided by the authors, by considering the mechanism associated with the polymer segmental dipole moment owing to solvation.

A number of studies on copolymer solutions under electric fields have been also reported. In a recent one, solutions of a triblock copolymer made of styrene and 5-N,N-

(diethylamino)isoprene in pure THF, DMF, or cyclohexane were investigated by Giacomelli et al²⁶. In THF, only random coil structures ($R_h \sim 4$ nm) were identified, which were not affected by the applied electric field. In DMF, micelles having R_h around 25 nm have self-formed, and their diffusion constant has increased linearly with the square of the applied electric field. The observed effect was attributed to the generation of a dipole moment on the micelles. In cyclohexane, huge aggregates of $R_h \sim 100$ nm and free chains were detected, the values of the relaxation rate for the slow mode (clusters) were displaced to smaller values when relatively high electric fields were applied. In this case, according to the authors, the induced dipole moment has the same direction of the field, favoring electrostatic interactions between the structures, since it was observed that the clusters dimensions have increased as a function of applied electric field time. As a consequence of the attractive forces, clusters amount in solution has decreased, which is supposed to be related to a precipitation process.

Another interesting study on the reversible tuning of block copolymer nanostructures (in solution) via electric fields was carried out by Schmidt et al²⁷. The authors showed that electric d. c. fields can be used to tune the characteristic spacing of a block-copolymer nanostructure of poly (isoprene-*b*-styrene) dissolved in common good solvents with high accuracy, in a fully reversible way on a timescale in the range of several milliseconds. The influence of various physical parameters on the tuning process was studied. More specifically, a linear dependence of the relative change in the lamellar distances (measured by Small Angle X-ray Scattering) on the electric field strength was found. Moreover, a stronger effect was found for solutions of lower concentration. Solvent also has an influence on the observed effect, since THF solutions were influenced more strongly by the electric field, compared to toluene solutions. These results were described by simple thermodynamic arguments, based on a balance between the interfacial (enthalpic) and the entropic energy of the chains that are stretched under the application of the field. Finally, copolymers with higher poly (isoprene) content show a stronger response to the external field. A tentative explanation of the studied effect was given on a basis of anisotropic polarizabilities and permanent dipole moments of the poly (isoprene) block.

1.6.2 LASER-induced association in polymer and micellar solutions

A series of experimental investigations concerning macromolecular associations in polymer solutions, induced by the application of sharply focused LASER beams was reported. Nevertheless, despite the clear experimental findings, the tentative explanations given by the groups involved are not satisfactory. Some of these investigations are presented in this Section.

Systems that respond to external stimuli, such as temperature, pressure, pH, electric and magnetic fields, could be used for the development of functional and intelligent materials, such as actuators and artificial muscles. Of special interest is the use of light as the external stimulus, owing to the versatility that LASER beams can offer. Along these lines, Ishikawa et al^{28, 29} reported on the phase transition in aqueous poly (N-isopropylacrylamide) (PNIPAM) solutions, induced by sharply focused (i.e. diffraction limited spot) near-infrared LASER beam ($\lambda = 1064$ nm). It is well known that PNIPAM is an amphiphilic polymer, containing hydrophobic and hydrophilic segments in the same molecule (**Figure 1.12**, right part), exhibiting a reversible phase transition at a lower solution critical temperature (LCST) of 31 °C when dissolved in water.

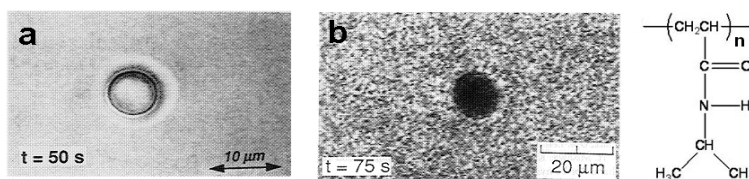


Figure 1.12: a) LASER-induced microparticle formation due to phase transition in a PNIPAM in water solution ($c = 3.6$ % wt, $T = 20$ °C) after 50 s of irradiation ($P = 1.2$ W), b) LASER-induced microparticle formation in a D_2O solution ($c = 3.6$ % wt, $T = 34$ °C, above LCST) after 75 s of irradiation ($P = 0.75$ W). In the right part, the chemical formula of PNIPAM can be seen²⁹.

The photothermal effect, due the local heating of water by the LASER light, was believed to be the primary origin of the observed micron-sized particle formation (**Figure 1.12**, a) at the focus of the beam. However, in addition to the role of the light as a local heat source, some evidence was found for the influence of radiation pressure upon this phase transition, as

stated by the authors. In fact, the authors have demonstrated a microparticle formation in D_2O , but only at $34^\circ C$, above the critical temperature (**Figure 1.12, b**).

In a following study, Hofkens et al.^{30, 31} observed similar behavior in solutions of PNIPAM and micellar solutions of the amphiphilic copolymer (PNIPAM-co-N-octadecylacrylamide) under similar irradiation conditions. In particular, reversible microparticle formation was observed upon LASER irradiation, which was believed to result from the combination of radiation forces and photothermal effects in the case of solutions in H_2O , and as a result of optical forces only in the case of D_2O solutions (**Figure 1.13**), since this solvent has negligible absorption at the used wavelength.

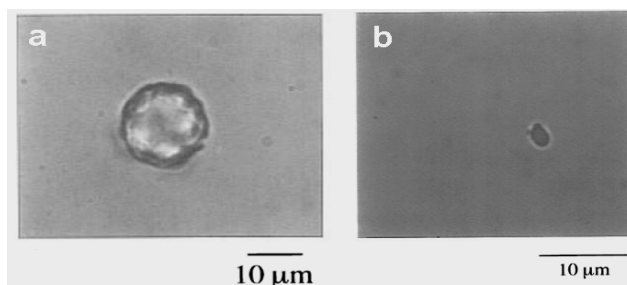


Figure 1.13: a) LASER-induced microparticle formation a PNIPAM in water after 320 s of irradiation ($c = 3.6$ wt, $T = 20^\circ C$, $P = 250$ mW) b) Microparticle formation in a D_2O solution ($c = 3.6$ % wt, $T = 20^\circ C$) after 1000 s of irradiation ($P = 250$ mW)³¹.

The same authors³² conducted fluorescence measurements in a microassociation formed by the LASER-induced assembly of pyrene-labeled NIPAM molecules dissolved in H_2O and D_2O , concluding that the fluorescence spectral data indicated complete different structures of the PNIPAM particles formed by radiation pressure and temperature elevation, respectively. In a more recent report, Juodkazis et al.¹⁷ showed that the radiation force generated by the LASER beam (similar irradiation conditions) induces reversible shrinkage in PNIPAM gels. The authors claim that the LASER-induced volume phase transitions are due to radiation forces, rather than local heating, modifying the weak interactions in the polymer gels.

In order to establish the molecular assembly by radiation pressure, further studies involving other polymeric systems were conducted. Such a study of a polymer in organic solvents was done by Borowicz et al.³³ who examined solutions of poly (N-vinylcarbazole)

(PVCz) in cyclohexanone and N, N-dimethylformamide (DMF). Similarly to the cases mentioned above, the formation of a microparticle at the focal spot of a sharply focused near-infrared LASER beam ($\lambda = 1064$ nm) was experimentally identified (**Figure 1.14**).

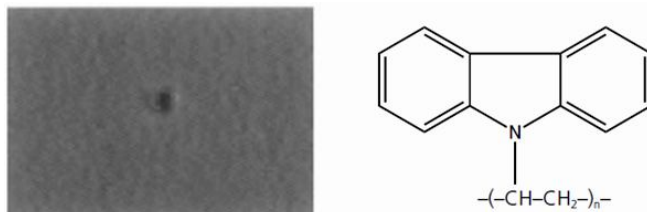


Figure 1.14: Left part: LASER-induced microparticle in a PVCz in DMF solution ($c = 3.5$ % wt, $T = 20$ °C) after 1740 s of irradiation. Right part: The chemical formula of PVCz³³.

This association process clearly exhibited power dependence. Above the critical LASER power for the particle formation, the diameter of the particle increases with increasing power. However, above a certain level, further increase provides no changes in the particle size. The time necessary to achieve this steady state, decreases when the power increases. The time needed to detect particle formation was found to be longer in the cyclohexanone than in the DMF solution (at equal polymer concentrations). The power threshold, above which the formation process is possible, was also slightly different for both solvents (lower for the DMF solutions). Moreover, a difference in the particle diameter was observed, as in the DMF solutions bigger particles could be observed under the microscope. This solvent dependence could be due to different solubility which may lead in slightly different conformations of the macromolecules, resulting in a different effective size from the point of view of the radiation pressure, as stated by the authors. This process of LASER-induced polymer association was found to depend also on the concentration of the solutions. The power threshold for particle formation shifted down for higher polymer concentrations. The diameters of the formed structures were different too, as the microparticles in solutions of higher concentration reached a larger diameter in the steady state at the same LASER power. All measurements during this study were done below the overlap concentration. In both solutions, after the beam was blocked, the particle disappeared in a few seconds.

Smith et al.³⁴ conducted similar experiments in order to find the minimum size of polymers that could associate due to radiation forces. The systems examined were aqueous

solutions of random copolymers of sodium 2-acrylamido-2-methylpropane-sulfonate (AMPS) and 2-(9-carbazoyl)-ethyl methacrylate (CzEMA), and AMPS and [3-(9-carbazoyl) propyl] methacrylamide (CzPMAM), with different carbazoyl (Cz) contents. Microassociations were similarly observed to form in each of the various copolymers studied, but the formation rate and final particle size varied between the samples. First, the observed onset of formation occurred in the higher Cz content copolymers in each series sooner than in the lower Cz content copolymers. Second, the onset from each of the (CzEMA) copolymers in water occurred sooner than for the corresponding (CzPMAM) copolymers of similar Cz content. **Figure 1.15** shows the formed microparticle and the structure of the copolymer used:

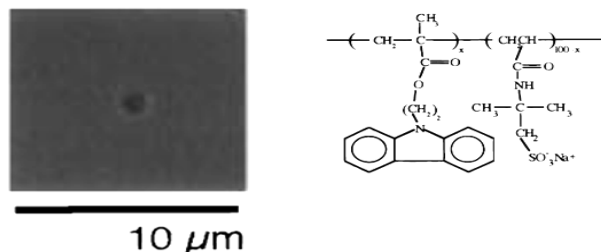


Figure 1.15: Left part: LASER-induced microparticle in a CzEMA in water solution ($c = 3.17\%$ wt) after 30 min of irradiation ($P \sim 250$ mW). Right part: The formula of the random CzEMA copolymer³⁴.

As reported by the authors, these results can be explained in terms of photon pressure exerted on the polymer chains, pointing out the important role of the polarizability in this process. By increasing the Cz content in the copolymer, the refractive index of the polymer is expected to increase, giving rise to stronger radiation pressure. In addition, the length, flexibility, or properties of the chain linking the Cz chromophore to the backbone also affect the particle formation. Finally, the authors concluded that the radius of gyration (R_g) of the polymer may also be a major factor in the microassociation process, claiming that polymers in solution with an R_g of 10-20 nm can be 'trapped' by the photon pressure. The particle formation was confirmed to be similar to H_2O and D_2O . Thus, the researchers concluded that the photothermal effect did not contribute in these systems. It has to be noted that

dissolution of the microassemblies upon removal of the LASER beam was very rapid in all cases, on the order of seconds.

Tsuboi et al.³⁵ demonstrated the photon pressure induced phase separation in solutions of poly (vinyl methyl ether) (PVME) in H₂O and D₂O. When the 1064 nm LASER beam was (strongly) focused in either of these solutions, a single PVME microparticle was assembled at the focal point. Nevertheless, obvious differences in the size, shape and formation time were observed between the two solvents. **Figure 1.16** shows the formations in H₂O and D₂O (a, b) and the chemical formula of PVME (right part):

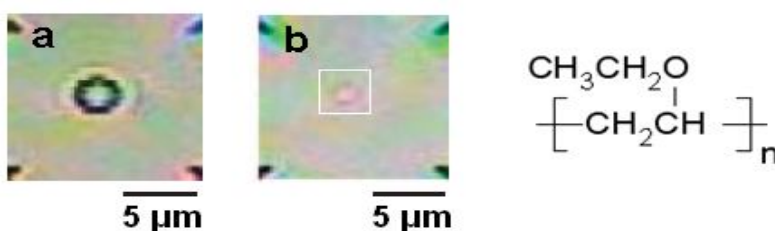


Figure 1.16: a) LASER-induced microparticle in an aqueous PVME solution ($c = 4 \%$ wt) after of irradiation ($P = 120 \text{ mW}$). b): LASER-induced microparticle in PVME in D₂O solution ($c = 4 \%$ wt) after of irradiation ($P = 230 \text{ mW}$)³⁵. Right part: The formula of PVME.

In the water solutions, a critical power for polymer association of 40-50 mW was found to exist, with the corresponding value for the D₂O solutions being 80 mW. For the former case, the time required for the particle formation to start was less than a second ($\sim 0.1 \text{ s}$), while the time to reach an equilibrium state was about 1 minute. In D₂O, the time necessary to observe particle formation was 1-2 min, while the time to reach the equilibrium state was several minutes. The particle diameter in this case, as measured in the equilibrium state, was $2 \mu\text{m}$, irrespective of the LASER power. On the contrary, in the H₂O solutions, the equilibrium particle size increased with an increase in power. At around the critical power, a spherical particle morphology was identified, whether for higher values, particles showed a doubled-layer structure. The dissociation time scales for the two solvents were also different: In H₂O, the formed microparticle disappeared immediately after LASER switching-off, while in D₂O, a few tens of seconds were required. The structures of the PVME microparticles were studied using Raman microspectroscopy. In solutions of PVME in H₂O,

where the microparticle formation is ascribed to the photothermal effect due to local heating of the solvent, the structure of the LASER-induced particle was found to be globular. This is indicated by the similar Raman spectra of the particle and of the solution in the globular state, which shows dehydration of the polymer chains. In the D_2O solutions, where the solvent is transparent, irradiation results in a microparticle with characteristic features of a globular structure too. On the basis of these observations, the authors concluded that the microparticle formation following the phase transition from a coil to globule is triggered by radiation pressure. It has to be mentioned that the concentration examined was 4% wt (in both solvents), for polymer molecular weight of ~ 90 kg/mol.

Masuo et al.³⁶ reported another case of radiation pressure-induced macromolecules association in solutions of poly (2, -(9, 9-bis (2-ethylhexyl) fluorene)) (PEHF) in THF. More specifically, ordered fibril- and particle-like assemblies have been achieved controllably by combining LASER ($\lambda = 1064$ nm) irradiation with convection in the cast solution on a glass substrate. When the viscous drag of the solution in the convection is stronger than the photon force, the fibril-like assemblies could be formed. It was confirmed that assemblies of various widths and lengths could be formed by controlling the following parameters; the power of the tightly focused LASER beam, the concentration of the cast solution, and the convection rate. Fluorescence and AFM images of the fibrillar structures are shown in **Figure 1.17**:

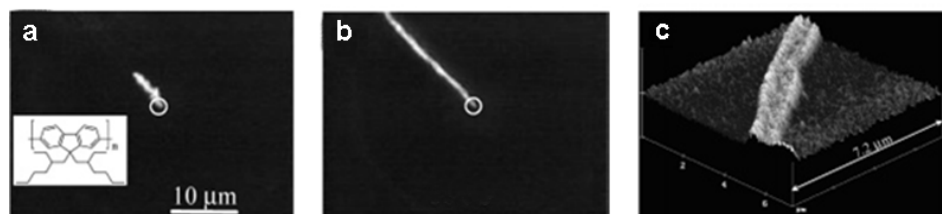


Figure 1.17: a), b) Fluorescence images of the LASER-induced fibril-like assembly formation. White circles show the focal point of the near-IR LASER beam. LASER power at the focal point was 45 mW. The chemical structure of PEHF is inset in image (a). c) AFM image of a 1.5 μm wide fiber.

It was demonstrated by fluorescent anisotropy imaging that the molecular orientation in the formed assembly was controlled by the direction of the linearly polarized near-infrared LASER beam in this case. The authors attributed the assembly formation at the focal point

solely to the photon force. The arguments were based in the fact that long π -conjugation like in PEHF possesses a high polarizability, and in the current case, the surrounding medium was THF, whose polarizability is lower than that of PEHF. That is to say, PEHF molecules in the THF solution are trapped by the photon force at the focal point, consequently, concentration at the focal point becomes high, which leads to the deposition of the assembly. As for the possibility to have the photothermal effect too, it was stated that PEHF and THF have practically no absorption at 1064 nm. Therefore, the authors claimed that it was not necessary to consider local heating as the origin of the deposition of PEHF, even when the temperature is elevated (estimated to be $\sim 0.14\text{K}$ under the experimental conditions). An important point in this study was the reversibility of the process. During the gradual evaporation of the solvent of the cast solution on the glass substrate, the concentration was increasing, and when the solution reached a saturated condition, polymers started to deposit on the substrate. When the irradiation started after the polymer deposition, the assemblies were not redissolved in the solution. On the contrary, when the LASER was shined in the solution before the deposition, the whole process was reversible.

The effects resulting from the application of radiation forces in micellar solutions were also experimentally demonstrated. Hotta et al.³⁷ reported on the LASER-controlled assembling of repulsive monomolecular micelles in aqueous solutions. Copolymers which were terpolymerized from sodium AMPS, *N*-Cyclodecyl-methacrylamide, and *N*-(1-pyrenylmethyl) methacrylamide (poly (A / Cd / Py) dissolved in D_2O (**Figure 1.18**, right), resulting in micelles with $R_g \sim 5.5$ nm, were irradiated by a strongly focused near-infrared LASER light ($\lambda = 1064$ nm). Assembling of the unimer-forming amphiphilic polyelectrolyte by photon pressure and the resultant formation of a single microparticle were shown (**Figure 1.18**, left).

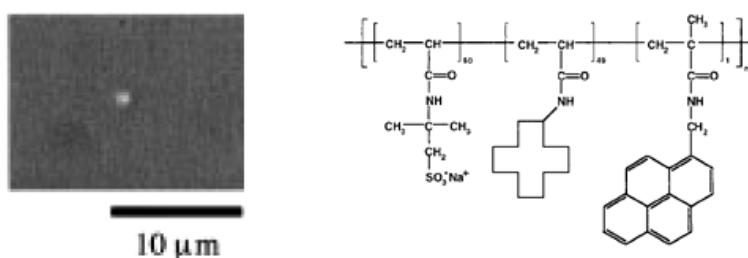


Figure 1.18: Left part: LASER-induced microparticle in a D₂O solution of the random copolymer poly (A / Cd / Py) after irradiation (P = 700 mW). Right part: The chemical structure of the random copolymer poly (A / Cd / Py)³⁷.

Examination in a concentration range (in the dilute regime) showed that solutions with higher *c* exhibit a faster and more pronounced effect, compared to the more dilute solutions. The formed microparticles disappeared quickly after switching off the LASER light. By contrast to other reported cases of polymer association³⁰⁻³³, the time scales for particle formation was much faster in this case, and no changes in the conformation. Fluorescence experiments revealed no changes in the microenvironmental conditions of the micelles.

Except for the case of micelles, D₂O solutions of giant vesicles made of didodecyldimethylammonium bromide, under similar irradiation conditions mentioned above, were studied by Kitamura et al.³⁸. The interesting concept of transformation and fission of vesicles due to radiation pressure was demonstrated.

Further experimental investigations have been carried out to support a radiation pressure effect upon molecular association and to show the applicability of this effect in more general terms. Hotta et al.³⁹ reported on the aggregation and fusion process of molecular micelles in aqueous solutions, where long chains were not present. The micelles consisted of sodium dodecyl sulfate (SDS) in water, xylene and 1-pentanol. The size of the swollen micelles was estimated to be less than 100 nm. A single small droplet was observed at the focal point of the sharply focused LASER beam ($\lambda = 1064$ nm), with a diameter of about 1 μm . By switching off the LASER light, the droplet underwent Brownian motion without dissolution and disappeared immediately from the ocular field. The whole process was reproducible. The same experiment was conducted in a D₂O micellar solution, in order to examine the mechanism behind this assembly process. Quite similar LASER-induced aggregation was confirmed, pointing towards a radiation pressure mechanism. The authors estimated the trapping potential to be two orders of magnitude bigger than the thermal energy in this system. In addition, fluorescence experiments showed that fusion of the micelles was achieved by the radiation pressure.

A demonstration of size-selective optical trapping and deposition of polymer and aromatic molecules from a binary mixed solution was reported by Nabetani et al.⁴⁰. As a LASER beam ($\lambda = 1064$ nm) was tightly focused in PS and perylene mixed solution in THF

(dilute regime) that was dropped on a glass substrate, a molecular assembly was deposited at the LASER focus and was fixed on the substrate. The authors compared the structures produced by evaporating the solvent, without irradiation, with the LASER-induced assemblies, using Atomic Force Microscopy (AFM) and fluorescence spectroscopy. AFM investigation showed that the former structures were very inhomogeneous, presenting dot-like and polygonal geometry. The corresponding fluorescent spectra showed a typical perylene monomer and an excimer emission, respectively. The latter shows that perylene crystals were formed in the case of polygonal morphologies. Upon LASER irradiation, a surface deformation of the solution layer was directly induced, and then the solution around the LASER focus disappeared within several seconds. Eventually, a molecular assembly trapped in the solution was left at the position of the focus on the glass substrate. The width of the assembly became narrower at higher LASER power. An interesting point is that the rough surface structures were observed at intermediate P (200-400 mW), whereas assemblies with smooth surfaces were obtained at higher P. Furthermore, the fluorescence spectra also showed clear power dependence. In the range of the LASER power below 400 mW, both monomer and excimer emission was observed. However, only monomer emission was observed in the LASER-power range above 500 mW. Results of further control experiments supported that the relative concentration of perylene in the PS microassembly is varied only by optical trapping force, and not by solvent evaporation. The formation of perylene crystals in the polymer microassembly was suppressed in the case of power higher than 500 mW, and perylene concentration may be below the critical concentration for crystallization so that crystals do not form and only monomer emission is observed at high P. This, according to the authors, happens due to size-selective trapping of the PS molecules.

Another similar but not very clear report of association of macromolecules by the utilization of a classical optical trap was carried out recently by Singer et al.⁴¹. The authors claim to have experimentally verified that optical tweezers can be used to manipulate single molecules of polyethylene oxide (PEO) suspended in water. In this study, a typical optical tweezers apparatus was used to focus the beam from a 1064 nm LASER to form the trap. A solution of PEO molecules was placed in the trap, and the concentration of macromolecules in the trap was monitored by measuring the backscattered light from another low power He-Ne LASER focused on the same position. When the polymers were 'trapped', the

concentration of PEO was observed to increase over several minutes. The increase in concentration was repeatable, reversible, and increased with increasing LASER power.

In a very recent experimental investigation, Toyama et al.⁴² explored the homogenization of a phase-separated droplet in aqueous solutions of binary polymers (water / polyethylene glycol (PEG) / dextran) caused by irradiation with a tightly focused 1064 nm LASER beam. The experiments were carried out at room temperature, in dextran-rich droplets inside the PEG-rich phase and in PEG-rich droplets inside the dextran-rich phase. In the former case, upon LASER irradiation, it was found that the size of the dextran-rich droplet (initially $\sim 20 \mu\text{m}$) gradually decreased, up to the complete disappearing of the droplet. When the LASER was turned off, the droplet re-appeared in the same region, followed by the formation of multiple smaller droplets both inside and outside the original dextran-rich droplet, to form a nested structure (**Figure 1.19**).

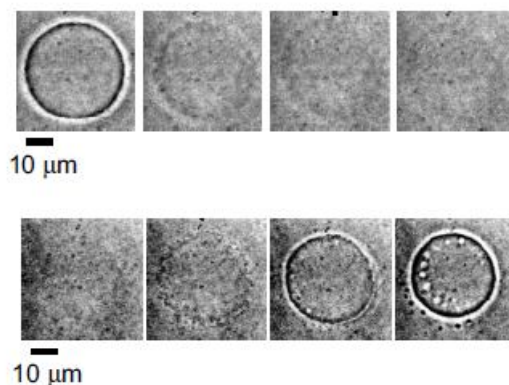


Figure 1.19: Top: Time series of images ($t \sim 1, 9, 15, 20$ s) of a gradually disappearing dextran-rich droplet around the focus of the LASER beam ($P = 1.5$ W) Bottom: Time series of images ($t \sim 1, 10, 20, 45$ s) of a reappearing dextran-rich droplet after LASER irradiation was discontinued. Micrometer-sized droplets are generated both inside and outside the original dextran-rich droplet⁴².

On the other hand, in the case of the PEG-rich droplets the situation was different. While being irradiated, the droplet diameter (initially $\sim 5 \mu\text{m}$) was decreasing up to vanishing, but the droplet did not re-appear after blocking the LASER light. In order to investigate the heating effect by LASER irradiation, the same experiments were conducted with a D_2O / dextran / PEG system. The authors confirmed that there was no essential difference in the experimental trends regarding the disappearance of droplets. Thus, it was attributed to the

LASER potential as the main driving force. These phenomena were described in terms of a phenomenological free-energy model, which included a LASER potential term based on a relational expression of the refractive indices of the compounds. In fact, numerical results on the two systems mentioned above, reproduced well the experimental findings.

Deformations and breakup of fluid interfaces under an applied field have been also studied in detail, owing to their scientific and technological importance. Casner et al^{43, 44} studied the giant light-induced deformation and optohydrodynamic instabilities of liquid-liquid interfaces. The experiments were performed in a near-critical water in oil micellar phase of a microemulsion consisted of water, SDS, toluene and n-butanol. For a temperature $T > T_c$ ($T_c = 35$ °C for this specific system), the mixture phase separates in two micellar phases of different micellar concentrations. The high micellar concentration phase, Φ_1 , is located below the low concentration phase, Φ_2 , owing to the higher density of water. Application of a weakly focused LASER light ($\lambda = 514$ nm), caused the deformation of the flat meniscus between the two phases. The light momentum discontinuity at the interface gives birth to a radiation pressure directed towards the phase of lower refractive index, which is Φ_1 . The authors found that the response of the surface can be local or non-local, depending on the ratio between the two restoring forces, buoyancy and Laplace forces, which could be experimentally changed by varying the beam waist. Moreover, the authors have reported on a new class of electromagnetically driven fluid interface instability in the same system, by using high beam powers (on the order of 1 W) relatively loosely focused (beam waist ~ 3.5 μm). For LASER power higher than a critical value, the interface becomes unstable, leading to the formation of a stationary, mm long, liquid jet (**Figure 1.20**).

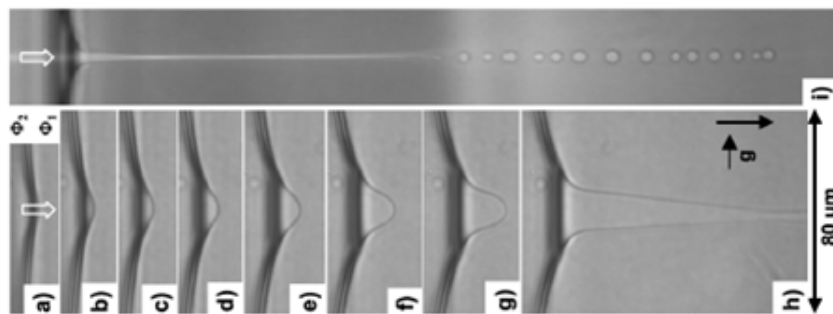


Figure 1.20: (a) –(h) Variation of the optical interface bending versus beam power until instability when $(T-T_c) = 15K$ and beam waist, $w_0 = 3.5 \mu m$: (a) $P = 310 mW$, (b) $P = 500mW$, (c) $P = 620mW$, (d) $P = 740mW$, (e) $P = 920mW$, (f) $P = 1110mW$, (g) $P = 1170mW$, and (h) $P = P_S = 1230mW$. For $P = P_S$ the interface becomes unstable, leading to the formation of a stationary liquid jet similar to that illustrated in the overview (i) for $(T-T_c) = 6K$, $w_0 = 3.5 \mu m$, and $P = P_S = 490mW$. The LASER beam is represented by the arrows, and the height of (i) is $1 mm^{44}$.

The whole effect is driven by the optical radiation pressure exerted by the LASER beam. Recently, more detailed studies on the statics and the dynamics of the light-induced instabilities were carried out by this group^{45, 46}.

References

1. Boyd, R. W., *Nonlinear Optics*. Academic Press: Burlington, 2008.
2. Menzel, R., *Photonics: Linear and Nonlinear Interactions of Laser Light and Matter*. Springer: Berlin, 2007.
3. Barthelemy, A., Maneuf, S., Froehly, C. *Opt. Commun.* **1985**, 55, 201-206.
4. Segev, M., Crosignani, B., Yariv, A., Fischer, B. *Phys. Rev. Lett.* **1992**, 68, 923-926.
5. Jones, R. A. L., *'Soft Condensed Matter'*. Oxford University Press: Oxford, 2002.
6. Conti, C., Ruocco, G., and Trillo, S. **2005**, 95, 183902.
7. Ashkin, A., Dziedzic, J. M., Smith, P. W. *Opt. Lett.* **1982**, 7, 276-278.
8. Khoo, I. C. *Phys. Rep.* **2009**, 471, 221-267.
9. Voit, A., Krekhov, A., Enge, W., Kramer, L., Köhler, W. *Phys. Rev. Lett.* **2005**, 94, 4.
10. Voit, A., Krekhov, A., and Köhler, W. *Phys. Rev. E* **2007**, 76, 011808.
11. Duhr, S., and Braun, D. *Proc. Natl. Acad. Sci* **2006**, 103, 19678–19682.
12. Delville, J. P., Lalaude, C., Freysz, E., and Ducasse, A. *Phys. Rev. E* **1994**, 49, 4145.
13. Delville, J. P., Lalaude, C., Buil, S., and Ducasse, A. *Phys. Rev. E* **1999**, 59, 5804.
14. Loppinet, B., Somma, E., Vainos, N., and Fytas, G. *J. Am. Chem. Soc.* **2005**, 127, 9678-9679.
15. Sigel, R., Fytas, G., Vainos, N., Pispas, S., and Hadjichristidis, N. *Science* **2002**, 297, 67-69.
16. de Gennes, P. G., *Scaling Concepts in Polymer Physics*. Cornell University Press: Ithaca, NY, 1979.
17. Juodkazis, S., Mukai, N., Wakaki, R., Yamaguchi, A., Matsuo, S., and Misawa, H. *Nature* **2000**, 408, 178-181.
18. Kewitsch, A. S., and Yariv, A. *Opt. Lett.* **1996**, 21, 24-26.
19. Wirtz, D., Berend, K., and Fuller, G.G. *Macromolecules* **1992**, 25, 7234-7246.
20. Wirtz, D., and Fuller, G.G. *Phys. Rev. Lett.* **1993**, 71, 2236-2239.
21. Gurovich, E. *Macromolecules* **1995**, 28, 6078-6083.
22. Tsori, Y.; Tournilhac, F.; Leibler, L. *Nature* **2004**, 430, (6999), 544-547.
23. Price, C., Deng, N., Lloyd, F.R., Li, H., and Booth, C. *J. Chem. Soc. Faraday Trans.* **1995**, 91, 1357-1362.

24. Wang, C. H., and Huang, Q.R. *J. Chem. Phys.* **1997**, 106, 2819-2823.
25. Sun, Z., and Wang, C. H. *Macromolecules* **1999**, 32, 2605-2609.
26. Giacomelli, F. C., Riegel, I.C., Petzhold, C.L., and da Silveira, N.P. *Macromolecules* **2008**, 41, 2677-2682.
27. Schmidt, K., Schobert, H. G., Ruppel, M., Zettl, H., Hänsel, H., Weiss, T. M., Urban, V., Krausch, G., and Böker, A. *Nat. Mater.* **2007**, 7, 142-145.
28. Ishikawa, M., Misawa, H., Kitamura, R., and Masuhara, H. *Chem. Lett.* **1993**, 22, 481-484.
29. Ishikawa, M., Misawa, H., Kitamura, N., Fujisawa, R., and Masuhara, H. *Bull. Chem. Soc. Jpn.* **1996**, 69, 59-66.
30. Hofkens, J., Hotta, J.-I., Sasaki, K., Masuhara, H., Faes, H., De Schryver, F. *Mol. Cryst. Liq. Cryst.* **1996**, 283, 165-172.
31. Hofkens, J., Hotta, J., Sasaki, K., Masuhara, H., and Iwai, K. *Langmuir* **1997**, 13, 414-419.
32. Hofkens, J., Hotta, J., Sasaki, K., and Masuhara, H. *J. Am. Chem. Soc.* **1997**, 119, 2741-2742.
33. Borowicz, P., Hotta, J.-I., Sasaki, K., and Masuhara, H. *J. Phys. Chem. B* **1997**, 101, 5900-5904.
34. Smith, T. A., Hotta, J.-I., Sasaki, K., Masuhara, H., and Itoh, Y. *J. Phys. Chem. B* **1999**, 103, 1660-1663.
35. Tsuboi, Y., Nishino, M., Matsuo, Y., Ijio, K., and Kitamura, N. *Bull. Chem. Soc. Jpn.* **2007**, 80, 1926-1931.
36. Masuo, S., Yoshikawa, H., Nothofer, H.-G., Grimsdale, A.C., Scherf, U., Müllen K., and Masuhara, H. *J. Phys. Chem. B* **2005**, 109, 6917-6921.
37. Hotta, J.-I., Sasaki, K., and Masuhara, H., and Morishima, Y. *J. Phys. Chem. B* **1998**, 102, 7687-7690.
38. Kitamura, N., Sekiguchi, N., and Kim, H.-B. *J. Am. Chem. Soc.* **1998**, 120, 1942-1943.
39. Hotta, J.-I., Sasaki, K., and Masuhara, H. *J. Am. Chem. Soc.* **1996**, 118, 11968-11969.
40. Nabetani, Y., Yoshikawa, H., and Masuhara, H. *J. Phys. Chem. B* **2006**, 110, 21399-21402.

41. Singer, W., Nieminen, T.A., Heckenberg, N.R., and Rubinsztein-Dunlop, H., 'Nanotrapping and the thermodynamics of optical tweezers'. In *Australian Institute of Physics (AIP) 17th National Congress*, Brisbane, 2006.
42. Toyama, H., Yoshikawa, K., and Kitahata, H. *Phys. Rev. E* **2008**, 78, 060801.
43. Casner, A., and Delville, J.P. *Phys. Rev. Lett.* **2001**, 87, 054503.
44. Casner, A., and Delville, J.P. *Phys. Rev. Lett.* **2003**, 90, 144503.
45. Wunenburger, R., Casner, A., and Delville, J.P. *Phys. Rev. E* **2006**, 73, 036315.
46. Wunenburger, R., Casner, A., and Delville, J.P. *Phys. Rev. E* **2006**, 73, 036314.

CHAPTER 2

MATERIALS AND METHODS

The materials (and their properties) which have been used will be presented in this chapter. The utilized experimental techniques will be also discussed.

2.1 Polydiene Solutions

2.1.1 General properties of polydienes

All the results presented in this thesis have been obtained by utilizing polydiene solutions in various organic solvents. Polydienes are macromolecules which result from the polymerization of dienes, hydrocarbon monomers that contain two double bonds (C=C). Isoprene and butadiene are two of the most commonly used dienes. Isoprene and butadiene polymerization can result in polymers with different microstructures, shown in **Figure 2.1**. By varying the polymerization conditions, the desired microstructures can be obtained¹.

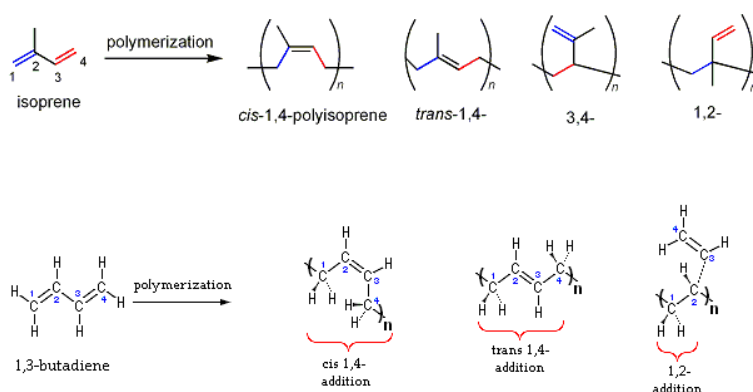


Figure 2.1: Different polymer microstructures resulting from the polymerization of isoprene and butadiene.

Analogous microstructures can be obtained for PB. The corresponding chemical structures in this case can be visualized by substituting the methyl group of PI with a hydrogen atom. Different polymerization processes with variable level of control are used to produce these synthetic rubbers. Alternatively, cis 1,4 – PI, the main compound of natural rubber (latex), is derived from a milky colloidal suspension of specific kinds of trees.

PI and PB are model systems of flexible polymeric chains and have been subject of extensive studies². Several rheological, dielectric and light scattering studies have been reported on these systems, both in the melt and in solution state.

Natural and synthetic PI and PB are the most common rubbery materials used in numerous applications and products, such as tires, motor mounts, gloves, toughened plastics and others. The low cost, high availability and unique properties of these materials make them extremely popular.

2.1.2 Polymer solutions

Since all the samples used in this study are polymer solutions, and since the studied effect relates to local modifications in the polymer concentration, a brief account of the standard physical description of dilute and semidilute polymer solutions is given below.

To describe the conformation of an ideal chain, a model of random walk can be used. In a hypothetical chain of N freely jointed links of length l , the root mean square end-to-end distance of the chain (R) can be calculated to be

$$R = N^{1/2}l \quad \text{(Equation 2.1)}$$

In real polymer chains, however, the excluded volume interaction between monomers prevents any two segments from simultaneously occupying the same region and the end-to-end distance of a real chain in a solvent is different than the one of an ideal chain. The general relation between R , N and l is:

$$R = N^\nu l \quad \text{(Equation 2.2)}$$

For good solvents, $\nu = 3/5$, larger than $\nu = 1/2$ for the ideal case. The ideal scaling is observed in solvents of reduced quality, the so-called θ solvents.

In dilute solutions, the chains can be viewed as isolated coils which do not interact, with the characteristic size being the radius of gyration R_g ($R_g = R/\sqrt{6}$). Due to their small size, polymer chains undergo substantial Brownian motion. The resulting self diffusion of a polymer coil in a dilute solution, D , is described by the Stokes-Einstein-Sutherland relation³,

$$D = \frac{k_B T}{6\pi\eta R_h} \quad (\text{Equation 2.3})$$

where k_B is the Boltzmann constant, η is the solution viscosity, and R_h is the hydrodynamic radius of the macromolecule, related to R_g through the equation $R_g = 0.7 R_h$

Due to the very low concentration within a coil, polymer coils have the unique property to be able to overlap with each other, in particular as the concentration c increases.

The overlap concentration c^* is defined as the concentration inside one coil

$$c^* = \frac{M_w}{\frac{4}{3}\pi R_h^3 N_A} \quad (\text{Equation 2.4})$$

where M_w is the polymer molecular weight, and N_A is the Avogadro number. **Figure 2.2** depicts the different concentration regimes:

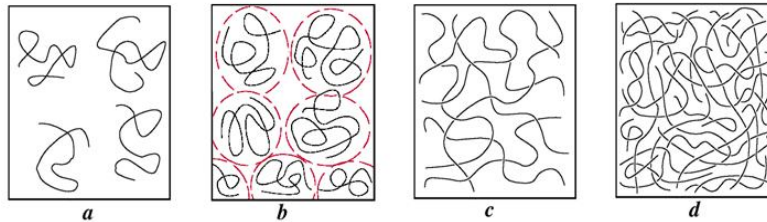


Figure 2.2: Concentration regimes for solutions of linear flexible polymers: a) dilute solution, $c < c^*$; b) crossover from dilute to semidilute solution, $c \sim c^*$, c) semidilute regime, $c > c^*$, d) concentrated regime, $c \gg c^*$.

At $c > c^*$ (and $c \ll 1$) chains start to interpenetrate. The physical picture of a semidilute solution is that of a network⁴ with an average mesh size ξ (known as blob) as depicted in **Figure 2.3 a**:

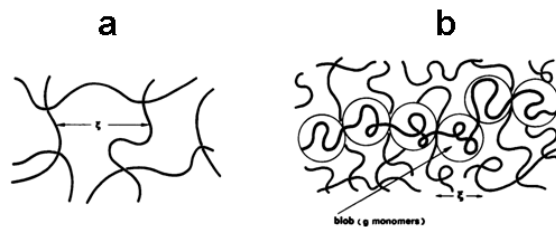


Figure 2.3: a) The spatial picture of a semidilute solution with a characteristic mesh size ξ . b) An individual chain in a semidilute solution can be visualized like a succession of blobs of size ξ .

ξ is the characteristic length scale of the screened monomer-monomer interaction. On length scales smaller than ξ , each monomer is surrounded by mostly solvent and other monomers belonging in the same chain. Therefore, the chain conformation is similar to dilute solutions. On larger length scales larger than ξ , the excluded volume interactions are screened by the overlapping chains. Thus, the conformation is a random walk of blobs with size ξ , as shown schematically in **Figure 2.3 b**. The mesh size depends only on the polymer concentration (it decreases as c increases) and not on the molecular weight, since each chain is much longer than ξ .

As concentration is further increased, the diffusion is strongly affected by the other solute molecules. In the physical network formed, the network chains impose topological constraints on each other because they cannot cross³. These constraints, called entanglements, greatly affect the system properties. In the case of entangled semidilute solutions, the so-called tube model has been successfully introduced to describe the polymer dynamics.

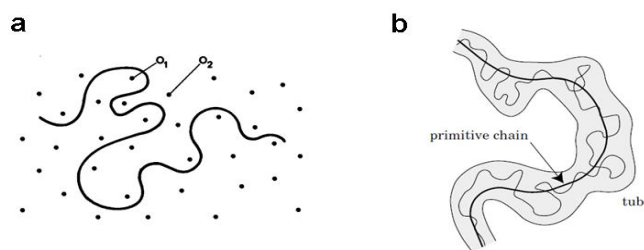


Figure 2.4: a) A single chain moving in a snake-like motion, called reptation, through a collection of fixed obstacles. b) A schematic illustrating the tube model.

Let us consider a single chain, called a primitive chain, moving in a given network of other chains. The network is described by fixed obstacles, as shown in **Figure 2.4 a**. The chain cannot cross any of them, but it can move in between in a wormlike fashion, a motion called reptation⁴. We can imagine a tube-like region, in which the primitive chain is being trapped (**Figure 2.4 b**). Over a short period of time, the chain wiggles within the tube just as the monomers in the blob move cooperatively without moving out of the blob. Beyond that time scale, the chain can move only along the tube. The tube and the blob models provide some simple scaling laws to describe the dynamics and its dependence on concentration and molecular weight of the polymer chains in semidilute solutions⁴.

2.1.3 Light scattering from polymer solutions

As the polymer solutions are irradiated by a light beam, part of this light will be scattered in direction different from the propagation direction. This scattering process is well described by the Rayleigh scattering theory and is the base of light scattering techniques widely used for the characterization of polymers structures and dynamics.

Rayleigh scattering theory is based on the concept of induced dipole: as the light field impinges a "scatterer" (that could be a molecule), it induces a dipole moment, μ in the direction of the field which is proportional to the field strength:

$$\mu = aE \quad \text{(Equation 2.5)}$$

The proportionality constant a is the polarizability of the scatterer. This induced dipole moment then radiates (scatters) electric field in all directions, giving rise to the scattered light.

For a small dielectric sphere of dielectric constant ε (refractive index n) immersed in a fluid of dielectric constant ε_0 (refractive index n_0), this description holds and the polarizability is given by the Clausius-Mosotti relation :

$$a = 3V \varepsilon_0 n_0^2 \left(\frac{m^2 - 1}{m^2 + 2} \right) \quad (\text{Equation 2.6})$$

where $m = n/n_0$. **Equation 2.6** shows that the scattering power of a sphere is proportional to the square of its volume as well as the refractive index difference between the sphere and the solvent. If $m = 1 + \frac{\delta n}{n_0}$, then

$$a = \frac{3M}{\rho} \varepsilon_0 n_0^2 \left(\frac{\frac{2\delta n}{n_0} + \left(\frac{\delta n}{n_0}\right)^2}{\frac{2\delta n}{n_0} + \left(\frac{\delta n}{n_0}\right)^2 + 3} \right) \quad (\text{Equation 2.7})$$

where M is the mass and ρ is the density of the scatterer. This relation holds more generally for the polarizability of any isotropic macromolecule immersed in a solvent of similar refractive index. The polarizability can be positive or negative, depending on whether the refractive index of the particle is higher or lower than that of the solvent. This equation relates the microscopic polarizability with the macroscopic refractive index.

For many non interacting macromolecules, the total intensity will be the addition of the intensity scattered by the different macromolecules. For larger macromolecules, the intensity will show some level of scattering wave vector dependence. The Rayleigh approximation is still valid and the intensity can be shown to be on the general form of

$$I(q) \sim 1 - \frac{q^2 R_g^2}{3} \quad (\text{Equation 2.8})$$

where q is the scattering wavevector

$$q = \frac{4\pi n_0}{\lambda} \sin\left(\frac{\theta}{2}\right) \quad (\text{Equation 2.9})$$

and θ is the scattering angle, and λ is the wavelength of the light. The scattering intensity for the polarized scattering geometry, I , is given by

$$I = cHM_w \left(1 - \frac{q^2 R_g^2}{3} - 2A_2 M_w c \right) \quad (\text{Equation 2.10})$$

where A_2 is the second Virial coefficient, and H is the optical constant

$$H = \frac{4\pi^2 n^2}{\lambda^4 N_A} \left(\frac{dn}{dc} \right)^2 \quad (\text{Equation 2.11})$$

A_2 is a direct measure interactions between pairs of chains. When in good solvents, chains repel each other and A_2 is positive. In θ solvent, the attraction between monomers just balances their repulsive interaction, so that the net excluded volume is zero and therefore $A_2 = 0$. In poor solvents, polymer-polymer interactions are attractive and $A_2 < 0$.

As concentration increases **Equation 2.10** loses its meaning and the scattering by overlapping polymer chains in semi-dilute solutions is best understood within the blob model. As ξ is the characteristic size of the formed network, the scattering is of the type

$$I(q) \sim \frac{I_0}{1 + q^2 \xi^2} \quad \text{Equation 2.12}$$

Given the typical ξ size, this will not lead to any q -dependence in the light scattering regime. The scattered intensity is given by the blob polarizability $a_{blob} = I_0 N_{blob} M_{blob}^2 = c M_{blob}$, where N_{blob} is the number of blobs and M_{blob} is the molecular weight of the blob. Using the scaling law, the weak concentration dependence of scattered intensity in polymer solutions can be shown.

Useful information concerning the dynamics of semidilute solutions can be obtained by Dynamic Light Scattering. In a transient gel model described above, the dynamic correlation length ξ_D deduced from the cooperative diffusion coefficient D_C

$$\xi_D = \frac{k_B T}{6\pi\eta D_C} \quad (\text{Equation 2.13})$$

is similar to the static correlation length ξ . As has been already mentioned above, for a distance longer than the correlation length, the segment-segment interaction is “completely” screened out in an athermal solvent.

Further details concerning the Static and Dynamic Light Scattering techniques are provided in **Appendix I**.

2.2 Sample preparation and characterization

The molecular characteristics of the used homopolymers and diblock copolymers will be presented here. Next, the semidilute solution preparation route and the characterization will be described.

2.2.1 Characterization of the linear and branched homopolymers

In order to characterize the anionically polymerized PI's, a series of dilute solutions was prepared (**Table 2.1**). The solvent used was toluene, known from the literature for being a good athermal solvent for the specific macromolecules. All polymer concentrations were in the dilute regime (i.e. $c \ll c^*$), in order to avoid interactions between isolated chains. The solutions were left to stir for 2 days, in order to finally obtain homogeneous samples. Then, they were carefully filtered through PTFE filters (pore diameter 0.45 μm) to dust-free glass cells, appropriate for light scattering measurements.

Figure 2.5 shows a typical plot of the inverse normalized Rayleigh ratio, $\frac{cH}{R_{VV}}$, as a function of polymer concentration for the intermediate cis-1,4 PI used in the present study see **Appendix I**). The data were obtained by Static Light Scattering measurements. Using the value⁵ $\text{dn}/\text{dc} = 0.03 \text{ ml/g}$, the weight-averaged molecular weight at the limit of zero dilution ($c \rightarrow 0$) can be calculated (**Equation 2.10**), which is $M_w = 378.8 \text{ kg / mol}$ for this specific polymer.

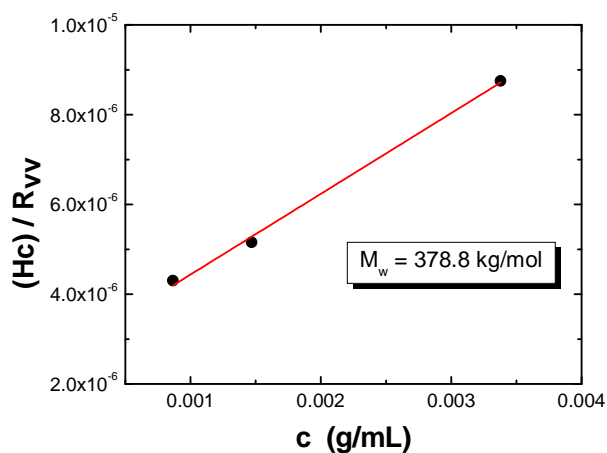


Figure 2.5 Plot of the inverse normalized Rayleigh ratio vs. polymer concentration, for a series of dilute solutions of cis-1,4 polyisoprene dissolved in toluene. The weight-averaged molecular weight is $M_w = 378$ kg/mol.

The results for the rest of the PI's are summarized in **Table 2.1**.

A typical correlation function of PI in toluene, in a concentration $c = 3.38 \cdot 10^{-3}$ g/ml, at a scattering angle $\theta = 20^\circ$, is shown in the left part of **Figure 2.6**:

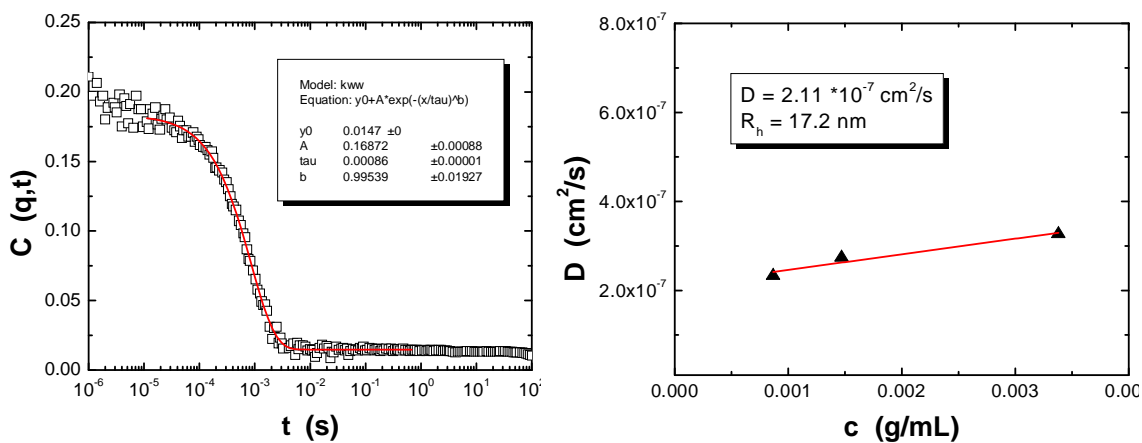


Figure 2.6 Left: Correlation function obtained from a cis-1,4-PI ($M_w = 378.8$ kg/mol) solution in toluene, at a scattering angle $\theta = 20^\circ$. The polymer concentration is $3.38 \cdot 10^{-3}$ g/mL. The red solid line is an exponential decay fit with the KWW function, $y = y_0 + A \exp(-t/\tau)^b$, where A is the amplitude, τ is the relaxation time and b is the stretching exponent. Right: Plot of the diffusion coefficient, D , as a function of polymer concentration, for the cis-1,4 PI ($M_w = 378.8$ kg/mol) in toluene dilute solutions. The hydrodynamic radius is $R_h = 17.2$ nm.

A single exponential decay is observed, which corresponds to the translational diffusion of the polymer chains, with a diffusion time of $\tau = 8.6 \cdot 10^{-4}$ s. A plot of D vs. polymer concentration is shown in the right part of **Figure 2.6**, summarizing the DLS results for this polymer in dilute toluene solutions. In the limit of zero dilution, the R_h of the chains for this specific M_w can be calculated, using **Equation 2.3**. For $\eta = 0.59 \cdot 10^{-3}$ Pa s, and $T = 293$ K, the result is $R_h = 17.2$ nm. The results for the rest PI's are summarized in **Table 2.1**:

Polymer	cis-1,4 PI low M	cis-1,4 PI intermediate M	cis-1,4 PI high M	PI (40% 1, 2 and 3, 4 60 % 1, 4 domains)
c_1 (g/mL)	$7.02 \cdot 10^{-3}$	$3.38 \cdot 10^{-3}$	$7.8 \cdot 10^{-4}$	$2.43 \cdot 10^{-3}$
c_2 (wt %)	$3.55 \cdot 10^{-3}$	$1.47 \cdot 10^{-3}$	$6.07 \cdot 10^{-4}$	$1.39 \cdot 10^{-3}$
c_3 (wt %)	$2.17 \cdot 10^{-3}$	$8.67 \cdot 10^{-4}$	$3.47 \cdot 10^{-4}$	$7.8 \cdot 10^{-4}$
M_w (g / mol)	$64.7 \cdot 10^3$	$37.8 \cdot 10^4$	$1.09 \cdot 10^6$	$93.6 \cdot 10^4$
R_h (nm)	9	17.2	53.6	30.1
M_n / M_w	1.02	1.07	1.07	1.06

Table 2.1: A list of the dilute solutions measured with light scattering, and the resulting polymeric characteristics.

The polydispersity M_w/M_n was calculated by Size-Exclusion Chromatography experiments.

The isomer composition (calculated from Nuclear Magnetic Resonance (NMR) data) is 90 % 1, 4 (cis and trans) and 10% 1, 2 and 3, 4 for the high cis content PI's.

The industrial branched cis-1, 4 PB used in this study⁶ was used without further characterization. The given molecular characteristics were the following: The molecular weight is $M_w = 390$ kg/mol, while the polydispersity is $M_w/M_n = 2.5$. These data were acquired by Size-Exclusion Chromatography and Light Scattering measurements.

2.2.2 Characterization of the copolymer solutions

Dynamic and Static Light Scattering (DLS and SLS, respectively) experiments were performed in dilute solutions of the anionically prepared diblock copolymer poly (isoprene-*b*-styrene) (IS4), in two solvents, hexane and ethyl acetate respectively. The molecular weight and the polydispersity of this copolymer were $M_w = 424$ kg/mol and $M_w/M_n = 1.04$, measured by Size Exclusion Chromatography. The composition was 25% poly (styrene) and 75% poly (isoprene), calculated from NMR data. Previous experiments on IS4 in hexane solutions showed that star-like micelles are formed, since hexane is a selective solvent for the PI block. A series of dilute solutions was prepared and were left to stir for 2 days, in order to finally achieve homogeneous samples. Then, they were carefully filtered through PTFE filters (pore diameter 0.45 μm) to dust-free glass cells.

A representative correlation function from an IS4 / hexane solution, $c = 2.85 \cdot 10^{-5}$ g/ml, at a scattering angle $\theta = 90^\circ$, is shown in the left part of **Figure 2.7**:

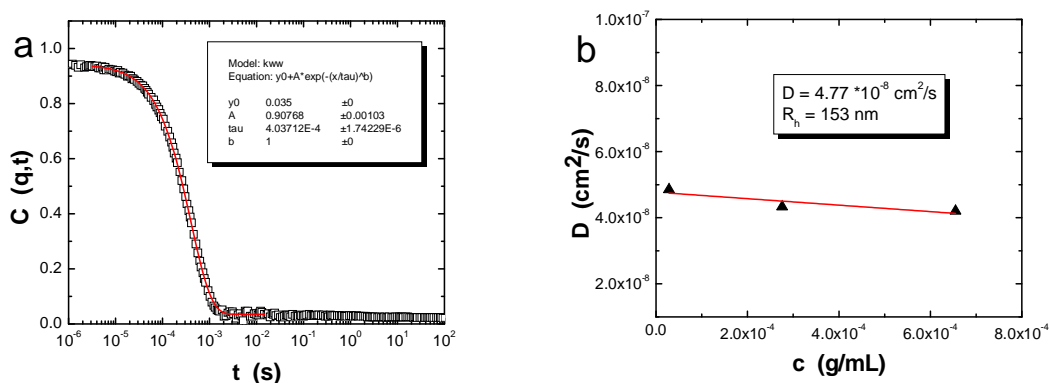


Figure 2.7 Left: Correlation function obtained from an IS4 / hexane solution, $c = 2.85 \cdot 10^{-5}$ g/ml, at a scattering angle $\theta = 90^\circ$. The red solid line is an exponential decay fit with the KWW function. Right: Plot of the diffusion coefficient, D , as a function of polymer concentration, for the IS4 in hexane dilute solutions. The hydrodynamic radius is $R_h = 153$ nm.

A single exponential decay is observed, which corresponds to the translational diffusion of the micelles, with a diffusion time of $\tau = 4.04 \cdot 10^{-4}$ s. A plot of D vs. polymer concentration is shown in the right part of **Figure 2.7**, summarizing the DLS results for the IS4 in hexane solutions. For $\eta = 0.29 \cdot 10^{-3}$ Pa s, and $T = 293$ K, the result is $R_h = 153$ nm. The presence of star-like micelles is further supported by the SLS results shown in **Figure 2.8**:

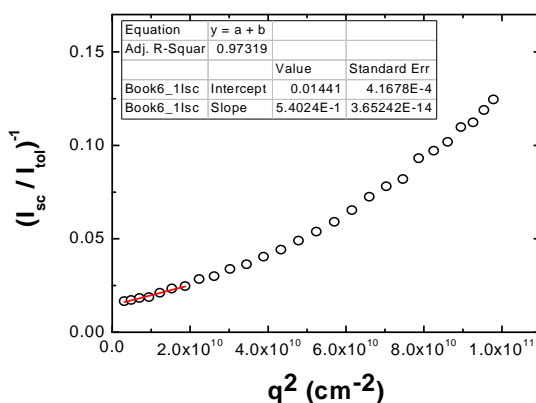


Figure 2.8 Plot of the inverse normalized (with the toluene scattering intensity) scattering intensity $\left(\frac{I_{sc}}{I_{tol}}\right)^{-1}$, as a function of the squared scattering vector q^2 . The red solid line is a linear fit to the data at low scattering angles. The R_g is 106 nm.

From the SLS data, the radius of gyration of the micelles was found to be $R_g = 106$ nm. The ratio $\frac{R_g}{R_h}$ is 0.69, a result in agreement with previously reported values for star-like micelles.

The case of IS4 in ethyl acetate was much more complicated. Ethyl acetate is a good solvent for polystyrene, while being a poor solvent for PI at room temperature. A typical

correlation function of an IS4 / ethyl acetate solution, $c = 8.79 \times 10^{-5}$ g/ ml, at scattering angle $\theta = 90^\circ$ is shown in **Figure 2.9**:

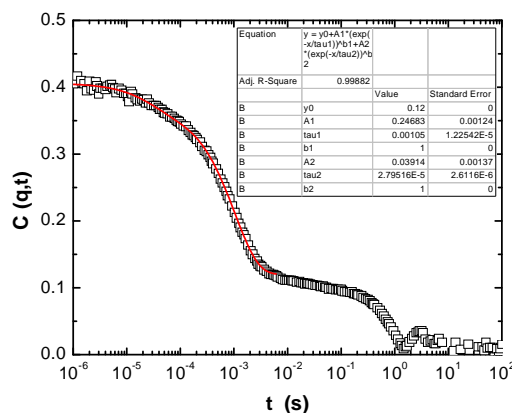


Figure 2.9: Correlation function obtained from an IS4 / ethyl acetate solution, $c = 8.79 \times 10^{-5}$ g/ mL, at scattering angle $\theta = 90^\circ$. The red solid line is an exponential decay fit with a double KWW function, $y = y_0 + A_1 \exp(-t/\tau_1)^{b_1} + A_2 \exp(-t/\tau_2)^{b_2}$

The correlation function is featuring 4 decay processes. The fast process, with a diffusion time of 2.8×10^{-5} is attributed to dissolved chains, while the second process with $\tau = 1.1 \times 10^{-3}$ s probably resembles the diffusive motion of aggregates. Finally, the very slow processes ($\tau \sim 0.05$ s and 0.5 s) correspond to huge aggregates. In fact, micron-sized aggregates are observed with optical microscopy, as will be described later. This is also the reason of increased turbidity at IS4 / ethyl acetate solutions in high polymer concentrations. It has been reported in the bibliography that self assembly of diblock copolymers PS-PI in ethyl acetate is a complicated process⁷. No further detailed characterization of the self-assembled structures in ethyl acetate was done, since this would be beyond the scope of this thesis.

2.2.3 General semidilute solution preparation route

The general solution preparation route used during this study was the following: Initially, the bulk polymer is left in a vacuum oven for about half an hour, in order to get rid of solvent (from the synthesis) or humidity traces. Next, the desired amount of polymer is put in a dust-free vial and the required amount of solvent is added. All solvents were filtered

through PTFE filters (pore diameters 0.2 and 0.45 μm). Since the solutions are directly prepared at the desired concentration, a magnetic stirring bar is always added in order to accelerate the mixing process. The solutions are left for stirring for 7-10 days, until homogeneous samples are acquired. In general, the same procedure was followed for the diblock copolymer solutions too.

2.2.4 Characterization of the semidilute homopolymer solutions

Light scattering experiments were conducted in semidilute solutions of cis-1, 4 PI in THF and decane too. Typical data are shown in **Figure 2.10**, for a THF solution of cis-1, 4 PI ($M_w = 1090 \text{ kg / mol}$), at $c = 1.88 \text{ \% wt}$:

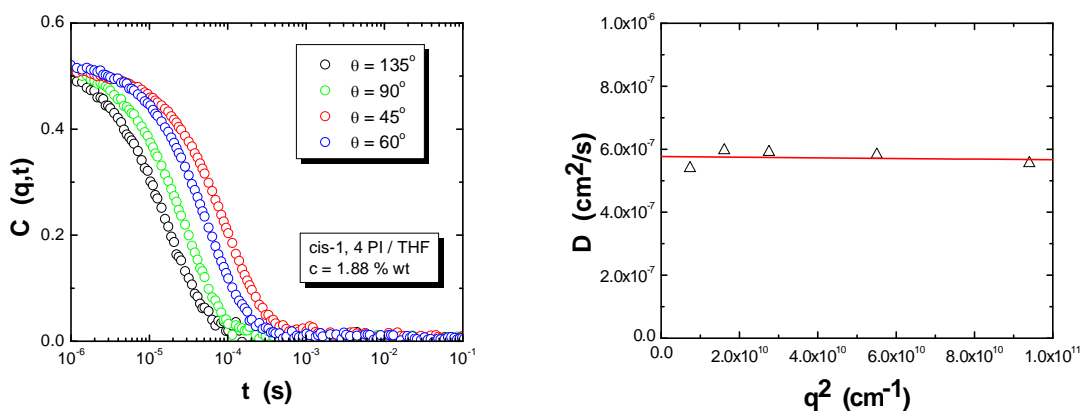


Figure 2.10: Left: Correlation functions at different scattering angles for a cis-1, 4 PI ($M_w = 1090 \text{ kg / mol}$) in THF solution, at $c = 1.88 \text{ \% wt}$. Right: Plot of the diffusion coefficient D as a function of the squared scattering wavevector, q^2 .

As expected for semidilute solutions in athermal solvents, only one fast diffusive mode was observed, attributed to thermally agitated fluctuation of chain segments (blob) confined in a non-interacting tube made of its surrounding chains (**Figure 2.4**). The dynamic correlation length, calculated using **Equation 2.13**, is found to be $\xi_D = 8 \text{ nm}$. The scattered intensity as a function of scattering wavevector is shown in **Figure 2.11**:

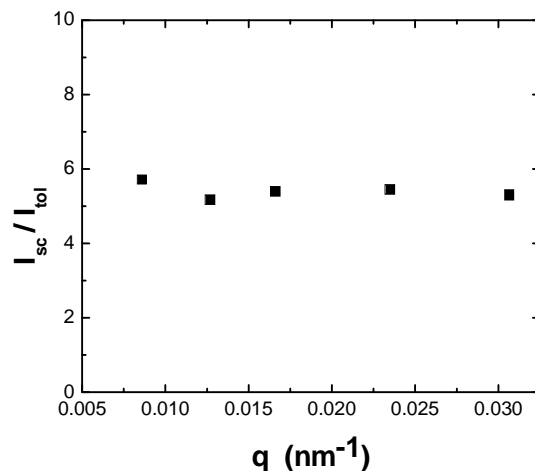


Figure 2.11: Plot of the normalized (with the scattering intensity of toluene) scattering intensity I_{sc} / I_{tol} vs. scattering wavevector q for a cis-1, 4 PI ($M_w = 1090$ kg / mol) in THF solution, at $c = 1.88$ % wt.

It can be seen that the scattered intensity is weak and q -independent, as expected from the small size of the characteristic size (blob) that scatters. This behavior is typically observed in semidilute solutions in good solvents.

2.3 Real time Phase Contrast Microscopy

In order to be able to quantify the writing phenomenon we used a quantitative version of optical microscopy. To do so, the necessary simple experimental setup based on a typical upright optical microscope combined with a LASER source was constructed. Thus, real-time imaging of the light-induced pattern formations is feasible. Under specific illumination conditions, quantitative microscope images can be acquired, as it will be described in detail in **Section 2.3.2**. From the quantitative images, the refractive index contrast of the formed patterns and its evolution with irradiation time can be measured. This enables us to study the pattern formation kinetics as a function of different parameters (such as material properties and irradiation conditions) and therefore quantify the observed phenomenon.

2.3.1 Experimental Setup

The experimental setup for pattern formation and simultaneous imaging of the light-induced structures consists of two basic parts. The one part is a typical upright optical microscope (Zeiss Axioskop 2). The second part is a metallic plate attached to the microscope stage, containing the optical and mechanical elements. As depicted in **Figure 2.12**, a CW LASER source ($\lambda = 671$ nm, $P = 300$ mW) is placed on the plate. The LASER beam is guided through two mirrors (M1 and M2) to a 4x microscope lens (L1, focal length, $f = 35$ mm, $NA = 0.12$), and is focused in the middle of the glass cell which contains the sample.

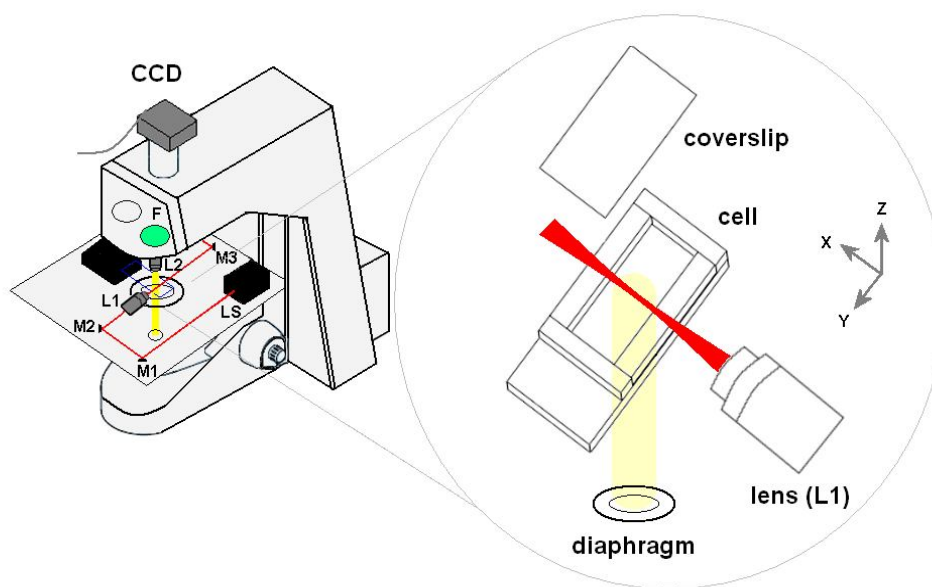


Figure 2.12: A schematic of the experimental setup for creating and simultaneously imaging the light-induced patterns.

The beam diameter at the focal spot is roughly $28 \mu\text{m}$. The sample cell is mounted on an x, y-translation stage, giving the ability to irradiate different sample positions. The lens L1 is also placed in an x-translation stage, which allows finding easily the focal point.

The home-made glass cells, shown in the right part of **Figure 2.12**, were specially

designed for the experiments. They consist of four glass pieces (thickness 2 mm), which are glued with UV-curable adhesive (resistant to the majority of the organic solvents) to a typical glass slide, forming the bottom of the cell. The resulting optical path of the cell is 2mm. Two of the pieces are thoroughly polished to achieve optical quality, avoiding undesired LASER reflections and beam distortions. These pieces are the windows from where the LASER beam passes through. The top part ('cap') of the cell is a typical coverslip (thickness 0.17 mm). This construction has several advantages; on the one hand it allows for relatively simple sample loading (usually samples are very viscous liquids). On the other hand, the optical quality of the cell in two dimensions allows for simultaneous LASER irradiation in the x-direction and transmission microscopy observations in the z-direction. In addition, the total thickness of the glass cell is 2.37 mm, small enough to allow even the use of high magnification objective lenses (short working distances).

Utilizing the above setup, someone can observe the writing phenomenon in all the three ways described in the introduction. The transmitted LASER beam is projected to a screen, after being reflected from the mirror M3. This allows detection of the changes occurring to the shape of the spot during irradiation. Moreover, the scattered LASER light during pattern formation can be detected through the objective lens L2 and the CCD camera that is attached on the microscope. Finally, by means of white light Kohler illumination and by using the bandpass filter F (which blocks the LASER light), real time imaging of the structures can take place. The illumination and imaging conditions will be described in detail in the next Section.

2.3.2 Quantitative Phase Contrast Microscopy

In microscopy, objects under investigation generally contain both phase ϕ and amplitude information, which means that the light passing through the material undergoes both phase retardation and absorption. Transmitted brightfield illumination is one of the most commonly utilized observation modes in optical microscopy, especially for fixed, stained specimens or other types of samples having high natural absorption of visible light (amplitude objects). On the contrary, when a specimen has no absorption, wavefronts which illuminate the specimen either pass through undeviated or are diffracted and retarded in

phase by structures and phase gradients present in the sample. These are called phase objects, and are extremely difficult to be observed under conventional brightfield conditions. Hence, a number of methods to render phase structure visible have been developed, such as the well known Differential Interference Contrast and Zernike Phase Contrast microscopies. However, neither of these methods is quantitatively, at least in a simple manner.

Quite recently, a new, non-interferometric technique for measuring phase has been demonstrated by Barty et al.^{8, 9}. The technique provides a simple and general method for making visible the magnitudes of the phase shifts in microscopic objects by use of existing, readily available microscope hardware in the form of an ordinary transmission microscope, using partially coherent illumination. This imaging methodology produces in general linear images of amplitude and phase.

Let us consider a perfect, aberrational-free microscope and an object which contains both phase and amplitude structure, illuminated by partially coherent light. The complex amplitude of the light field leaving the object may be written

$$E(\mathbf{r}) = \sqrt{I(\mathbf{r})} \exp[i\phi(\mathbf{r})] \quad (\text{Equation 2.14})$$

where $I(\mathbf{r})$ is the intensity distribution, $\phi(\mathbf{r})$ is the phase distribution and $i = \sqrt{-1}$. The propagation of this light along the optical axis z (direction of white light illumination) obeys the equation

$$\frac{\partial I(\vec{r})}{\partial z} = -\frac{\lambda}{2\pi} I(\Delta z = 0) \nabla^2 \phi(\vec{r}) \quad (\text{Equation 2.15})$$

In most conditions relevant to optical microscopy (that is, in the absence of optical phase dislocations), knowledge of $I(\mathbf{r})$ and the spatial derivative $\frac{\partial I(\mathbf{r})}{\partial z}$ on the left-hand side of the equation uniquely specifies the phase distribution. In this case, the phase and intensity distributions may be determined independently. $I(\mathbf{r})$ is directly measured with an in-focus image ($\Delta z = 0$). The derivative information may be obtained by defocusing the microscope

slightly in both positive and negative directions and obtaining the difference between the two images.

Roberts et al.¹⁰ demonstrated the application of the above technique to refractive index profiling of optical fibers, which were immersed in index matching liquid. Optical fibers possess a cylindrical symmetry. The phase $\phi(y, x)$ of the light transmitted through the fiber is given by the Abel Transform

$$\phi(y, x) = \frac{4\pi}{\lambda} \int_y^R n(r, x) r (r^2 - y^2)^{-\frac{1}{2}} dr \quad (\text{Equation 2.16})$$

where R is the radius of the fiber, $n(r, x)$ is the refractive index of the fiber (taken to be axially symmetric), the x direction is taken to be along the axis of the fiber (propagation direction of the LASER beam too), r is the radial distance from the axis of the fiber, and the y direction is perpendicular to the direction of propagation of the light in the microscope (**Figure 2.14** f). Hence, the refractive index can be found by application of the inverse Abel transform to the phase image:

$$n(r, x) = -\frac{\lambda}{2\pi^2} \int_r^R \frac{\partial \phi(y, x)}{\partial y} (R^2 - y^2)^{-\frac{1}{2}} dy \quad (\text{Equation 2.17})$$

The technique is simple and particularly well suited for the type of cylindrically symmetric patterns formed. In the following, the procedure that was followed to acquire the phase contrast images is described. Using a collimated white light beam (diameter ~ 2mm) and a slightly out of focus microscopic detection leads to an image where the intensity can be quantitatively related to the refractive index variation. It has to be mentioned that defocusing the objective above the focal plane (that is, positive Δz) leads to the observation of bright structures, when the refractive index difference between the structure and the background solution is positive. Oppositely, lower refractive index structures appear as dark objects. The defocusing distance Δz used is typically 20 μm above the focal plane (**Figure 2.13**, second image). The objective typically used is a x32 microscope lens. A series of progressively defocused images of a formed fiber can be seen in **Figure 2.13**. The sample used in this case is a cis-1, 4 PB ($M_w = 390 \text{ kg / mol}$), $c = 9.32 \text{ \% wt}$.

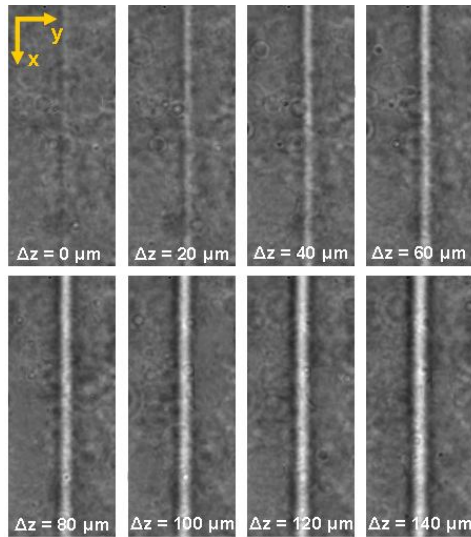


Figure 2.13: Image of the fiber at the focal plane of the microscope objective ($\Delta z = 0 \mu\text{m}$) and at different planes above the focal plane. The in-focus image is almost featureless, while the slightly defocused images have an enhanced contrast.

Due to the relatively small refractive index variation, the in-focus image ($\Delta z = 0$) is almost featureless. In order to analyze the phase contrast images, the normalized intensity profile across the fiber, averaged over a portion of the fiber is calculated. A typical analysis box of rectangular shape with dimensions $60 \mu\text{m} \times 45 \mu\text{m}$ is used. The averaged normalized image intensity

$$I_{nor} = \frac{I(\Delta z)}{I(\Delta z = 0)} \quad (\text{Equation 2.18})$$

is plotted as a function of y , yielding the normalized intensity profiles across the fiber. The profiles at different defocusing distances are shown in **Figure 2. 14**:

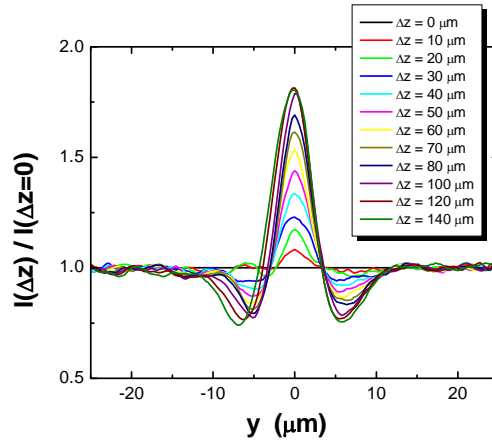


Figure 2.14: Normalized intensity profiles for different defocusing distances.

The evolution of the maximum value of I_{nor} , I_{max} , as a function of Δz , is shown in **Figure 2.15:**

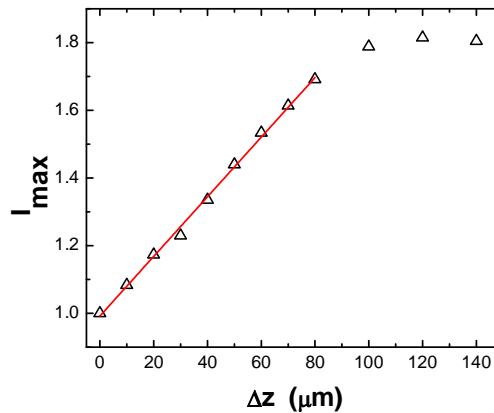


Figure 2.15: Dependence of the maximum value of $I(\Delta z)/I(\Delta z=0)$ on the defocusing distance. For small Δz , the dependence is linear, as shown from the red line (linear fit to the data).

We can see that the measured I_{max} scales linearly with Δz for relatively small values of Δz , and saturates for larger defocusing distances. Therefore, we can assume that

$$\frac{\partial I(\vec{r})}{\partial z} \simeq \frac{\Delta I(\vec{r})}{\Delta z} \quad (\text{Equation 2.19})$$

for the small Δz that we use (typically 20 μm). By combining **Equations 2.15** and **2.19**, we end up with the relation

$$\frac{I_{\max} - 1}{\Delta z} = -\frac{\lambda}{2\pi} \nabla^2 \phi_{\max} \quad (\text{Equation 2.20})$$

Therefore within the approximations, the imaged intensity is directly proportional to the Laplacian of the phase. This in turn can be traced back to the gradient of refractive index, through an Abel transform. It becomes possible to compute the refractive index profile from the image by inverting the relation. Instead of the full rigorous calculation, a simplified approach was followed in this study, where we assume a simple Gaussian functional form for the refractive index profile:

$$n(r, t) = n_0 + \delta n \exp\left(-\frac{r^2}{a^2}\right) \quad (\text{Equation 2.21})$$

The phase ϕ can be calculated using the Abel transform (**Equation 2.16**):

$$\phi(y, x) = \frac{2\pi}{\lambda} a \sqrt{\pi} \delta n e^{-\frac{y^2}{a^2}} \quad (\text{Equation 2.22})$$

The gradient of phase $\nabla \phi$ is:

$$\nabla \phi(y, x) = \frac{-4\pi \sqrt{\pi} \delta n}{a\lambda} y e^{-\frac{y^2}{a^2}} \quad (\text{Equation 2.23})$$

and the Laplacian of phase $\nabla^2 \phi$ is:

$$\nabla^2 \phi(y, x) = \frac{-4\pi\sqrt{\pi}\delta n}{a\lambda} \left(1 - \frac{2y^2}{a^2}\right) e^{-\frac{y^2}{a^2}} \quad (\text{Equation 2.24})$$

The calculated intensity $I(\vec{r})$ describes accurately enough the imaged intensity, as can be seen in **Figure 2.16**, where the intensity profile $I(\Delta z, y)/I(\Delta z = 0, y)$ for a given Gaussian refractive index difference profile $\delta n(r)$ is calculated:

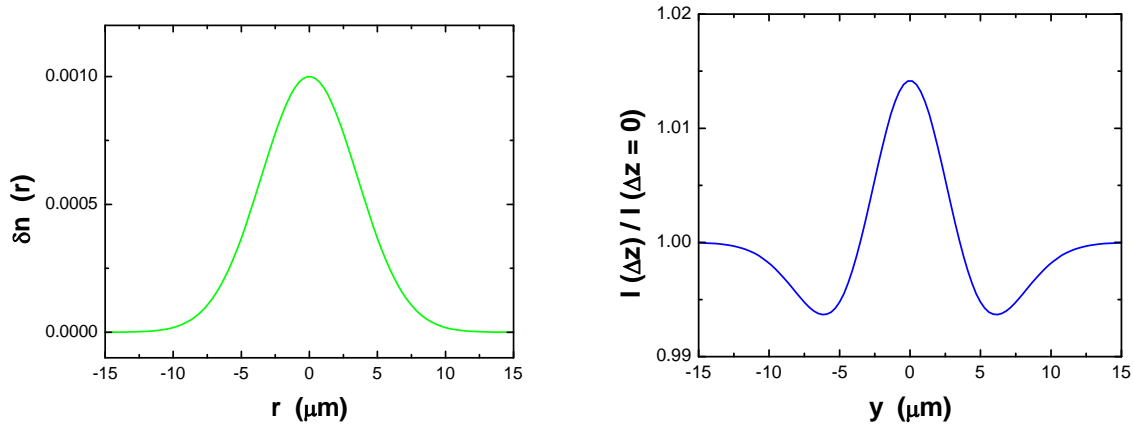


Figure 2.16: Left: A Gaussian refractive index difference profile, $\delta n(r)$ with $a = 5 \mu\text{m}$. Right: The calculated intensity profile $I(\Delta z, y)/I(\Delta z = 0, y)$.

By combining **Equation 2.20** and **Equation 2.24**, the relation between I_{max} and the maximum refractive index change δn_{max} can be obtained:

$$\delta n_{\text{max}} = \left(\frac{I_{\text{max}} - 1}{2\sqrt{\pi}} \right) \left(\frac{a}{\Delta z} \right) \quad (\text{Equation 2.25})$$

Assuming that modifications in the index of refraction (δn) arise solely from concentration changes δc , the latter can be calculated from the relation:

$$\delta c = \left(\frac{dn}{dc} \right)^{-1} \delta n \quad (\text{Equation 2.26})$$

Therefore, by following the time evolution of δn , the kinetics of the writing phenomenon can be studied, as will be presented in **Chapter 3**.

The sensitivity and range of the technique as implemented here is limited by the relatively low dynamic range of the used CCD camera (8 bit). The smallest measurable value of I_{\max} is ~ 1.01 , corresponding to a change of $\sim 7 \cdot 10^{-4}$ (for $a = 5 \mu\text{m}$) in refractive index. As the illumination was kept constant during a measurement with a background intensity of the order of half of the full scale, an value of $I_{\max} \sim 2$ was the maximum to be detected, corresponding to an increase of refractive index of the order of $7 \cdot 10^{-2}$ (for $a = 5 \mu\text{m}$).

A comparison of our measurements with a full quantitative approach developed by D. Papazoglou and co-workers¹¹ was done in order to check the validity of our simplified approach. For a fiber formed in a cis-1, PB / tetradecane solution ($M_w = 390 \text{ kg / mol}$, $c = 17.3 \text{ \% wt}$) after 5 min of irradiation ($P = 150 \text{ mW}$), the quantitative holographic microscopy returned the refractive index profile $\delta n(r)$ shown in **Figure 2.17**:

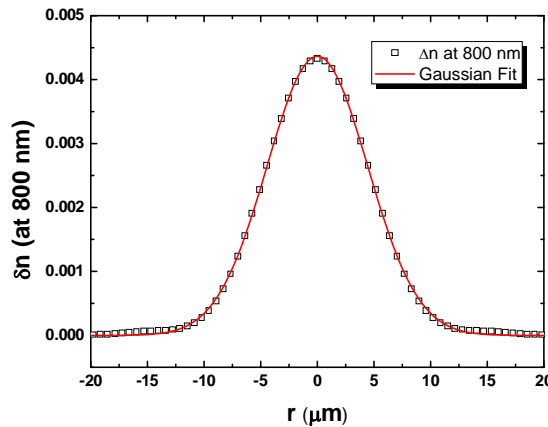


Figure 2.17: Refractive index profile of fiber formed in a cis-1, PB / tetradecane solution ($M_w = 390 \text{ kg / mol}$, $c = 17.3 \text{ \% wt}$) after 5 min of irradiation ($P = 150 \text{ mW}$), measured by quantitative holographic microscopy¹¹. The maximum refractive index change is $\delta n_{\max} = 4.37 \cdot 10^{-3}$, while the fiber diameter is $d = 10 \mu\text{m}$.

The refractive index profile is well fitted by a Gaussian profile (red line), with the maximum refractive index change equal to $\delta n_{\max} = 4.37 \times 10^{-3}$, and a fiber diameter (FWHM) of $d = 10 \mu\text{m}$.

In our simplified approach, $I_{\max} = 1.856$ was measured at $\Delta z = 20 \mu\text{m}$. The dimension of the fiber was $a = 3.1 \mu\text{m}$. From **Equation 2.25** we calculate $\delta n_{\max} = 3.74 \times 10^{-2}$.

The quantitative holographic microscopy confirmed the Gaussian refractive index profile and the small δn_{\max} assumptions, but led to different contrast values. The origin of the discrepancy between the values obtained by our phase contrast method and the holographic microscopy is not yet identified, and it is still investigated. It could be possibly ascribed to different magnifications used by the two methods. However, our method can be calibrated using the results of holographic microscopy.

2.4 Raman Scattering

The technique of Raman Scattering was employed during this study to characterize the LASER-induced structures. The basic principles of Raman Scattering are briefly described in the following.

When incident light encounters a molecule, the electric field of light induces a dipole moment μ in the molecule due to its polarizability, a , according to **Equation 2.5**. Due to the oscillation of the electric field, which can be described as

$$E = E_0 \cos(2\pi\nu_0 t) \quad (\text{Equation 2.27})$$

where E_0 is the amplitude of the oscillation, ν_0 is the frequency of the incident light, and t is the time, the induced dipole moment of the molecule also oscillates. An oscillating dipole moment can absorb or emit energy by transitions between different oscillation energy levels. Through the energy transfer from photons of the incident light to molecules, the latter can be excited to their higher energy levels. Subsequently, the excited molecules go back to their lower energy levels by the emission of scattered light. This energy transition is usually

energetically elastic (Rayleigh scattering). However, when the energy of the incident light is similar to the energy difference between different rotational or vibrational energy levels of molecules, the scattering process may involve energy transition of the excited molecules to a different energy level from their initial energy level. The scattering associated with this inelastic energy transition is called Raman scattering. The energy transitions during Rayleigh scattering, Stokes Raman scattering and anti-Stokes Raman scattering are depicted in **Figure 2.18**¹²:

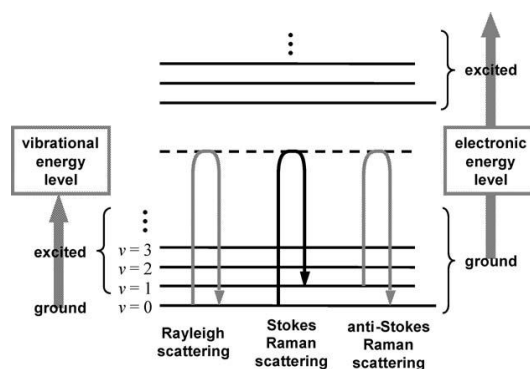


Figure 2.18: A schematic diagram for energy transitions during Rayleigh scattering, Stokes Raman scattering and anti-Stokes Raman scattering

If a molecule is vibrating with a certain frequency, the displacement of the k -th atom in the molecule from its equilibrium position can be written by

$$q_k = q_k^0 \cos(2\pi\nu_m t) \quad (\text{Equation 2.28})$$

where q_k^0 is the amplitude of the displacement, and ν_m is the frequency of the vibration. The polarizability a of the molecule can be expanded in the form of Taylor series

$$a = a_0 + \sum_k \left(\frac{\partial a}{\partial q_k} \right)_{q_i=0} q_k + \frac{1}{2} \sum_{i,j} \left(\frac{\partial^2 a}{\partial q_i \partial q_j} \right)_{q_i=q_j=0} q_i q_j + \dots \quad (\text{Equation 2.29})$$

The displacement q_k concerning the molecular vibration is considered to be very small, and the high order terms (from the 3rd term in the right-hand side of the equation and above) can be neglected. The combination of the above equations gives

$$\mu = a_0 E_0 \cos(2\pi\nu_0 t) + \sum_k \left(\frac{\partial a}{\partial q_k} \right)_{q_k=0} q_k E_0 \left\{ \cos[2\pi(\nu_0 - \nu_m)t] + \cos[2\pi(\nu_0 + \nu_m)t] \right\}$$

(Equation 2.30)

In **Equation 2.30**, the first term is related to the Rayleigh scattering, while in the second term, the part containing $(\nu_0 - \nu_m)$ is related to the Raman scattering for which the vibrational energy of the molecule moves to a higher energy level than its initial energy level (Stokes Raman scattering). In contrast, the scattering with the vibrational energy transition of the molecule from its initial energy level to a lower energy level (anti-Stokes Raman scattering) is related to the part with $(\nu_0 + \nu_m)$. It can be easily realized that the condition for a vibrational mode to be Raman active is shown by

$$\left(\frac{\partial a}{\partial q_k} \right)_{q_k=0} \neq 0 \quad \textbf{(Equation 2.31)}$$

which indicates that the molecular polarizability of the vibrational mode should be neither maximum nor minimum when the atoms are at their equilibrium positions ($q_k = 0$)¹³.

The experimental setup used during this study (Nicolet Almega XR Raman spectrometer) is based a confocal microscope. A LASER beam ($\lambda = 780$ nm, P = 15 mW) is focused on a micron-sized spot in the sample through a microscope objective of high numerical aperture. Light scattered from this spot in backward direction is collected and collimated by the same objective lens. The Rayleigh line is blocked by an appropriate notch filter. The different frequency components of the inelastically scattered light are dispersed in a monochromator, whose entrance slit is replaced with a pinhole. A CCD detector is placed in its exit focal plane so the whole Raman spectrum is recorded¹⁴. Due to the confocal scheme, only light from the focus can penetrate through the pinhole; light from other depths

in the sample is efficiently blocked. As a consequence, out-of-focus regions do not blur the signal, but are dark. A schematic of a typical micro-Raman setup is shown in **Figure 2.19**:

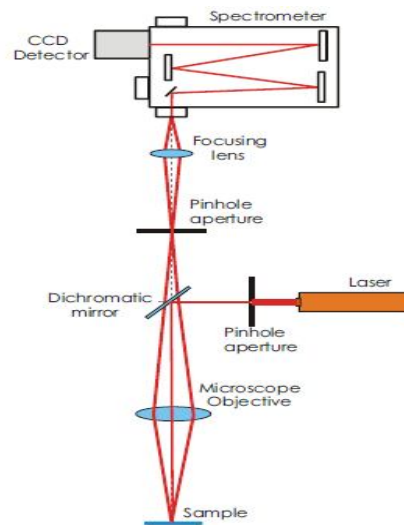


Figure 2.19: A schematic of a typical experimental micro-Raman setup

References

1. Hadjichristidis, N., Iatrou, H., Pispas, S., Pitsikalis, M. *J. Polym. Sci. Part A: Polym. Chem.* **2000**, 38, 3211-3234.
2. Watanabe, H. *Prog. Polym. Sci.* **1999**, 24, 1253–1403.
3. Rubinstein, M., and Colby, R. H., *Polymer Physics*. Oxford University Press: New York, 2003.
4. de Gennes, P. G., '*Scaling Concepts in Polymer Physics*'. Cornell University Press: London, 1979.
5. Brandrup, J., and Immergut, E. H., '*Polymer Handbook*'. John Wiley and Sons: New York, 1989.
6. A. Barty, K. A. N., D. Paganin, and A. Roberts. *Opt. Lett.* **1998**, 23.
7. Mountrichas, G., Mpiri, M., and Pispas, S. *Macromolecules* **2005**, 38, 940-947.
8. Barty, A., Nugent, K. A., Paganin, D., and Roberts, A. *Opt. Lett.* **1998**, 23, 817-819.
9. Barone-Nugent, E. D., Barty, A., and Nugent, K. A. *J. Microsc.* **2002**, 206, 194–203.
10. Roberts, A., Ampem-Lassen, E., Barty, A., Nugent, K. A., Baxter, G. W., Dragomir, N. M., Huntington, S. T. *Opt. Lett.* **2002**, 27, 2061-2063.
11. Papazoglou, D. G., and Tzortzakis, S. *Appl. Phys. Lett.* **2008**, 93, 041120.
12. Tanaka, M., Young, R. J. *J. Mater. Sci.* **2006**, 41, 963-991.
13. Ferraro, J. R., Nakamoto, K., and Brown, C. W., *Introductory Raman Spectroscopy*. Elsevier Science: USA, 2003.
14. Smith, E., Dent, G., *Modern Raman Spectroscopy-A Practical Approach*. John Wiley and Sons: Chichester, 2005.

CHAPTER 3

LASER-INDUCED FIBER FORMATION

LASER-induced fiber formation and its relation with Optical Spatial Solitons and associated phenomena are discussed in this Chapter. Quantification of the early stage kinetics of the formation process and characterization of the induced structures is also investigated.

3.1 Introduction

To gain insight into the phenomenon of LASER-writing in polydiene solutions, a number of experiments were carried out, which will be presented in this Section.

In order to explore the kinetics of the light-induced pattern formations, real time phase contrast imaging at the LASER beam focus was employed. As mentioned in **Chapter 2**, this experimental technique offers the capability of studying the refractive index evolution of the formed pattern as a function of irradiation time. Thus, the kinetics of the formation at the focal point of the writing beam and its dependence on several parameters can be investigated. Material parameters include the polymer concentration, the molecular weight, the microstructure, and the optical contrast between the solute and the solvent. Moreover, the effect of irradiating conditions, such as the LASER power and the beam size was studied.

Optical phenomena reminiscent of Optical Spatial Solitons and Modulation Instabilities were observed in the used polydiene solutions. These systems are found to exhibit similar non linear optical behavior to other soft matter systems, such as colloidal dispersions and liquid crystals.

The last Section of this Chapter deals with the characterization of the written microstructures. Video microscopy was utilized to explore the behavior of the fibers after LASER switching-off. The writing phenomenon was found to be reversible for short sample exposures to the LASER beam, while for prolonged illuminations the effect of irradiation is irreversible. Polarized Raman Scattering was utilized to study the effect of the applied optical field to the microstructures of the used polydienes.

3.2 Pattern formation kinetics

In order to quantify the local variation of refractive index induced by the laser illumination, we use quantitative phase contrast microscopy (**Section 2.3**). In the following, we describe the procedure followed to obtain the refractive index contrast of the formed pattern.

Using a collimated white light beam and a slightly out of focus microscopic detection leads to an image where the intensity can be quantitatively related to the refractive index variation (**Section 2.3**). In all experiments during this study, the area at the focus of the writing LASER beam was imaged. **Figure 3.1** a shows the scattering image (at a scattering angle $\theta = 90^\circ$) of the focused beam (using a spherical lens of $f = 35$ mm, resulting in a beam diameter of about $28 \mu\text{m}$) when the irradiation starts ($t=0$ s). **Figure 3.1** b shows the scattering image obtained after irradiating the sample for $t = 180$ s.

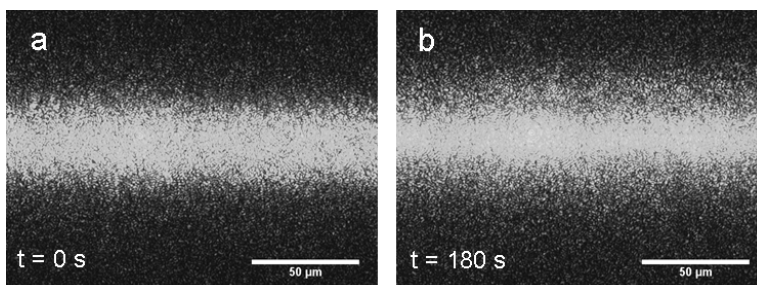


Figure 3.1: a) Scattering image of the LASER beam in a cis-1, 4 PB in tetradecane solution ($M_w = 390$ kg / mol, $c = 14.7$ % wt). The beam ($P = 238$ mW) is focused through a spherical lens ($f = 35$ mm). b) Scattering image showing the self-focusing of the beam.

It can be clearly seen that due to self-focusing, the LASER beam appears to have a smaller diameter of about $19 \mu\text{m}$. The sample in this case is a cis-1, 4 PB / tetradecane solution ($M_w = 390$ kg / mol, $c = 14.7$ % wt) and the power used is $P = 238$ mW. Similar behavior was observed for all the solutions studied in this Chapter. The corresponding phase contrast images of the solution are presented in **Figure 3.2**:

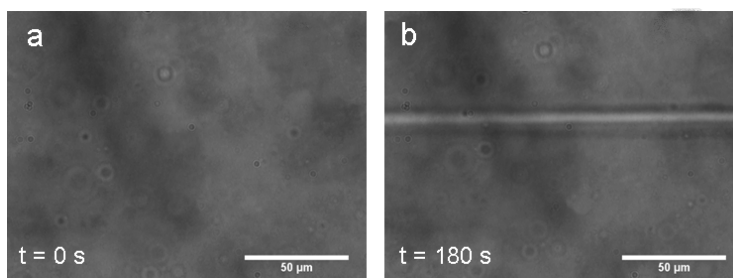


Figure 3.2: a cis-1, 4 PB in tetradecane solution ($M_w = 390$ kg / mol, $c = 14.7$ % wt). The LASER beam ($P = 238$ mW) is focused through a spherical lens ($f = 35$ mm).

In **Figure 3.2 a**, when the LASER irradiation starts, a featureless image can be observed. On the contrary, after 3 minutes of irradiation, a $10\ \mu\text{m}$ wide fibrillar structure is formed (**Figure 3.2 b**). As described in **Chapter 2**, the imaged intensity directly relates to the Laplacian of the phase and the refractive index profile can be deduced. In particular, a higher refractive index (compared to the background solution index, n_{sol}) microstructure (n_{str}) appears as a bright stripe.

As the imaged local refractive index increase is attributed to a local variation in the polymer concentration, the positive δn corresponds to a local increase in polymer concentration ($\delta c > 0$) in solutions where $dn/dc > 0$.

In an effort to quantify the positive writing process, a detailed study of the kinetics of the pattern formation at the focus of the LASER beam will be presented above. The influence of various parameters including illumination power and sample parameters are examined.

3.2.1 Quantitative Phase Contrast Microscopy

Real Time Phase Contrast Microscopy was utilized (as described in **Section 2.3**) in order to study the kinetics of the microstructure formations. The imaged area is always at the focus of the LASER beam (typically placed in the middle of the sample cell). As time evolves, the contrast of the imaged pattern is observed to increase. **Figure 3.3** shows a typical example of an observed phase contrast sequence when the transparent solutions are irradiated by LASER light (as depicted in **Figure 2.13**). The corresponding sample is a solution of cis-1, 4 PB in tetradecane at $c = 14.7$ % wt. Starting from a transparent solution with no visible pattern, a region of higher intensity (larger phase gradient) appears in the image along the position of the propagating beam.

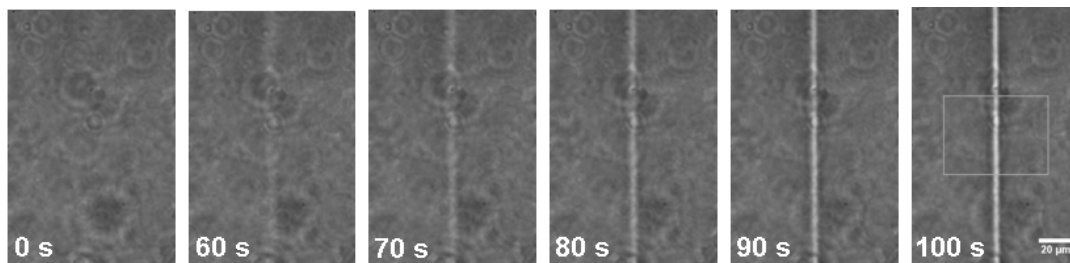


Figure 3.3: Time series images of the fiber formation in cis-1,4 PB in tetradecane solution, at $c = 14.7\%$ wt. The LASER power is $P = 238$ mW.

In order to analyze the phase contrast images, the normalized intensity profile across the fiber, averaged over a portion of the fiber was calculated. A typical analysis box of rectangular shape with dimensions $60\ \mu\text{m} \times 45\ \mu\text{m}$ was used, as shown in the last image of **Figure 3.3**. The averaged normalized image intensity of the imaged region, $I(t)/I(t=0)$, where $I(t=0)$ is the image intensity before irradiation, is plotted as a function of y (shown in **Figure 3.4**), yielding the normalized intensity profiles across the fiber. The evolution of the profiles at different irradiation times is shown in **Figure 3.4**:

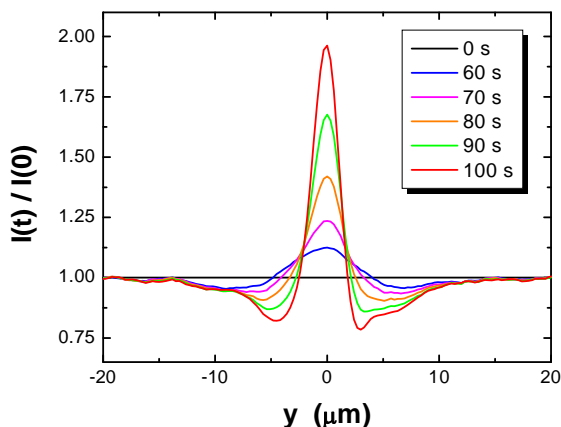


Figure 3.4: Time evolution of the normalized intensity profiles of the images in **Figure 3.3**.

As can be observed, the contrast of the imaged fiber grows rapidly with irradiation time. Very similar kinetics evolutions were observed in nearly all cases of reported samples and LASER irradiation conditions: formation of a fiber with almost constant (in time) size, but

increasing refractive index. The maximum value of the intensity profiles shown above, corresponds to the maximum refractive index difference between the background solution and the written structure. Therefore, a simple way to follow the kinetics of the structure formation, is to see how the maximum value of $I(t)/I(0)$ changes with time. The corresponding plot is shown in **Figure 3.5**:

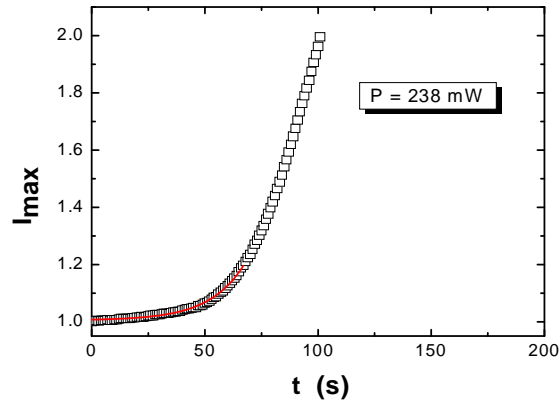


Figure 3.5: Time evolution of the maximum value of the normalized intensity, $I(t)/I(0)$. The early stage of the fiber formation is well described by a simple exponential growth fit, $I_{\max} = A \exp(\Gamma t)$ (red line).

The early stage of the fiber formation can be described well with a simple exponential growth fit of the form

$$I_{\max} = A \exp(\Gamma t) \quad (\text{Equation 3.3})$$

where A is the amplitude and Γ is the fiber formation rate. The later stages of the writing process do not follow the simple exponential growth, as deviations are observed. The early stage rate Γ is used to study the kinetics as a function of the LASER power and the material properties. The latter include the polymer concentration, the molecular weight, the macromolecular microstructure and the refractive index difference between the polymer and the solvent. The detailed investigation of these dependencies will be described in the following Sections.

3.2.2 LASER power dependence

The influence of the LASER power on the writing process was the first parameter to be examined. By using a stepped density neutral filter, the incident power on the sample cell was varied at will. The plot of I_{\max} as a function of irradiation time for a solution of cis-1, 4 PB in tetradecane, at $c = 14.7\%$ wt, for different P is shown in the left part of **Figure 3.7**:

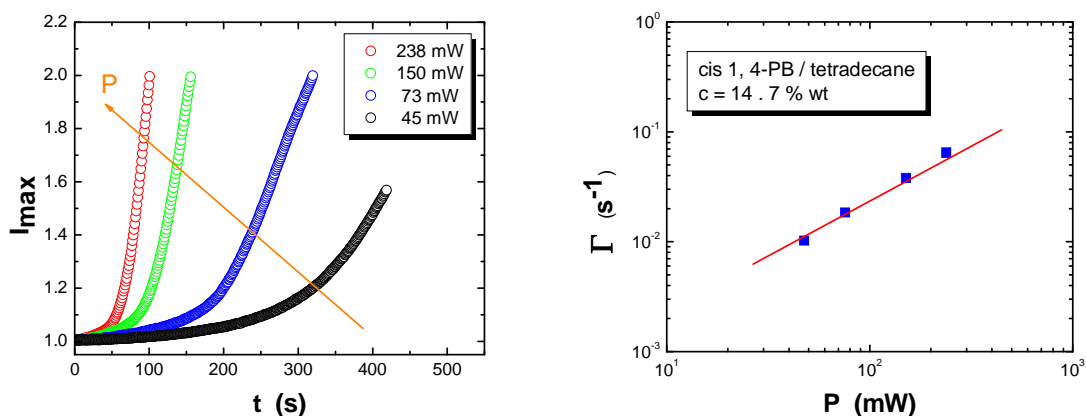


Figure 3.7: Left: Kinetics curves showing the maximum normalized image intensity I_{\max} as function of irradiation time, for different LASER powers P . The solution is cis-1, 4 PB in tetradecane, at $c = 14.7\%$ wt. Right: Power dependence of the growth rate for the cis-1, 4 PB in tetradecane solution, at $c = 14.7\%$ wt. The red line is a linear fit to the data. The slope is 1, indicating linear dependence of the rate on LASER power.

It can be clearly seen that the writing process becomes faster as the LASER power increases. In the right part of **Fig. 3.7**, the growth rates obtained from the kinetics curves as a function of P are shown. Increasing P , causes a linear increase of the early growth rate, as can be seen by the linear fit which is indicated with the red solid line (slope = 1). A summary of the results for the different solutions used is shown in **Figure 3.8**:

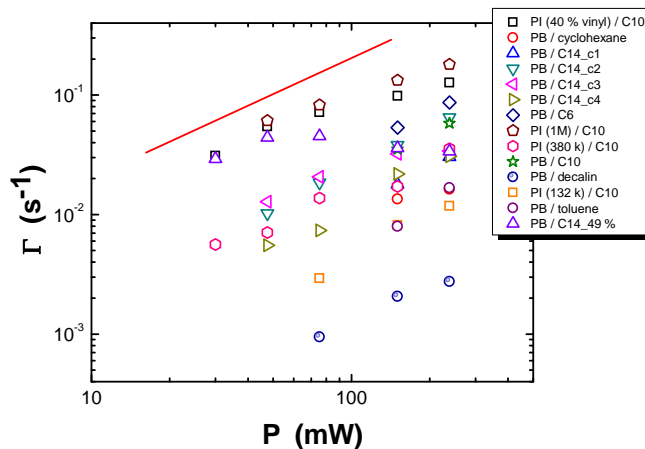


Figure 3.8: Power dependence of the growth rate for different polydiene / solvent systems examined in this thesis. The red line has a slope of 1, indicating that the majority of the solutions exhibit an almost linear dependence on LASER power.

As can be seen, a behavior very close to linear was confirmed in the majority of the examined polydiene solutions.

3.2.3 Polymer concentration dependence

The effect of the polymer concentration on the fiber formation rate was studied in a series of cis-1, 4 PB in tetradecane solutions, in a range from 9.33 – 48.6 % wt. The solutions in the range from 9.33 % wt to 19.85 % wt showed similar behavior. The linear dependence of the growth rate on the incident power was confirmed in almost all cases, and the kinetics curves exhibit similar features. On the contrary, the situation for the highly concentrated PB solution ($c = 48.6$ % wt), was different. It is important to note that this sample, in contrast to the viscous solutions (in the c range from 9.33 – 19.85 % wt), it doesn't flow. Macroscopically, it looks like a PB melt of relatively low molecular weight. In order to measure this sample, a piece was cut with a razor blade and was put in the sample cell. A waiting time of a few hours until the sample flows covering the whole cell volume had to be used. The kinetics curves show different features, as can be seen in **Figure 3.9**:

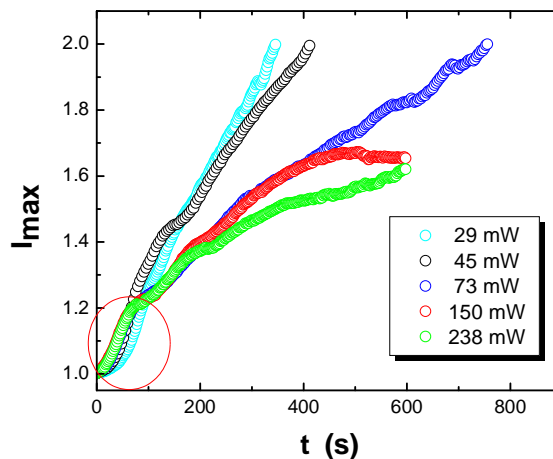


Figure 3.9: Kinetics curves of I_{\max} vs. irradiation time for the highly concentrated cis-1, 4 PB / tetradecane solution ($c = 48.6\%$ wt) for different LASER powers. The early stage fiber formation kinetics is indicated by the red circle.

It can be clearly seen that the form of the kinetics curves are quite different compared to the more dilute solutions. However, the early stage of the I_{\max} increase (indicated by the red circle) can still be described by a simple exponential growth. The obtained growth rates as a function of P is shown in **Figure 3.10**:

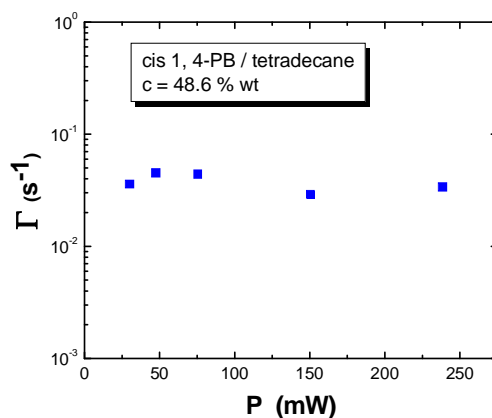


Figure 3.10: Dependence of the growth rate Γ on LASER power P . In contrast to the other solutions, Γ in this case appears to be independent on P .

A crucial difference with the more dilute solutions is that Γ does not depend on P . This means that the fibers are starting to form equally fast at any given P .

The concentration effect on growth rate is summarized for the whole series of the cis-1, 4 PB / tetradecane solutions in **Figure 3.11**. In the graph on the left, the kinetics curves I_{\max} vs. t obtained at different concentrations and using the same power ($P = 238$ mW) are shown. On the right, the growth rate Γ is plotted as function of the polymer concentration, for different LASER P.

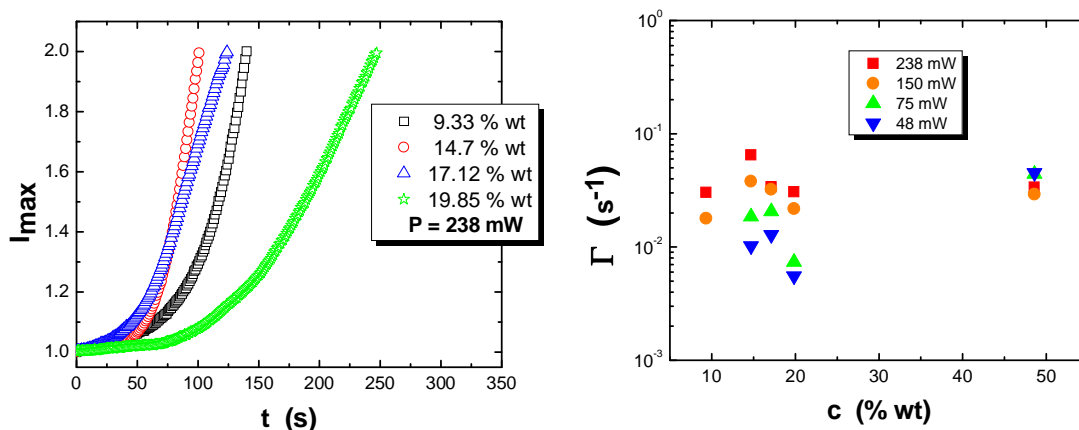


Figure 3.11: Concentration dependence of the kinetics for the series of cis-1, 4 PB / tetradecane solutions, at the range of 9.33 – 48.6 % wt. Left: Kinetics curves I_{\max} vs. irradiation time for the different concentrations measured for the same LASER power ($P = 238$ mW). Right: Dependence of the growth rate on polymer concentration, for all the powers used.

First of all, it can be seen that the rate values for all solutions are scattered within about one decade. No obvious concentration dependence is found. Moreover, it can be noticed that the LASER power is a crucial parameter defining the fiber growth rate for the solutions in the concentration range of about 9 – 20 % wt. Oppositely, this is not the case for the highly concentrated PB solution, since in this case the growth rate is almost constant at all powers used.

3.2.4 Influence of solvent refractive index

The effect of the refractive index difference between the polymer and the solvent used in each case, Δn

$$\Delta n = n_{pol} - n_0 \quad (\text{Equation 3.4})$$

on the fiber formation kinetics was studied in detail. For this purpose, a series of cis-1, 4 PB solutions in various organic solvents was prepared, as shown in **Table 3.1**:

Solution	c (% wt)	Δn
cis-1,4 PB / hexane	15.04	0.145
cis-1,4 PB / decane	14.54	0.109
cis-1,4 PB / tetradecane	14.7	0.091
cis-1,4 PB / cyclohexane	14.39	0.094
cis-1,4 PB / toluene	14.7	0.024
cis-1,4 PB / cis-decalin	14.57	0.039

Table 3.1: Solutions of cis-1, 4 PB ($M_w = 390$ kg / mol) in various solvents that were used to study the refractive index difference dependence Δn of the growth rate. The polymer concentrations and the Δn values are shown.

The refractive index difference between the solute and the solvent plays a crucial role in the well-known case of optical trapping of colloidal particles in suspensions. As will be described in more detail in Chapter 4, when $\Delta n > 0$, the colloidal particles are attracted to the center of the LASER beam due to the optical gradient force and they are pushed towards the beam propagation axis due to the optical scattering force. Both of these forces that are exerted on the colloidal particles depend on the Δn value. As Δn increases, the optical forces are stronger. Therefore, it is important to see if Δn plays a role in the writing procedure that we are examining.

Figure 3.12 summarizes the results obtained for all the solutions of **Table 3.1**. In the left part, I_{max} as a function of irradiation time for the same LASER power ($P=238$ mW) for solutions in the different solvents is shown. On the right, growth rate as a function of optical contrast (Δn) is shown for different LASER powers:

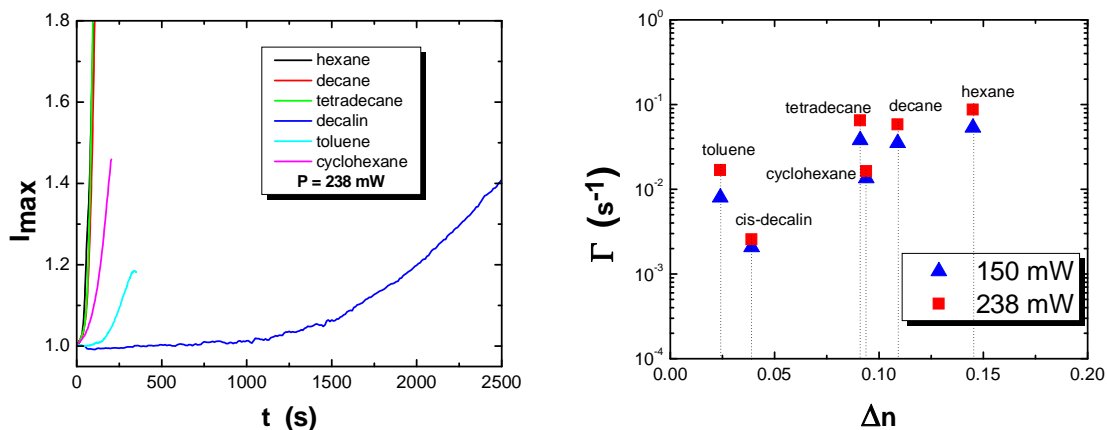


Figure 3.12: Left: I_{\max} as a function of irradiation time for the same LASER power ($P=238$ mW) for solutions in the different solvents Right: Growth rate of the fiber formation vs. refractive index difference between polymer and solvent for a series of cis-1, 4 PB solutions at very similar concentrations. Data for the two highest LASER powers used are shown.

As can be seen, there is clearly a Δn dependence on the fiber formation growth rate. When linear alkanes are used as solvents, the fastest fiber formations are observed. Among linear alkanes, hexane appears to be the solvent with the fastest growth rate, while the difference between decane and tetradecane is not very clear. Use of cyclic hydrocarbon solvents leads to slower growth rates. The slowest formations are observed in cis-decalin solutions. No significant difference on the time scales for toluene and cyclohexane is observed.

It is clear from the experimental data that the refractive index difference Δn affects the growth rate Γ of the early stage of the fiber formation. However, Γ shows a weaker dependence on Δn than the one expected for optical gradient forces. In the latter, the characteristic time should scale linearly with the optical contrast. In our case, the dependence is clearly much weaker than linear.

3.2.5 Microstructure and molecular weight dependence

The effect of the microstructure of the macromolecules on the writing process was studied. As mentioned in **Chapter 1 (Figure 1. 8)**, polymerization of isoprene can result in polymers with four different microstructures (cis, trans, 1, 2 and 3, 4), while for butadiene

polymerization, three macromolecular microstructures can be obtained (cis, trans, and 1, 2). It was already reported by Sigel et al.¹ that 1, 2-PB ($M_w = 204 \text{ kg / mol}$) does not show the writing phenomenon (up to $c = 0.15 \text{ g / ml}$). This was verified also in our experiments. The sample tested was 1, 2-PB ($M_w = 20 \text{ kg / mol}$) in hexane, at $c = 57.73 \text{ \% wt}$. After 1 hour of irradiation ($P = 300 \text{ mW}$, no LASER-induced refractive index changes were detected. In order to gain more insight into the microstructure effect, a solution of PI with a higher percentage (40 x %) of 1, 2 and 3, 4 units than the rest rich cis PI's was studied. Typically, the high cis PI's contain 92 % 1, 4 (mostly cis) and 8 % 1, 2 and 3, 4 units. The molecular weights were $M_w = 936 \text{ kg / mol}$ and 1090 kg / mol for the low and high cis PI, respectively.

The kinetics curves for the two polymers mentioned above are shown in **Figure 3.13**. The data for the high 1, 4 PI decane solutions ($c=5.51 \text{ \% wt}$) are shown with circles, while the corresponding data for the high vinyl content PI decane solution ($c=5.56 \text{ \% wt}$) are shown with solid lines:

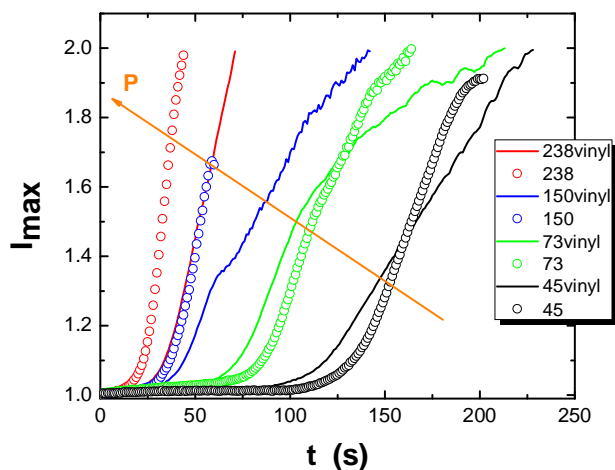


Figure 3.13: Kinetics curves for decane solutions of high (~98 %, circles) and lower (~60 %, solid lines) 1, 4 content PI's.

It can be clearly observed that the time evolution of I_{\max} is faster for the high 1, 4 PI solution, for the two highest P used. Given that 1, 2-PB does not show the writing phenomenon, we can assume that the vinyl segments (1, 2 and 3, 4) do not contribute to the writing process. Thus, the effect is more pronounced in the PI macromolecules with the highest percentage of C=C along their backbone. The situation is quite different for the two

lower LASER powers. It seems that for these P, the early stage of the writing process for the high 1, 4 PI solution is slower than the one for the solution of the lower 1,4 content PI.

In order to check the response of trans-1, 4 units, a 99% trans-1, 4 PI solution in a mixture of toluene and hexane was examined. The molecular weight of the commercial trans-1, 4 PI was $M_w = 410 \text{ kg / mol}$ and the polymer concentration of the sample was $c = 14.61 \text{ \% wt}$. Since trans-1, 4 PI is highly crystalline, the solution was prepared at $T = 58 \text{ }^\circ\text{C}$. Fiber formation was clearly confirmed. No kinetics measurements were carried out since the solution is not thermodynamically stable for long time at room temperature (it undergoes recrystallization).

The effect of polymer molecular weight on the fiber formation kinetics was also investigated through kinetics measurements. Based on previous studies, solutions of high viscosity are required for mechanically stable written microstructures. From our recent observations, irradiation of solutions of lower viscosities leads to formation of fibers, however very unstable. In order to achieve high solution viscosities and stable formations, solutions were prepared at a concentration $c \sim 3c^*$, sufficient to ensure well entangled viscoelastic solutions (**Table 3.2**). Since polymer concentration was found not to affect the formation kinetics, this criterion was followed.

M_w (kg/mol)	microstructure	c^* (% wt) in decane	c (% wt) in decane
64.7	92 % 1, 4 (mostly cis) 8 % 1, 2 and 3, 4	13.01	58.9
132	92 % 1, 4 (mostly cis) 8 % 1, 2 and 3, 4	7.17	43.33
378	92 % 1, 4 (mostly cis) 8 % 1, 2 and 3, 4	4.03	39.1
1090	92 % 1, 4 (mostly cis) 8 % 1, 2 and 3, 4	0.39	5.56
936	60 % 1, 4 (mostly cis) 40 % 1, 2 and 3, 4	1.86	5.51

Table 3.2: Solutions of the different PI's in decane that were used to study the effect of microstructure and molecular weight on the fiber formation kinetics.

Figure 3.14 summarizes the results for four of the polymer solutions of **Table 3.2**. On the left, I_{\max} vs. irradiation time for the three high cis-1, 4 PI / decane solutions is shown. Pattern growth rate as a function of polymer molecular weight for different LASER powers is shown on the right:

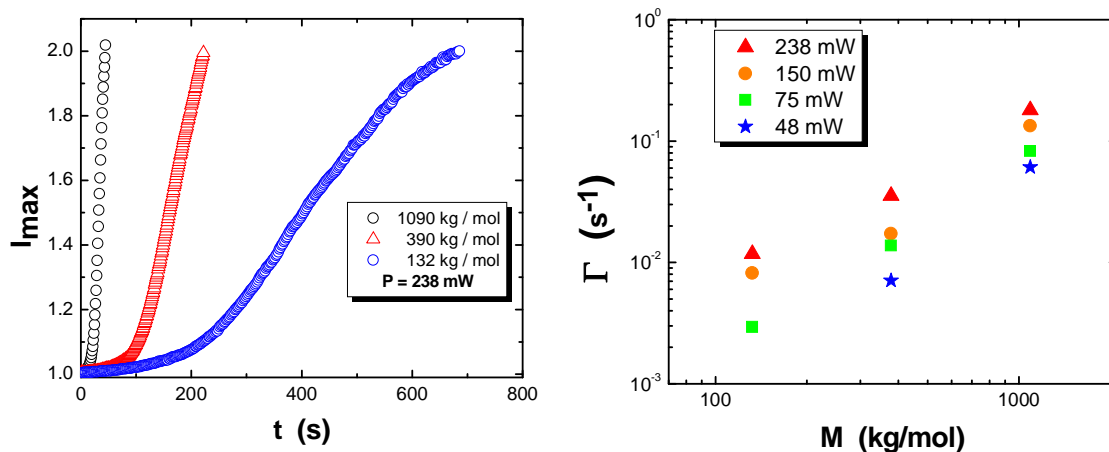


Figure 3.14: Left: I_{\max} vs. irradiation time for the three high cis-1, 4 PI / decane solutions. The power used is $P = 238$ mW. Right: Growth rate of the fiber formation, Γ vs. polymer molecular weight, M_w for a series of cis-1, 4 PI solutions. The solution concentrations were selected in order to obtain almost equally viscous samples. Data for different LASER powers are shown.

Obvious molecular weight influence on Γ can be observed. Solutions of higher molecular weight polymers exhibit clearly faster fiber formation.

It is important to notice that the lower M_w PI (shown in **Table 3.2**) also exhibited the writing phenomenon. However, it is so weak, that no quantitative measurements were possible. For example, after 1300 s of LASER irradiation ($P = 238$ mW), the low value of $I_{\max} \sim 1.1$ was measured.

3.2.6. Late stage

The results presented in the previous sections describe the pattern formation kinetics at the early stage of the writing phenomenon. As mentioned in **Chapter 2**, the adopted imaging technique imposed limits on the quantifiable refractive index increment ($I_{\max} \sim 2$).

Most of the experiments, however, were run longer and the transmitted pattern was also observed. In a later stage, the evolution of the transmitted pattern was observed to slow down. The time needed to reach this very slow down stage was found to correlate with the rate of the early growth in a way that faster rate lead to faster slowing down. However, no clear indication of saturation of the full transmission pattern was observed. Smaller secondary patterns seemed to superimpose on the frozen primary transmission pattern. These smaller patterns showed a time evolution similar to the one of the primary pattern. This is supported by the direct observation that other features (extra filaments) appear upon prolonged writing while the main feature (single filament) remains stable. Examples of these microscopic formations of more complex secondary patterns when the illumination is left for long times are given in **Figure 3.15**. The complex structures include twisted and multiple fibers (using focused LASER beam).

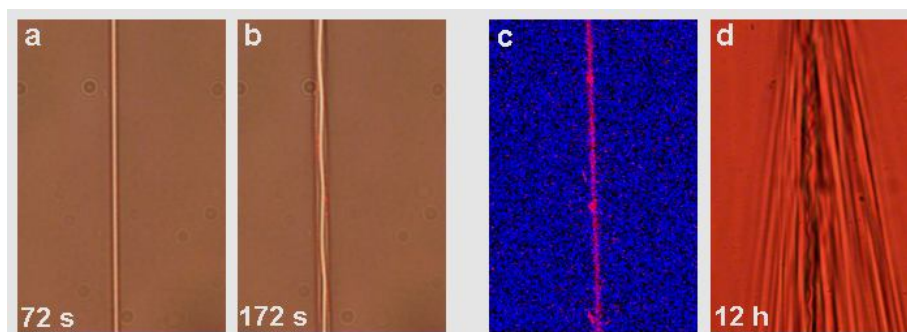


Figure 3.15: Complex patterns formed upon prolonged irradiation. a-b) Formation of a twisted fiber after $t = 172$ s of irradiation in cis-1, 4 PI / decane solution ($M_w = 1090$ kg / mol, $c = 5.6$ % wt) c-d) A focused beam (diameter ~ 17 μm) (c) results in an extended multi-fiber structure after irradiating for $t = 12$ h a cis-1, 4 PI / tetradecane solution ($M_w = 1090$ kg / mol, $c = 18.58$ % wt)

It is not very clear whether this formation is inherent to the specific light-matter interaction and the subsequent mechanism of patterning or if it results from some instabilities or other imperfections in the experimental setup, like the presence of flow, the lack of long time mechanical stability in the setup or others. The reproducibility of the secondary pattern formation was difficult to establish. The belief is that one filament formation is optically unstable and any small perturbations will give rise to extra formations. This is supported by the observation of optical instabilities that will be discussed in **Section 3.3**.

3.2.7. Discussion on the pattern formation kinetics

As shown in the Sections above, very similar kinetics evolutions were observed in nearly all cases of the studied samples and LASER irradiation conditions: formation of a filament with constant (in time) size, but increasing refractive index. An exponential-like growth rate is describing well the experimental findings. Exponential growth is generally associated to cases of amplified mechanisms where the driving force increases with time as the process goes on. It is worth noting that since the imaged region corresponds to the focus of the beam, large increase of the LASER light intensity as a consequence of self-focusing is not expected. A decrease in the friction of the system could provide an alternative channel to accelerated kinetics.

The effect of the LASER power on the formation kinetics is so that an increase of the laser power is found to lead to a speed up of the growth in all the samples, but the most viscous one (**Figure 3.8**). The linear speed up in the majority of the cases points to a driving force proportional to the LASER intensity, as expected for example in electrostriction. The higher intensities should lead to stronger forces and consequently shorter formation time scales. For the most concentrated solution, exhibiting a rubbery behavior, the growth rate becomes almost independent of the power.

Solutions in different solvents exhibit different growth rates (**Figure 3.12**). Linear alkanes appear to be the most effective solvents used for writing experiments. Nevertheless, the observed behavior does not lead to any clear conclusion on the effect of the optical contrast Δn on the kinetics. This is opposed to electrostrictive mechanisms, in which Δn plays a major role, as will be described in more detail in **Chapter 5**. In the case of dielectric particles suspended in a lower refractive index solvent, optical forces exerted are proportional to Δn .

Concentration c does not seem to play an important role on the early stage growth rate (**Figure 3.11**). On the contrary, polymer molecular weight M_w is found to affect strongly the formation kinetics, as increasing M_w speeds up the microstructure formation (**Figure 3.14**). The effects of the concentration and the molecular weight on the formation kinetics cannot be easily explained. In entangled semidilute polymer solutions the M_w and c

dependence of physical properties (like viscosity, rubbery plateau, etc...) are somewhat intricate.

Finally, microstructure seems to play an important role in the writing phenomenon. It seems that the amount of the 1, 4 (cis and trans) units of the polydiene chains affects the writing effect. This was verified by the following two facts: First, 1, 2-PB solutions did not show any non linear optical behavior. Second, the growth rate was found to be affected by the percentage of 1, 4 units (**Figure 3.13**). We speculate that the large polarizability of the C=C bond plays a major role in the writing effect.

3.3 Fiber formation: Similarities to Optical Spatial Solitons and Modulational Instabilities

In **Section 3.2**, the pattern evolution kinetics at the focus of the LASER beam was examined in detail. As already mentioned in **Chapter 1**, the light-induced fibrillar structures extend in the whole size of the sample cell used. Self-focusing and self-trapping of light, reminiscent of Optical Spatial Solitons and Modulation Instabilities were observed due to the local alteration of the refractive index.

3.3.1 Optical Spatial Solitons and Modulation Instabilities

The best-known characteristic of wave propagation is that beams that are finite in space tend to broaden due to diffraction. That this paradigm can be broken is perhaps one of the most fascinating features of Nonlinear Optics. For this to occur, it requires a strong nonlinear interaction between the wave and the medium through which the beam is propagating. As a result, a self-trapped beam or an optical spatial soliton (OSS) can form^{2, 3}. Spatial solitons are optical beams that propagate in a nonlinear medium without diffraction, i.e., their beam diameter remains invariant during propagation. Intuitively, a spatial soliton represents an exact balance between diffraction and nonlinearly induced self-lensing or self-focusing effects. This is depicted schematically in **Figure 3.15**³:

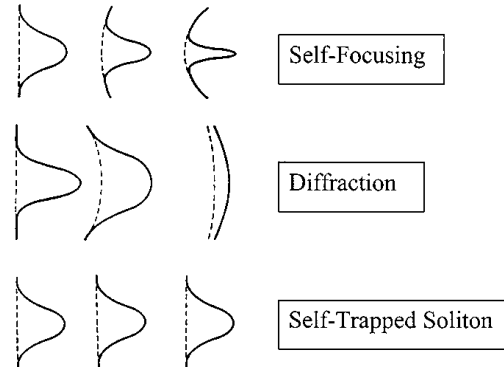


Figure 3.16: Schematic showing the spatial beam profiles (solid line) and phase fronts (dashed line) for (a) beam self-focusing, (b) normal beam diffraction, and (c) soliton propagation.

Self trapping and related OSS can exist by virtue of many different physical mechanisms, yet these solitons have many properties in common. The universal principle unifying all solitons is that the wave-packet creates, through the nonlinearity, a potential well and captures itself in it. It becomes a bound state of its own induced potential well². In general, two major categories of optical nonlinearities are well-known. Kerr nonlinearities are characterized by a local, instantaneous refractive index change, Δn ,

$$\Delta n = n_2 I \quad (\text{Equation 3.5})$$

with I being the local intensity and n_2 the Kerr constant. It has been shown that Kerr type solitons are stable only in planar, (1+1)D, systems, since catastrophic self-focusing occurs in bulk media. The other type is the saturable nonlinearities. These nonlinearities typically arise because resonances give rise to a maximum change in the optical susceptibility and thus higher order (than n_2) nonlinearities are included to describe the arrest in the refractive index increase. Saturation of the nonlinearity implies that there is a maximum value for Δn ,

$$\Delta n(I) = \frac{\Delta n_{sat} I}{I + I_{sat}} \quad (\text{Equation 3.6})$$

so that for $I \gg I_{sat}$, $\Delta n(I)$ approaches Δn_{sat} asymptotically. Just like a Kerr medium, a saturable medium acts as a focusing lens at high intensities. However, because the index change cannot exceed Δn_{sat} , the induced lens eventually becomes wider instead of stronger and has less focusing power at its center. Thus, the process that leads to catastrophic collapse in Kerr media can be arrested. Thus, saturable nonlinearities are able to lead to stable (2+1)D solitons.

OSS have been predicted and experimentally observed in a plethora of systems, such as gases, liquids, photorefractive crystals and others³, but also in Soft Matter systems. Despite their very different microscopic origins and mechanisms, the underlying nonlinearities in different materials lead to a similar phenomenology. The optical non linear response of soft materials was generally overlooked with the exception of colloidal suspensions and liquid crystals. Especially in the case of nematic liquid crystals, low power levels are required to observe OSS formation (called 'Nematicons'), due to the very large nonlinearity involved. An experimental observation of OSS in such a system⁴ is shown in **Fig 3.17**. A linearly polarized beam from an argon-ion LASER ($\lambda = 514$ nm) propagates in the plane containing the axes of the nematic molecules in a planar cell (**Figure 3.17 i**). When the beam is polarized orthogonally to the molecules, the nonlinearity is inactive and as a result, natural diffraction occurs (**Fig 3.17 ii, a**).

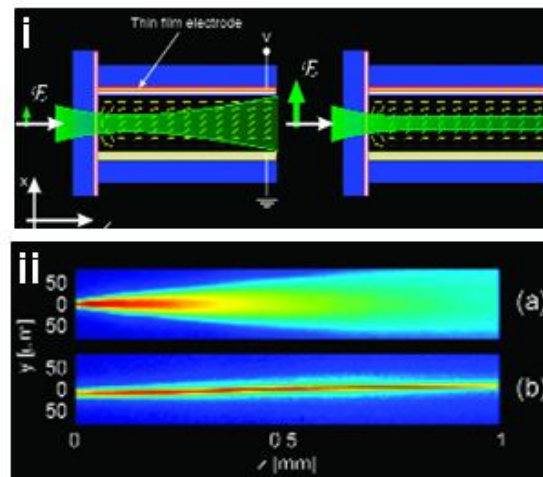


Figure 3.17: i) Schematic showing the planar liquid crystal cell employed in the experiments. Voltage V is applied through the thin film electrodes to induce a pre-tilt of the molecular axes with respect to the electric field. The glass cell and molecule distribution at (*left*) low beam intensity and (*right*) high-beam intensity. When the level of reorientation is sufficient, an OSS is obtained. ii) Photographs of (a) a linearly diffracting and (b) a soliton beam of 2 mW LASER beam ($\lambda = 514$ nm). In (a), the light was polarized orthogonally to the reorientation plane (x - z)⁴.

On the contrary, when the LASER light is polarized parallel to the nematic liquid crystals, the nonlinearity is active and the beam is self trapped, forming an OSS (**Figure 3.16** ii, b). It is worth noting that the LASER power used in this case was only 2 mW.

Another phenomenon related to OSS, is the appearance of Modulational Instabilities (MI). MI is a process that appears in most nonlinear wave systems. Because of MI, small amplitude and phase perturbations (from noise) grow rapidly under the combined effects of nonlinearity and diffraction. As a result, a broad beam tends to disintegrate during propagation, leading to filamentation (periodic arrays of OSS). MI typically occurs in the same parameter region as OSS. The relation between MI and solitons is best manifested in the fact that the filaments emerging from MI are actually trains of almost ideal solitons⁵. Apart from other materials, MI had been studied in Soft Matter systems too. The established case of dielectric colloidal hard spheres dispersed in a dielectric fluid has recently received renewed attention and MI were demonstrated both theoretically^{6, 7} and experimentally⁸ by Reece et. al. In this experiment, optically induced self-organization of colloidal arrays in the presence of unpatterned counterpropagating evanescent waves was demonstrated.

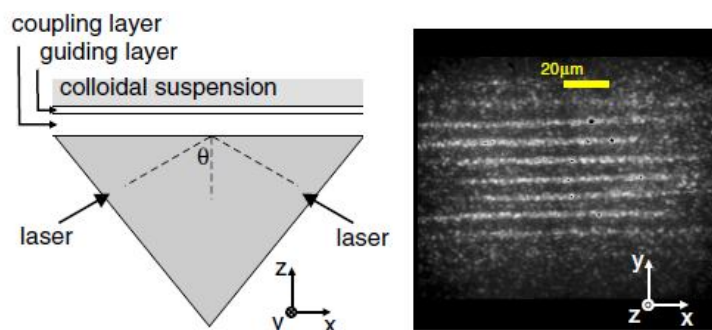


Figure 3.18 Left part: A schematic diagram outlining the geometry of the experimental setup. The propagation directions of the two counterpropagating modes are along the x direction and the observed array formation is aligned along the x direction with a periodic spacing in the y direction. Right part: A light scattering image of spontaneous ordering of 410 nm polymer colloids seen under typical experimental conditions⁸.

In **Figure 3.18** (left part), the optical waveguide geometry used in this experiment is shown. Two counterpropagating LASER beams ($\lambda = 1064$ nm) are along the x directions and the observed array formation of the 410 nm polymer colloids is aligned along the same direction, with a periodic spacing in the y direction. The authors have shown that the arrays are linked to the breakup of the incident field into OSS, the lateral spacing of which is related to MI of the soft condensed matter system.

3.3.2 Relation of LASER writing in polydiene solutions to OSS and MI

The effect of LASER-induced pattern formation in polydiene solutions exhibits similar behavior to the systems mentioned above. Both OSS and MI instabilities are evidenced through microscopy observations. **Figure 3.19** shows a typical OSS formation in a semidilute solution of cis-1,4 PI in decane ($M_w = 1090$ kg / mol, $c = 6.6$ % wt). The medium is irradiated with a red LASER ($\lambda = 671$ nm) focused by a x16 (NA = 0.32) microscope lens.

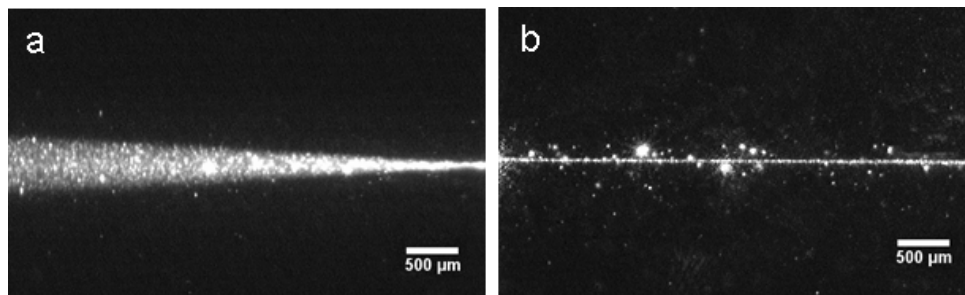


Figure 3.19: Single OSS formation in a cis-1, 4 PI in decane solution ($M_w = 1090$ kg / mol, $c = 6.6$ % wt). The LASER beam ($P = 29$ mW) is focused through a spherical lens (x16, NA = 0.32). a)

Spreading of the beam due to diffraction at $t = 0$ s, b) OSS formation after a few minutes of irradiation. The beam propagation axis is from right to left.

At $t = 0$ s, when the LASER is turned on, a normal diffraction of the sharply focused beam is observed through the 90° scattering image (**Figure 3.19 a**). However, after a few minutes of irradiation, the beam is self-focused and a single OSS is formed (**Figure 3.19 b**). It is propagating with a constant diameter of about $15 \mu\text{m}$ along the whole cell length (5 mm in this case).

The single fiber formation shown above is definitely very reminiscent of OSS. Moreover, the correspondence to OSS is strengthened by another striking observation: The formation of a 3D bundle array of regularly spaced parallel filaments oriented along the propagation direction when the writing lens is defocused. Defocusing the lens results in a wide ($\sim 200 \mu\text{m}$) beam (**Figure 3.20 a**). The LASER self-guiding from the fibers of the bundle is shown in **Figure 3.20 b**, for an irradiation of $t = 10$ min ($P = 300$ mW):

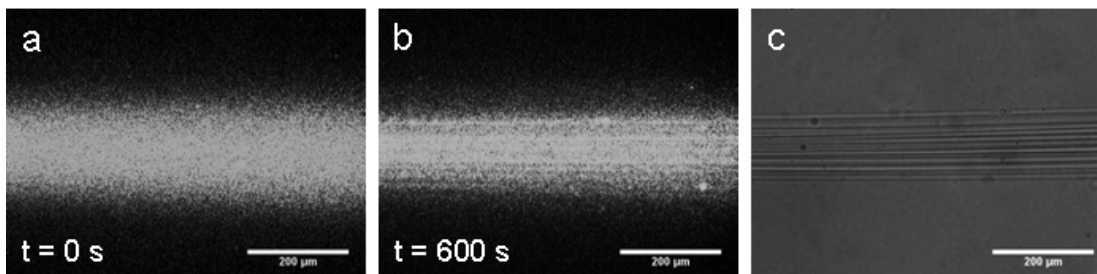


Figure 3.20: 3D fiber bundle formation in a cis-1, 4 PB in tetradecane solution ($M_w = 390$ kg / mol, $c = 14.7$ % wt). The LASER beam ($P = 300$ mW) is focused through a defocused spherical lens ($f = 35$ mm) to form broad light beam. a) the initial broad beam, b) waveguiding of the beam through the (2+1)D OSS filaments formed, as seen from the scattered light and c) phase image showing the 3D fiber bundle

The corresponding phase image is shown in **Figure 3.20 c**. Each fiber has roughly a diameter of $10 \mu\text{m}$, just as the single fiber formation case. A further demonstration of multi-fiber formation is obtained when the writing lens is replaced by a cylindrical lens ($f = 10$ mm), producing a wide 2D sheet of light (**Figure 3.21 a**). These irradiating conditions give rise to the formation of fibers regularly spaced in one plane, as shown in **Figure 3.21 b, c**:

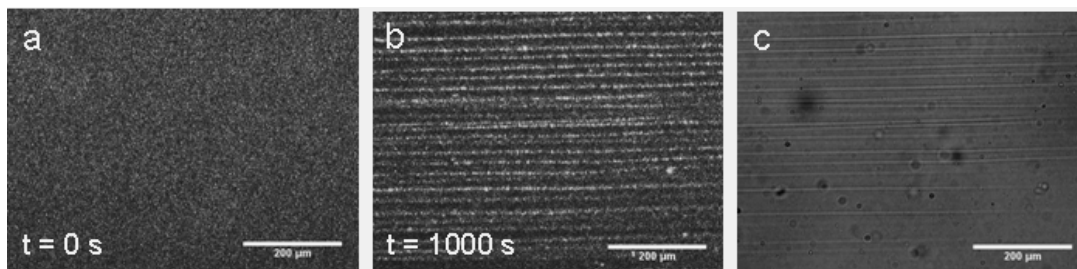


Figure 3.21: 2D filament array formation in a cis-1, 4 PB in tetradecane solution ($M_w = 390$ kg / mol, $c = 14.7$ % wt). The LASER beam ($P = 300$ mW) is focused through a cylindrical lens ($f = 10$ mm) to form a sheet of light. a) the initial sheet of light at $t = 0$ s, b) (1+1)D OSS planar array of filaments, as seen through the scattered light and c) the resulting phase image.

The waveguiding of each fiber in the 2D array is clearly seen in the scattering image (**Figure 3.21 b**), whether the phase contrast image shows that the different fibers appear to have the same transverse dimension (~ 10 μm), very similar to that of the single fiber formation. We may conclude that the constant width of the fibers in all cases studied is fixed by the interaction of the optical field with the material. Upon irradiation, the medium form a waveguide for the incident LASER beam, resulting in the observed 10 μm -sized fibrillar structure.

As it has been already mentioned, multi-filament patterns are usually explained as a result of MI, i.e., small wavefront perturbations that cause the optical field to break up into a periodic array. The present polydiene solutions therefore provide a very clear example, the first to the best of our knowledge, of a binary mixture where MI can be clearly observed with both (1+1)D and (2+1)D solitons⁹. The above observations clearly point toward a nonlocal and non-instantaneous light–matter interaction, where entangled polymer solutions specific properties, e.g., nonlinear mechanical response, might play a role. The polydiene solutions offer an unexpected, simple, and versatile system for nonlinear optics studies, with, however, unclear physical origins, as it will be discussed in detail in **Chapter 5**.

3.4 Characterization of the fibers

A couple of experiments were conducted in order to investigate the properties of the light-induced fibers in the polydiene solutions. Optical video microscopy and polarized Raman scattering results are presented in this section of the thesis.

3.4.1 Reversibility of the phenomenon

A crucial question that immediately arises relates to the reversibility of the writing phenomenon. In order to examine if fibers are redissolved in the surrounding solution, video microscopy was used. The stability of the LASER-induced formations was found to depend on both the properties of the polydiene solutions and on irradiation time used.

For short irradiation times, fibers appear to be re-dissolved in the polymer solution, with the re-dissolution time scale being much longer compared to the formation time scale. For relatively short irradiation periods, fiber formation appears to be a reversible phenomenon.

For long sample exposures to the LASER beam, the situation changes dramatically, as fiber formation becomes irreversible. The mechanical stability of the formed filaments depends on the viscosity of the solutions. For very viscous solutions, fibers are extremely stable for long time (weeks to months). Fiber bending (due to gravity) is nevertheless apparent in most cases.

For lower viscosity samples, fibers are less stable. **Figure 3.22** shows a series of microscope images of a fiber formed after irradiating a cis-1, 4 PI ($M_w = 378 \text{ kg / mol}$) / decane solution ($c = 9.51 \text{ \% wt}$) for 45 s ($P = 238 \text{ mW}$). The first image ($t=0 \text{ s}$) is captured directly after switching off the LASER light, while the other images correspond to later times:

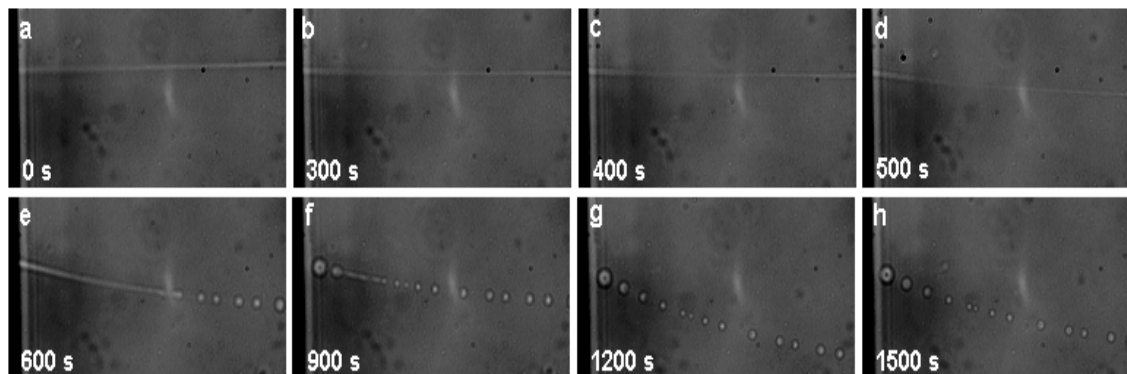


Figure 3.22: Microscope images of the fiber decay process at different times after switching off the LASER beam. The fiber was formed after irradiating a cis-1, 4 PI ($M_w = 378$ kg / mol) / decane solution ($c = 9.51$ % wt) for 45 s ($P = 238$ mW).

As can be seen, the fiber bends 300 s after stopping the LASER (**Figure 3.22** b) due to gravity. After about 400 s, the fiber eventually gets thinner at specific points and other points appear to swell (**Figure 3.22**, c and d). Finally, the structure breaks and retraction of the pieces result in globular structures at later times (**Figure 3.22**, e). However, the dots formed seem to be spatially correlated, since they move down and up in a similar fashion, due to gravity and bubble motion, respectively (**Figure 3.22**, f-h). One possible explanation is that thin sub-micron threads connect the dots, not resolved by optical microscopy. At much later stages (not shown here) the dot-like structures appear to be almost uniform in size (roughly $5 \mu\text{m}$) and are insoluble in the surrounding solution.

Similar observations were made for several polydiene solutions. Fibers formed in solutions of intermediate or low M_w (i.e. 132 - 378 kg / mol) were less stable than the structures formed in high M_w (i.e. 1090 kg / mol) polymer solutions. Representative microscope images of light-induced fibers, long after their formation, are shown in **Figure 3.23**:

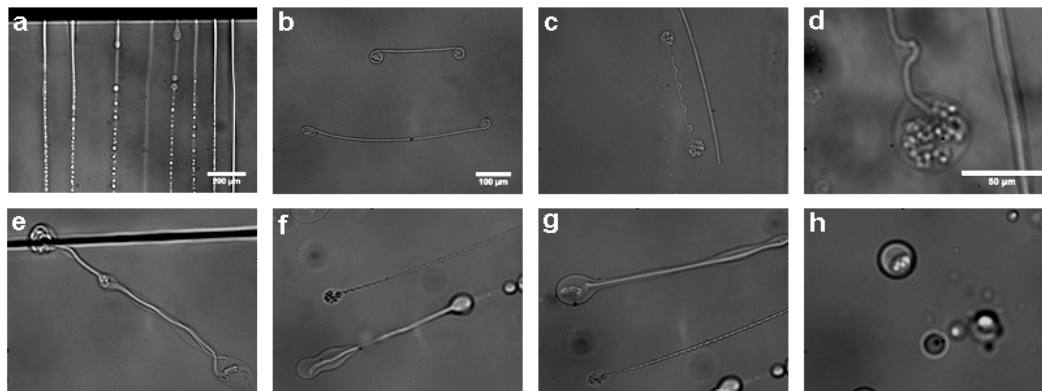


Figure 3.23: Microscope images of various fiber decays.

Figure 3.23 a shows the decay of fibers formed in a solution of cis-1, 4 PI ($M_w = 132 \text{ kg / mol}$) in decane ($c = 43.33 \text{ \% wt}$). The image was acquired about 2 hours after stopping LASER irradiation, showing that the formed structures break quickly into arrays of dots. The latter appear not to redissolve. **Figure 3.23 b, e** show pieces of fibers formed in a cis-1, 4 PI ($M_w = 1090 \text{ kg / mol}$) / decane solution ($c = 6.3 \text{ \% wt}$), 5 days after the formation. The fibers clearly remain stable, they do not break in dot-like structures. **Figure 3.23 c, d** show decaying pieces of fibers in the same sample (1 day after formation). Bending of the fibrillar structure is observed at regularly spaced distances. The edges of the structure seem to contract and associate, forming the complex shapes shown. Finally, **Figure 3.23 f-h** show the transition from fiber to globular (dot-like structures), in a cis-1, 4 PI ($M_w = 378 \text{ kg / mol}$) / decane solution ($c = 9.49 \text{ \% wt}$), 1-2 hours after sample irradiation.

The insolubility of the structures in good solvents for the original polymer is surprising. It indicates the presence of 'crosslinks' created upon LASER irradiation. The nature (physical or chemical) of these crosslinks remains to be established.

Dense fiber bundles, obtained by prolonged irradiation of viscous polydiene solutions with defocused spherical lens, are mechanically very stable. This allowed for isolation of the written structures. The procedure followed to obtain such (dry) structures was the following. After the formation, the whole glass cell was immersed in a pot with pure hexane. After 4 hours, the coverslip was removed gently from the cell, and the solution (containing the light-induced structures) was put again in pure hexane. After a few hours, the resulting dilute solution was replaced by pure hexane, and this procedure was repeated 3

times. After this step, the glass cell is put in vacuum oven for 3 hours, until the remaining solvent evaporates and a dry, solution free bundle is obtained. A typical image of an isolated bundle is shown in **Figure 3.24**:

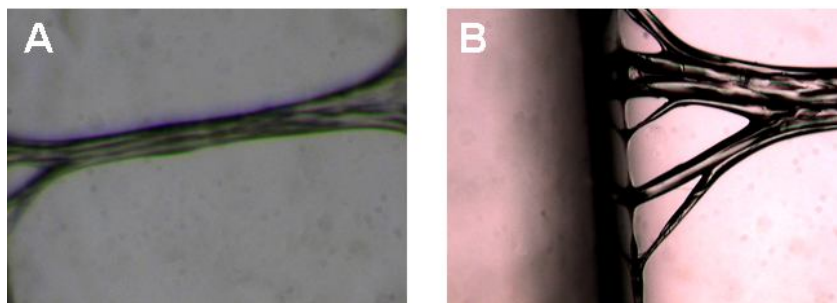


Figure 3.24: Microscope image from a dry fiber bundle formed by prolonged irradiation of a cis-1, 4 PB / tetradecane solution ($c = 14.7\%$ wt). A) The whole cell is imaged (2mm long). B) Magnified image of the bundle end attached to the glass cell window.

As was mentioned in **Chapter 1**, the length of the LASER-induced structures was found to be limited only by the size of the cell used. To demonstrate this, a multi-fiber bundle was written along the axis of a 3 cm long glass cuvette. The solution used in this case was cis-1, 4 PI ($M_w = 1090$ kg / mol) / decane, at $c = 6.6\%$ wt. LASER irradiation resulted in 2.5 cm long structure, extending between the bottom of the cell and the solution meniscus. After the formation, the cuvette was put in a vertical position. Sedimentation of the long multi-fiber structure was followed by video microscopy, as shown in **Figure 3.25**:

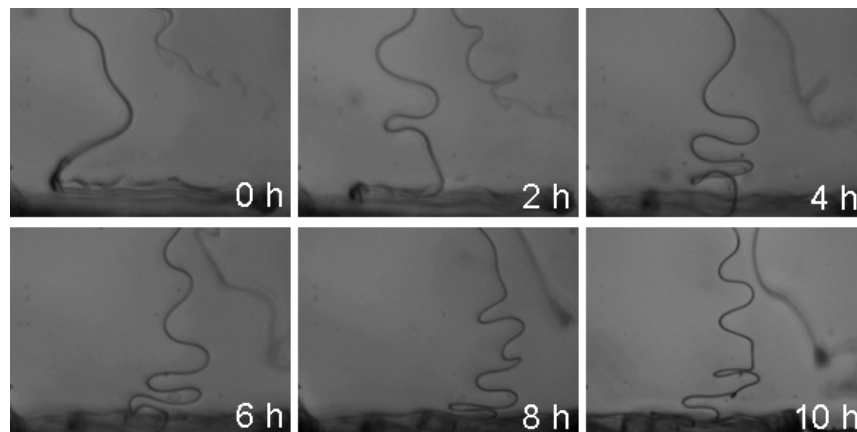


Figure 3.25: Microscope images of a long fiber bundled upon sedimentation. The bundle was formed after prolonged irradiation of a cis-1, 4 PI ($M_w = 1090 \text{ kg / mol}$) / decane solution ($c = 6.6 \%$ wt), and its length was about 2.5 cm. After formation, the sample cell was placed vertically to allow sedimentation of the written structure due to gravity.

The sedimentation provides insight to the mechanical properties of the structure. As seen in **Figure 3.25**, the fiber bundle shows a buckling behavior and no breaking could be observed. It reflects the enhanced mechanical stability of the bundle structure (compared to the single fibers). The structure evolution is reminiscent of buckling of an elastic filament and the characteristic length of the buckled structure (apparent in **Figure 3.25**) should relate to the persistence length. At the end of the process, a thick layer of insoluble fibers is formed at the bottom of the cuvette.

3.4.2 Micro-Raman scattering of the irradiated material

The above findings of insolubility of the irradiated material points towards local microstructure modifications of the polydienes. Micro-Raman Scattering was employed to study possible LASER-induced changes in the microscopic structure of the polydienes. A LASER beam of $\lambda = 780 \text{ nm}$ was used, along with a microscope x50 objective ($NA = 0.5$).

Initial experiments were conducted on LASER-written multi-fiber bundles inside the polydiene solutions in which the structures were formed. The resulting Raman spectra were compared to the corresponding spectra of 'clear' ('fiber-free') areas inside the same sample.

A comparison between such two spectra is shown in **Figure 3.26**. The red line corresponds to a multi-fiber bundle, while the blue line corresponds to a clean area:

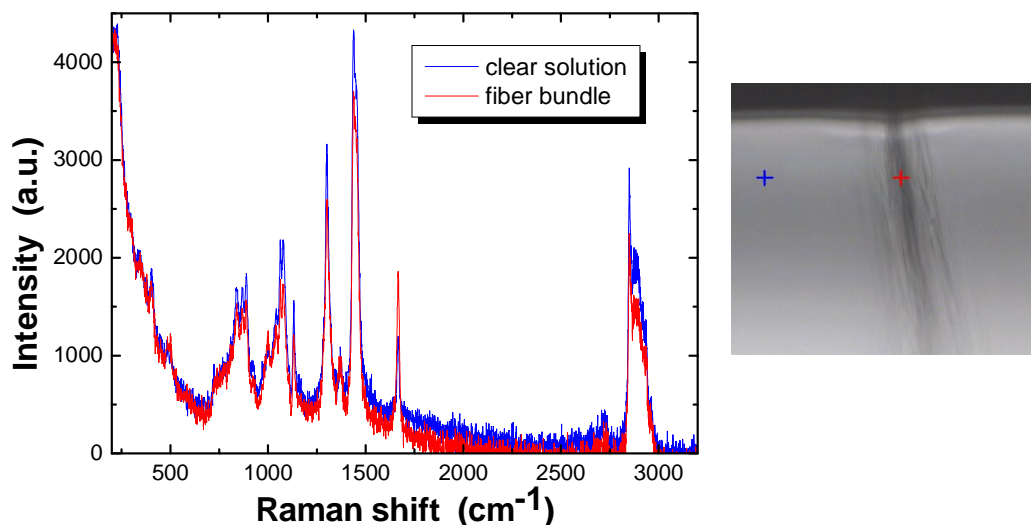


Figure 3.26: RAMAN spectra obtained from a multi-fiber bundle (red line) and a clear area (blue line) in a solution of cis-1, 4 PI ($M_w = 1090$ kg / mol) in tetradecane, at $c = 8.96$ % wt. The clean and the written area are shown with blue and red crosses in the microscope image on the right.

It can be observed that the two RAMAN spectra are almost identical. There is neither an appearance of new peaks nor a shift of the positioning of the peaks. However, some changes in the RAMAN intensity could be resolved. In order to examine the intensity ratio, two representative peaks were selected in both the clean and the written area. The peak positioned at 1666 cm^{-1} , attributed to the double bond C=C stretching, and the one at 1132 cm^{-1} , which corresponds to the single bond C-C stretching. The intensity ratio I_{1666} / I_{1132} is 1.532 and 0.767 for the fiber bundle and the clear solution, respectively. This is indicative of a higher percentage of C=C bonds in the written area, which are present in the polymer, but absent in the solvent. In other words, the fiber bundle is a region of increased polymer concentration. This confirms the assumption that the increase in refractive index observed in the phase contrast measurements are due to higher polymer concentration.

Subsequently, the RAMAN spectrum of a dry piece of multi-fiber bundle was isolated from the tetradecane solution and was measured. The obtained spectrum was compared to the measured spectrum of bulk cis-1, 4 PI ($M_w = 1090$ kg / mol), which was in

agreement with the results reported in literature^{10, 11}. **Figure 3.27** shows the comparison of the spectrum of the dry written piece (red line), with the one of the bulk polymer (black line):

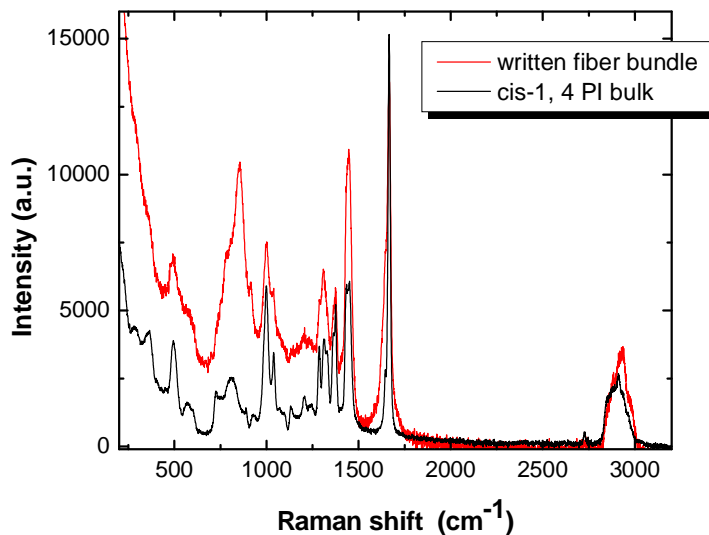


Figure 3.27: RAMAN spectra of bulk cis-1, 4 PI ($M_w = 1090$ kg / mol) (black line) and written PI fiber bundle (red line).

There are obvious differences in both the relative intensities and peak positioning between the two spectra., The region where the biggest differences are observed (1350 cm⁻¹ to 3100 cm⁻¹) is shown in **Figure 3.28**:

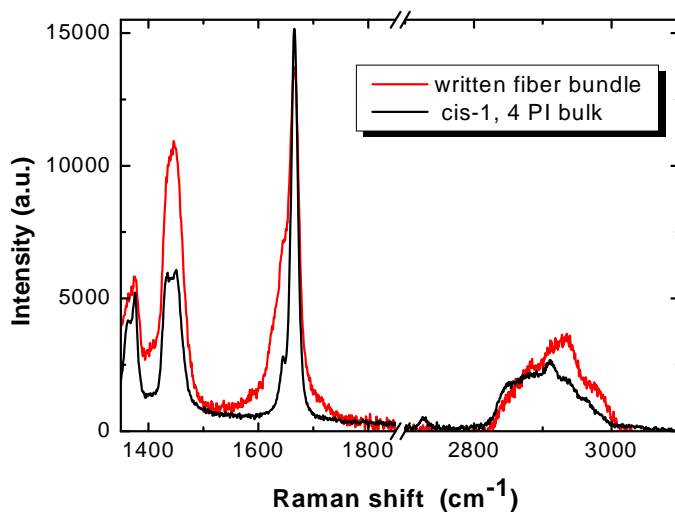


Figure 3.28: RAMAN spectra of bulk cis-1, 4 PI (Mw = 1090 kg / mol) (black line) and written PI fiber bundle (red line) in the region 1350 cm⁻¹ – 3100 cm⁻¹.

The relatively narrow peak at 1666 cm⁻¹ (C=C stretching), is clearly more broad in the spectrum of the written PI bundle. The peak is positioned at the same frequency and has almost the same intensity for both samples. Moreover, changes are detected in the broad peak around 2900 cm⁻¹, which refers to several modes of symmetric and asymmetric CH₂ and CH₃ stretching. It seems that this broad band is shifted to higher wavenumbers for the written sample. In addition to these, a factor of 2 in the intensity of the relatively broad band at 1443 cm⁻¹ is observed. This band corresponds to the deformation of the CH₂ groups of the macromolecules. Other less obvious differences between the spectra are observed in the lower wavenumber region, however not clear conclusions can be delivered.

These clear differences cannot be ascribed to any specific changes in the polymer microstructure, but nonetheless confirm some level of modification upon LASER irradiation. Ongoing RAMAN experiments are needed for a clear identification.

3.5 Summary

The study of LASER-induced formation of micron-sized fibrillar structures in semidilute and concentrated solutions of 1, 4 PI and PB in various lower refractive index

solvents was presented in this Chapter. Single and multiple fiber formation are observed, depending on the beam size employed. The relation of the phenomenon with Optical Spatial Solitons and Modulation Instabilities was clearly evidenced. The low power levels (down to ~0.7 mW) required to observe these impressive nonlinear optical effects, along with the versatility of the soft materials used, clearly offer several possibilities for nonlinear optics experiments.

Single fiber formation was imaged at the focus of the LASER beam. Using a thin collimated white light beam from the microscope's illumination unit and slightly defocused detection, quantitative phase contrast images were acquired. The imaged intensity corresponds to the phase gradient of the fibers observed. Assuming a Gaussian-like refractive index profile, the phase gradient is directly related to the refractive index difference between the formed structure and the surrounding solution (δn). The time evolution of the intensity at the middle of the fiber, I_{\max} (corresponding to δn_{\max}) was used to quantify the fiber formation kinetics. An exponential growth of I_{\max} is identified with a constant filament radius. The growth rate (Γ) dependence on a number of parameters has been investigated for the early stage of the effect.

The effect of the laser power on the formation kinetics is so that an increase of the laser power is found to lead to a linear increase of Γ , in the majority of the samples examined. Polymer concentration was found to play no role in the formation kinetics. The optical contrast (Δn) between the macromolecules and the solvent seems to affect Γ , however, not in a clear manner. Solutions in linear alkanes were found to exhibit the fastest kinetics, while cyclic alkane solutions are the slowest cases. Polymer molecular weight seems to play an important role, since growth rate is much faster for high M_w . Finally, the polymer microstructure affects the kinetics, since it depends on the amount of the 1, 4 units of the polydiene examined. As for the late stage of the effect, no clear indication of saturation of the complete transmission pattern was observed. The findings regarding very long irradiation times indicate that the single filament formation is relatively unstable as any small variation will give rise to extra formations.

The reversibility of the writing phenomenon was also explored. It is found that short irradiation times lead to reversible refractive index changes. On the contrary, prolonged irradiation results in insoluble structures. Depending primarily on the polymer molecular

weight, the fibrillar structures can remain stable for long periods (~weeks), or break in pieces. Broken fibers form globular structures that are insoluble in the surrounding solution. Multi-fiber bundles obtained from prolonged irradiation with a defocused lens, are mechanically stable. Isolation of such structures from the polydiene solutions was possible. Early micro-Raman scattering results indicate changes between the microstructure of the bulk (non-irradiated) polydienes and the written structures. Further investigation is ongoing.

References

1. Sigel, R., Fytas, G., Vainos, N., Pispas, S., and Hadjichristidis, N. *Science* **2002**, 297, 67-69.
2. Stegeman, G. I., and Segev, M. *Science* **1999**, 286, 1518-1523.
3. Stegeman, G. I. A., Christodoulides, D. N., and Segev, M. *IEEE J. Sel. Top. Quant.* **2000**, 6, 1419-1427.
4. Assanto, G., Peccianti, M., and Conti, C. *'Optics and Photonics News'* **2003**, 14, 44-48.
5. Kip, D., Soljacic, M., Segev, M., Eugenieva, E., Christodoulides, D. N. . *Science* **2000**, 290, 495-498.
6. Conti, C., Ghofraniha, N., Ruocco, G., Trillo, S. *Phys. Rev. Lett.* **2006**, 97, 123903.
7. El-Ganainy, R., Christodoulides, D. N., Musslimani, Z. H., Rotschild, C., and Segev, M. *Opt. Lett.* **2007**, 32, 3185-3187.
8. Reece, P. J., Wright, E. M., and Dholakia, K. *Phys. Rev. Lett.* **2007**, 98.
9. Anyfantakis, M., Loppinet, B., Fytas, G., and Pispas, S. *Opt. Lett.* **2008**, 23, 2839-2841.
10. Cornell, S. W., and Koenig, J. L. *Macromolecules* **1969**, 2, 546-549.
11. Nallasamy, P., and Mohan, S. *Arab. J. Sci. Eng* **2004**, 29, 17-26.

CHAPTER 4

SIGN OF THE INDUCED CONCENTRATION CHANGE IN VARIOUS SOLVENTS

Other cases of LASER-induced pattern formation in various homopolymer and diblock copolymer solutions are presented here. Additionally, patterning of turbid copolymer solutions and the resulting Self-Induced Transparency is described.

4.1 Introduction

So far we have reported cases of polydienes dissolved in a lower refractive index solvent (positive Δn) where application of LASER light leads to an increase of the refractive index of the irradiated region. This increase was attributed to an increase of the local polymer concentration. The following question arises: what happens if the macromolecules are dissolved in a higher refractive index solvent (i.e. $\Delta n < 0$) ? In the case of LASER irradiation of colloidal suspensions, the sign of the resulting optical forces is equal to the sign of Δn . When positive, the particles are attracted to the high intensity regions, while for a negative sign the particles are expelled from the LASER beam. In order to answer this question, writing experiments were carried out in higher refractive index solvents, presented in **Section 4.2**. In some higher n solvents (i.e. bromonaphthalene, chlorobenzene), the polymer was found to be expelled from the irradiated volume, leading to a formation of higher n , solvent-rich formations. This finding is qualitatively compatible with electrostrictive-like forces. It was further observed that the phenomenology of the writing effect in polydienes dissolved in THF and tetralin (a lower and a higher n solvent, respectively) was opposite: solvent-rich formations were observed in THF solutions, while polymer-rich structures were optically induced in tetralin solutions.

In **Section 4.3**, LASER writing experiments on more complex solutions of a diblock copolymer (PI-PS) in two different selective solvents (hexane and ethyl acetate) are presented. As known from previous experiments, that LASER-induced patterning also occurs in polydiene containing copolymers. Copolymer solutions can open new possibilities of LASER patterning. An impressive demonstration of Self-induced Transparency is given in **Section 4.2**. It is shown that turbid solutions of PI-PS in ethyl acetate (strong light scattering due to huge aggregates) become locally transparent upon LASER irradiation through a complex patterning mechanism.

4.2 The inverse case: Solvent-rich channel formation

4.2.1 Polydienes in bromonaphthalene ($\Delta n < 0$)

All the solutions investigated in **Section 3.2**, included macromolecules of higher refractive index dissolved in good solvents of lower refractive index. Despite the not clear relation between the early stage growth rate Γ and the refractive index difference Δn (**Figure 3.12**), the effect is qualitatively compatible with electrostrictive-like forces. To further check the relation between the sign of dn/dc and the local variation of polymer concentration, polydiene solutions in bromonaphthalene were examined. This solvent has a large refractive index ($n=1.657$), higher than the one of cis-1, 4 PB ($n= 1.520$) and cis-1, 4 PI ($n= 1.519$), so that $\Delta n = -0.137 < 0$.

The first experiments were conducted using the experimental setup described in **Section 2.3** and $P = 238$ mW. By employing the imaging conditions described in **Section 2.3** (defocusing distance $\Delta z = 20$ μm above the focal plane), minute changes in the refractive index of the irradiated solution were detected. However, obvious changes in the transmitted beam spot could be observed, indicating modifications in the index of refraction of the solution. In order to be able to capture such small δn values ($< 10^{-4}$), much longer defocusing distances for the image acquisition were utilized. A typical image series during the irradiation ($P = 238$ mW) of a cis-1, 4 PI ($M_w = 1090$ kg / mol) dissolved in bromonaphthalene, at $c = 2.79$ % wt ($c = 0.0413$ g / ml) is shown in **Figure 4.1**, a-e. The images were acquired in a plane roughly 500 μm above the focal plane. Under these conditions, I_{max} corresponds to the refractive index change δn , even though not in a known quantitative manner. In particular, because the diameter of the formed structure increases with time, the proportionality constant between I_{max} and δn changes with time (see **Chapter 2**).

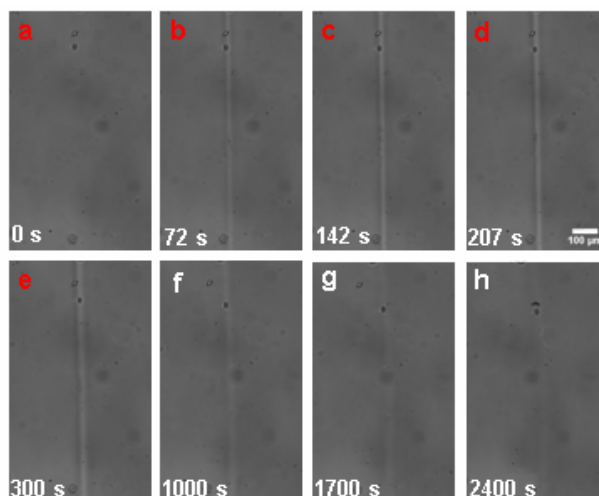


Fig. 4.1: Phase contrast images of the solvent fiber formation and decay. Red letters indicate that the LASER light is on, while white letters correspond to images obtained after stopping the LASER beam. The sample is cis-1, 4 PI (Mw = 1090 kg / mol) dissolved in bromonaphthalene, at $c = 2.79\%$ wt ($c = 0.0413\text{ g / ml}$) power used is $P = 240\text{ mW}$. The defocusing distance is $z = 500\text{ }\mu\text{m}$.

The light-induced formation of a fibrillar structure along the beam propagation direction is clearly evidenced. The structure exhibits higher imaged intensity arising from a higher refractive index than the surrounding PI solution. Given that bromonaphthalene has a higher n than PI, we conclude that the LASER-induced stripe has a reduced polymer concentration compared to the surrounding solution. Again, we assume that only concentration variations are responsible for the observed δn . The contrast of the formed structure remains very weak and large defocusing distances (Δz) had to be used. As a consequence, only quantitative interpretation of the δn changes can be obtained.

The structure's width is progressively increasing as the irradiation time increases. Very weak or no waveguiding is observed, which can be explained by the very small value of δn . Self-focusing and self-trapping of light are not observed, in contrast to the higher local polymer concentration fibers formed in the different solvents mentioned in **Section 3.2**, which exhibit high δn values and eventually guides the LASER light. For the latter systems, the constant fiber size of $\sim 10\text{ }\mu\text{m}$ and subsequent waveguiding could be understood as a material response to the LASER light. On the contrary, in the bromonaphthalene systems, there is no waveguide formation, and no constant fiber diameter is observed.

Qualitative results for the time scale of the phenomenon in the bromonaphthalene solutions are shown in **Figure 4.2**, where I_{\max} is reported as a function of time. Red symbols correspond to measurements with the LASER beam on (**Figure 4.1 a-e**), while black symbols correspond to the measurement of I_{\max} when the beam is blocked (**Figure 4.1 f-h**):

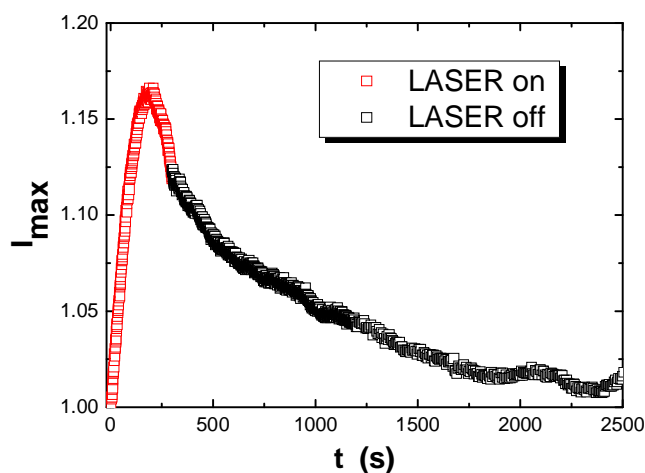


Figure 4.2: Kinetics of the solvent fiber formation and decay. Red symbols indicate that the LASER light is on, while black symbols correspond to measurements after stopping the LASER beam. The sample is cis-1, 4 PI (Mw = 1090 kg / mol) dissolved in bromonaphthalene, at $c = 2.79$ % wt ($c = 0.0413$ g / ml) power used is $P = 240$ mW.

The above plot clearly shows that I_{\max} is increasing while the solution is being irradiated, up to a maximum value of $I_{\max} = 1.17$, which is reached after $t = 207$ s (**Figure 4.1, d**). For longer irradiation times, I_{\max} decreases. At $t = 300$ s, the LASER beam is stopped, and I_{\max} further decreases. After $t = 2300$ s, I_{\max} almost reaches the value of 1, meaning that the sample returns to its initial condition of homogeneous refractive index (**Figure 4.1, h**).

Analogous behavior was also observed in cis-1, 4 PB solutions in bromonaphthalene, indicating no obvious difference between the two polydienes.

The observation that the polymer is expelled from the irradiated volume leading to solvent-rich formations of positive optical contrast ($\delta n > 0$) is qualitatively compatible with

electrostrictive-like forces, since the high n component is attracted to the LASER beam. The maximum δn values are quite small and self-focusing and related non linear optical phenomena are absent in the bromonaphthalene systems. Finally, the LASER-induced patterns appear to be reversible, since after LASER-switching off the solutions return to its initial condition (homogeneous refractive index).

4.2.2 Polydienes in THF ($\Delta n > 0$)

Compared to the lower n alkane solvents presented in **Section 3.2**, tetrahydrofuran solutions respond in a radically different way to the application of LASER light. THF has a lower refractive index ($n = 1.407$) than PI and PB. It is known to be an athermal solvent for both macromolecules. Similarly to the bromonaphthalene case (**Section 4.1.1**), while a clear change in the transmitted beam spot was evident upon irradiation, no changes could be detected during phase contrast imaging, unless a long defocusing distance was used. **Figure 4.3** shows a time series of phase contrast images acquired employing $\Delta z = 1000 \mu\text{m}$. The sample is a cis-1, 4 PI ($M_w = 1090 \text{ kg/mol}$) in THF, at $c = 5.47 \text{ \% wt}$ ($c = 0.0486 \text{ g/ml}$).

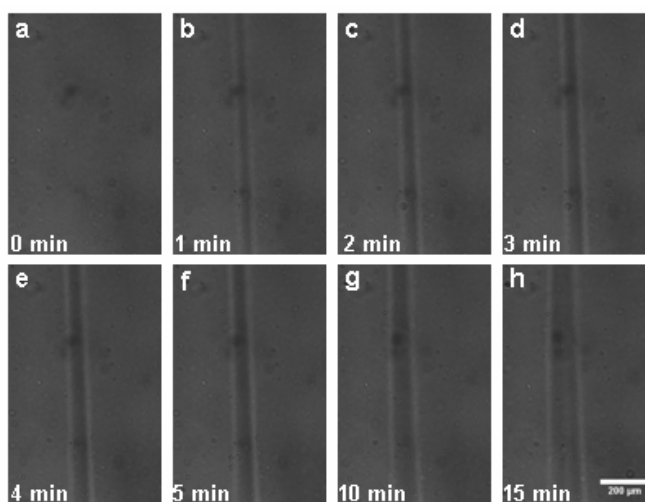


Figure 4.3: Phase contrast images of the writing process in a cis-1, 4 PI ($M_w = 1090 \text{ kg/mol}$) in THF solution ($c = 5.47 \text{ \% wt} = 0.0486 \text{ g/ml}$). The LASER power used is $P = 238 \text{ mW}$ and the

defocusing distance is $\Delta z = 1000 \mu\text{m}$. A lower refractive index tubular structure is formed upon irradiation.

Shortly after starting the LASER beam, a lower refractive index (dark) stripe-like pattern (**Figure 4.3, b**) is formed in the polydiene solution. The sign of the optical contrast of the structure ($\delta n < 0$) was also confirmed to be negative from images obtained for negative defocusing distances ($\Delta z < 0$) i.e. below the focal plane of the objective), which showed bright patterns. This structure seems to widen as irradiation is going on for prolonged times (**Figure 4.3, c-h**). As mentioned, the contrast (δn) of the light-induced formation is very small. As seen from comparison between the scattering and the phase contrast images, the resulting structure has a larger lateral dimension than the beam size used (beam diameter $\sim 28 \mu\text{m}$). This clearly indicates that a non-local effect, as the irradiated medium undergoes changes in its optical properties at length scales much larger than the beam size.

This behavior is clearly opposite to the one observed for PI and PB solutions in other lower n solvents mentioned previously (e.g. hexane and toluene). An electrostrictive-like mechanism cannot account for the observed effects. Obviously, the sign of the refractive index differences between polymer and solvent (Δn) does not determine the system's response to the optical field. The new findings strongly support the relevance of specific solute-solvent interactions in the writing phenomenon.

Again, analogous behavior has been observed in cis-1, 4 PB solutions in THF, indicating no obvious difference between the two polydienes.

4.2.3 Summary of the solvents examined

Since it was clear that depending on the system polymer-solvent used, different patterns are induced upon irradiation, a series of cis-1, 4 PI and PB solutions have been studied to gain more insight into the light-polymer concentration coupling in different solvents.

To check if dipole moment of the solvent defines or not the response of the polydiene solution to the application of the optical field, a solution of cis-1, 4 PB ($M_w = 390 \text{ kg / mol}$) in bromocyclohexane ($c = 7.37 \text{ \% wt} = 0.0976 \text{ g / ml}$) was studied. This solvent

has a lower n ($n=1.495$) than the polymer (i.e. $\Delta n > 0$) and possesses the largest dipole moment ($\mu = 2.3$ D) of all solvents used in this study, due to the presence of the Br atom. **Figure 4.4** shows the result after irradiating the solution for $t = 1200$ s ($P = 238$ mW):

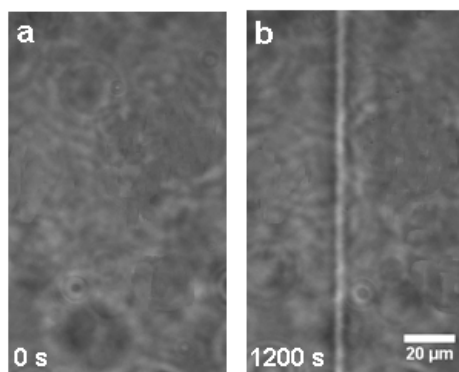


Figure 4.4: Polymer-rich fiber formation in a solution of cis-1, 4 PB ($M_w = 390$ kg / mol) in bromocyclohexane ($c = 7.37$ % wt = 0.0976 g / ml). The LASER power used is $P = 238$ mW.

As can be seen from the phase contrast image, a higher refractive index fiber-like pattern is formed ($\delta n > 0$). Taking into account the other solvents (i.e. linear alkanes) that lead to a similar result (fibers with $\delta n > 0$) are roughly apolar, we may conclude that dipole moment of the solvent is not the factor that determines system's behavior upon irradiation. This is further supported by the behavior of THF solutions. Despite the fact that THF is polar ($\mu = 1.63$ D), irradiation results in solvent-rich lower refractive index ($\delta n < 0$) channels.

Another physical property that could play an important role to the writing process, is the dielectric permittivity. However, neither this property seems to define the type of LASER-induced pattern: Both low ϵ_r alkanes ($\epsilon_r \sim 2$) and high ϵ_r bromocyclohexane ($\epsilon_r = 8$) lead to fibrillar structures of $\delta n > 0$, while another high ϵ_r solvent, THF ($\epsilon_r = 7.52$) results in channels with $\delta n < 0$.

In addition, other solvents of higher n than the polymers were also studied ($\Delta n < 0$). The fact that the sign of optical contrast does not determine the system's behavior was confirmed in cis-1, 4 PB ($n = 1.52$) in chlorobenzene ($n = 1.524$) and 1, 2, 3, 4-tetralin ($n =$

1.541) solutions. Phase contrast images for both solutions are shown in **Figure 4.5**, along with images of the transmitted beam spot:

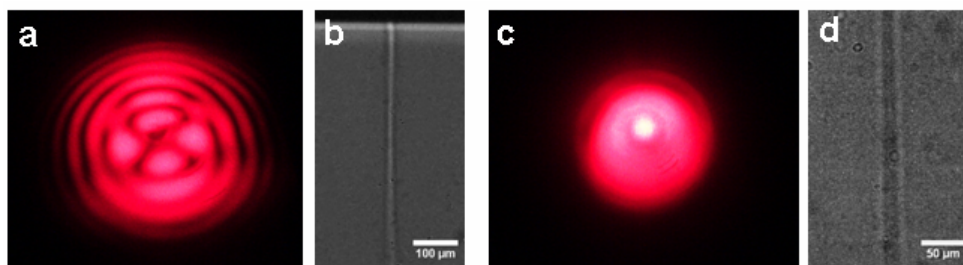


Figure 4.5: a-b) Transmitted beam spot and phase contrast images of solvent-rich stripe formed in a cis-1, 4 PB ($M_w = 390$ kg / mol, $c = 7.99$ % wt = 0.0884 g / ml) / chlorobenzene solution. c-d) Transmitted beam spot and phase contrast images of polymer-rich channel formed in a cis-1, 4 PB ($M_w = 390$ kg / mol, $c = 8.75$ % wt = 0.0851 g / ml) / tetralin solution.

A brief summary of all results for the different polymer solvent couples are presented in **Table 4.1**. Additionally, the physical properties mentioned above are also shown, along with the sign of the optical contrast between the solvent and the polymer (Δn) and the optical contrast between the LASER-induced structure and its surrounding solution (δn):

Solvent	n_0	μ (D)	ϵ_r	Δn	δn	Structure
Hexane	1.375	0	1.89	+	+	
THF	1.407	1.63	7.52	+	-	
Decane	1.411	0	1.99	+	+	
cyclohexane	1.426	0	2.02	+	+	
tetradecane	1.429	0	2.03	+	+	
cis-decalin	1.481	0	2.22	+	+	
bromocyclohexane	1.495	2.3	8.00	+	+	

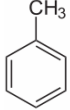
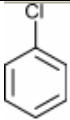
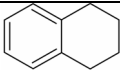
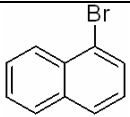
Toluene	1.497	0.375	2.38	+	+	
chlorobenzene	1.524	1.69	5.69	-	+	
1,2,3,4-tetralin	1.541	0.22	2.77	-	-	
1-bromonaphthalene	1.657	1.55	4.77	-	+	

Table 4.1: Summary of the solvents used to prepare different polydiene solutions. The index of refraction (n_0), the dipole moment (μ) and the permittivity (ϵ_r) for each solvent are shown^{1, 2}. Δn is the polymer-solvent refractive index difference and δn is the LASER-induced structure-solution refractive index difference. The chemicals structures are also shown.

What can be clearly observed is that neither the sign of Δn , nor any of the mentioned physical properties define solely the response of each polydiene solution (expressed by different pattern formations) to the applied LASER beam. It seems that at this point we are not able to predict the type of structure that will be formed upon LASER irradiation. It is of high importance that none of the cis-1, 4 PI or PB solutions examined during this study showed neutral behavior when exposed to the optical beam (which should mean no pattern formation), under the irradiation conditions mentioned so far.

4.2 LASER patterning of diblock copolymer solutions

The positive effect (LASER-induced fibers with $\delta n > 0$) and negative effect (LASER-induced formations with $\delta n < 0$) presented in **Chapter 3** and **Section 4.1** respectively, were further extended to more complex polydiene solutions. Solutions of the asymmetric diblock copolymer of poly (isoprene-*b*-styrene) (75% PI, 25% PS, $M_w = 424$ kg / mol) (IS4) in different solvents were used to explore the possibilities of different pattern formations. It was found that solutions of the same copolymer in different selective solvents

lead to both positive and negative writing processes. The various aspects of this fascinating diversity are explored in this part.

4.2.1 Diblock copolymers: Positive case

Solutions of the asymmetric diblock copolymer poly (isoprene-b-styrene) (PI-PS) in a selective solvent for the isoprene block, such as hexane, are well-known to form star-like micelles. This was also confirmed (for dilute solutions) through Light Scattering results presented in **Chapter 2 (Section 2.1.5)**. While dilute solutions are transparent, at higher polymer concentrations, the samples are slightly turbid, due to the increased number of big micelles ($R_h = 153\text{nm}$) that scatter strongly the light.

LASER-induced fiber formation (positive writing, $\delta n > 0$) was observed upon irradiation of the micellar solutions in hexane. **Fig. 4.6** shows a time series of phase contrast images of the fiber formation in a PI-PS / hexane solution ($c = 5.62\%$ wt). The irradiation conditions are $P = 25.1\text{ mW}$, $\lambda = 660\text{ nm}$, beam size $\sim 17\ \mu\text{m}$, and the defocusing distance for detection used is $\Delta z = 20\ \mu\text{m}$.

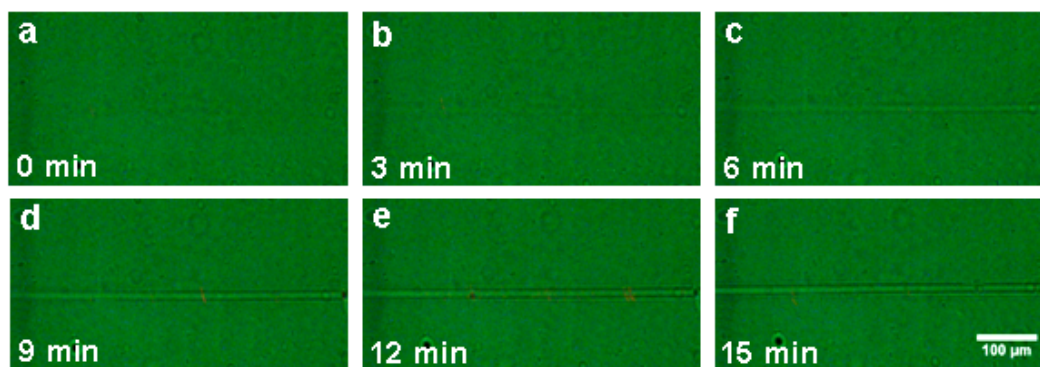


Figure 4.6: Real time phase contrast imaging of the fiber formation in a micellar solution of poly (isoprene-b-styrene) (IS4) in hexane, $c = 5.62\%$ wt (0.0368 g / ml) (total $M_w = 424\text{ kg / mol}$, 75% isoprene content). The LASER beam size at the focus is $\sim 17\ \mu\text{m}$ ($P = 25.1\text{ mW}$).

The fiber formation is very similar to the homopolymer cis-1, 4 PI in hexane solutions. The higher refractive index fiber extends from the one side of the sample cell to the other, having

a constant diameter ($\sim 10 \mu\text{m}$). Similarly to the fiber-like patterns formed in solutions of the homopolymers PI and PB in the solvents mentioned in **Section 3.2**, self guiding of the LASER beam is clearly evident (not shown here).

4.2.2 Diblock copolymers: Negative case

The LASER-patterning process was also investigated in more complex copolymer solutions. More specifically, solutions of the asymmetric diblock copolymer IS4 in ethyl acetate were prepared. Ethyl acetate is a good solvent for PS, and a poor solvent for PI at room temperature. As mentioned in **Section 4.1**, LASER-induced patterning is not limited only to homopolymers, and extension to more complex architectures can open possibilities for interesting applications, such as the Self-induced Transparency that will be presented later in this Chapter.

As has been shown in **Chapter 2 (Section 2.2.2)**, solutions of IS4 in ethyl acetate ($n=1.372$) consist of various ill-defined aggregates³ along with single (not assembled) chains, with sizes ranging from $\sim 11 \text{ nm}$ (single chains) to a few microns. The precise micellar formation is not clearly established, but most probably consist on vesicles³. The strong scattering of light from these big structures leads to a large drop of light transmission, i.e. turbid solutions in high polymer concentrations.

A transparent sample could be obtained if temperature was applied: a solution of IS4 / ethyl acetate ($c = 4.1 \text{ \% wt}$) was heated (under mechanical stirring) at $T \sim 40 \text{ }^\circ\text{C}$ for 2 days. The sample was left to cool down to room temperature for 1 hour, before the writing experiments were carried out. The solution was transparent though it still contained very large structures (**Figure 4.7 a**). **Figure 4.7** shows the result of the irradiation ($P = 38.4 \text{ mW}$). The defocusing distance for the detection is $\Delta z = 150 \mu\text{m}$ above the focal plane.

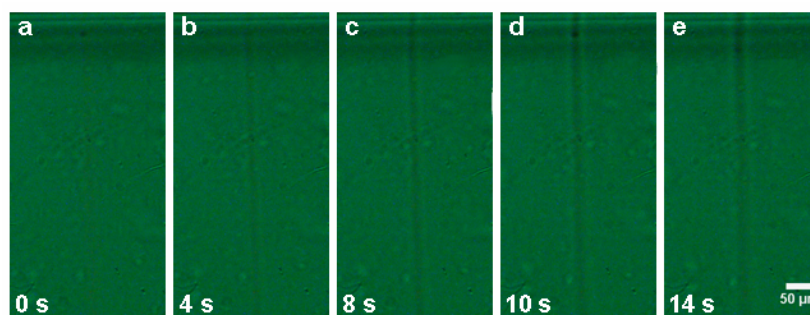


Figure 4.7: Real time phase contrast imaging of the fiber formation in a micellar solution of IS4 in ethyl acetate, $c = 4.1$ % wt (0.037 g / ml) (total $M_w = 424$ kg / mol). The irradiation conditions are $P = 38.4$ mW, beam size ~ 17 μm ($\lambda = 660$ nm). The defocusing distance is $\Delta z = 150$ μm .

As can be observed from the images above, a dark stripe corresponding to a lower refractive index region ($\delta n < 0$) is formed very quickly after switching on the LASER beam (**Figure 4.7 b**). The light-induced stripe appears simultaneously in the whole field of view, and clearly extends to the whole cell length (0.9 mm). Though clearly visible, the contrast of the formed structure remains very weak. Assuming that changes in the refractive index are caused solely by local variations in the polymer concentration, the negative δn value will correspond to a lowered polymer concentration in the stripe (solvent-rich). In a later stage, an increase of the size of the formed structure is evident. This phenomenology resembles the one observed in THF solutions (**Section 4.1.2**), as both systems possess a positive Δn and the optical field induces structures of negative δn .

4.2.3 Self-Induced Transparency in turbid solutions

As mentioned already, the not heated solutions are turbid, with the transmission being $T \sim 40$ % for 0.9 mm thick samples consisting of IS4 / ethyl acetate, at a concentration $c = 5.44$ % wt. The effect of LASER irradiation on the turbid solutions is reported in **Figure 4.8**, for a power of $P = 35$ mW and microscope detection using a defocusing distance of a few hundred μm .

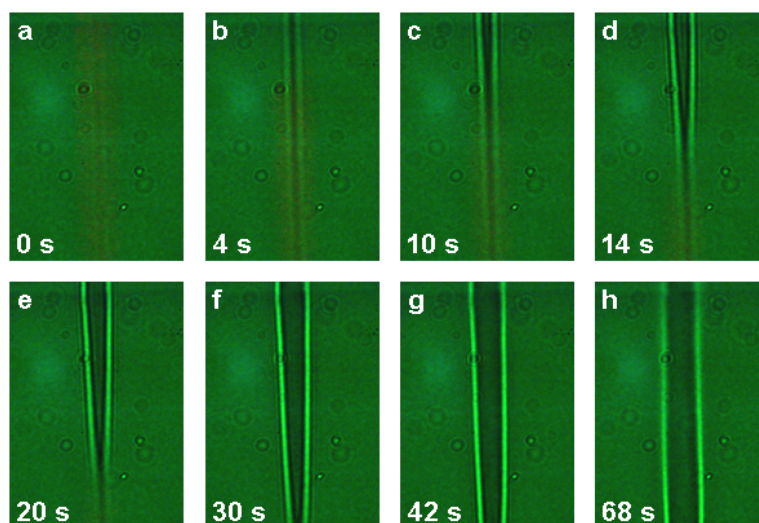


Figure 4.8: Real time phase contrast imaging of the Self-Induced Transparency process in a solution of IS4 in ethyl acetate, $c = 5.44$ % wt (0.0491 g / ml) (total $M_w = 424$ kg / mol, 75 % isoprene content). The LASER beam ($P = 35$ mW, $\lambda = 660$ nm) diameter (~ 17 μm) is similar to the diameter of the dark stripe formed immediately after switching on the LASER, shown in (a).

After very short irradiation time (< 1 s) a dark stripe can be observed, corresponding to a region of lower refractive index, i.e. depleted of polymer. This primary formation is very similar to the one observed in the heated solution. The optical contrast of the structure is very weak, requiring a large defocusing distance to be observed. However, contrarily to the case of the heated solution, the primary formation is followed by a secondary process where a narrow front seems to propagate in the direction of the beam propagation (top to bottom on **Figure 4.8**), followed by an opening of the formed structure into a tubular formation that eventually spreads over the entire cell thickness. This hollow structure has the astonishing property of guiding the LASER light, and the light transmission is found to increase over time. This guiding property was clearly observed by imaging of the transmitted beam at different irradiation times (**Figure 4.9 a**):

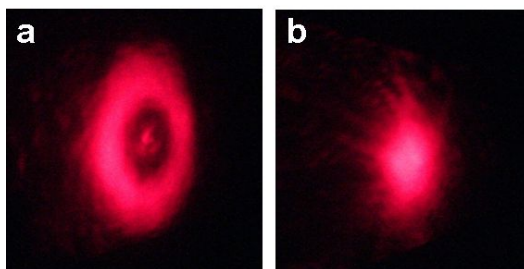


Figure 4.9: Images of the transmitted LASER beam spot during irradiation of IS4 / ethyl acetate solution (total Mw = 424 kg / mol), $c = 11.79\%$ wt). The power was $P = 35$ mW.

The initially relatively weak transmitted beam spot ($T \sim 40\%$, not shown here) eventually changes to a bright ring of increased intensity with a dark region within, which includes a tiny bright spot. The ring is increasing with irradiation time, which is in agreement with the phase contrast images that show an increase of the structure's size (**Figure 4.8**, b-f). At later times, where the full structure has been formed (**Figure 4.8** h), a Gaussian-like beam spot can be observed in the transmission image (**Figure 4.9** b). At this point, the transmittance of the sample reaches a value of $T \sim 90\%$. Some typical examples of the evolution of T vs. irradiation time are shown in **Figure 4.10** for an IS4 / ethyl acetate solution ($c = 4.2\%$ wt) and the LASER P varies from 37.2 mW down to 1.1 mW:

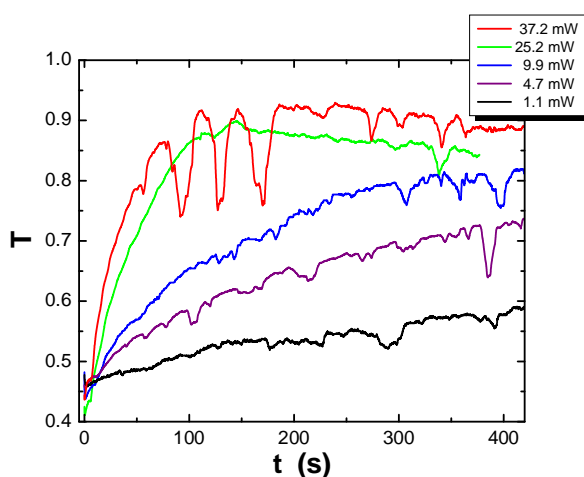


Figure 4.10: The evolution of transmittance as a function of irradiation time, for different LASER powers. The sample used is a solution of IS4 in ethyl acetate, $c = 4.2\%$ wt (0.0377 g / ml).

The transmission T clearly increases faster with increasing LASER power P . After reaching its maximum value of $T \sim 0.9$ (i.e. for the two higher P 's), the transmission remains stable for longer irradiation times.

The effect presented above provides an exceptional demonstration of Self Induced Transparency (SIT) in soft matter.

Recently, the interesting prospect of SIT has received much attention owing to its scientific and technological interest⁴. In particular, El-Ganainy et al⁵. conducted simulations and showed that suspensions of air-bubbles in water can exhibit SIT at high power levels. At low P levels, strong Rayleigh scattering occurs and huge losses are observed. On the contrary, for high P , the optical gradient forces expel the lower refractive index bubbles out of the high intensity regions, reducing the local concentration in the irradiated volume. This in turn gives rise to SIT and self-trapping effects, so that the high P beam effectively reduces the 'haze' while at the same time can establish its own waveguide structure⁵. SIT was also experimentally observed recently by Dai et al^{4, 6, 7}. The system that was used was PS spheres (diameter $\sim 1.9 \mu\text{m}$) suspended in water, at relatively high volume fractions ($\sim 10\%$). The authors utilized a Z-scanning optical trapping technique to demonstrate a transition from a disordered to an ordered state. At low P levels, where no trapping occurs, the spheres are randomly distributed in the aqueous phase and the LASER beam suffers strong backscattering. However, an increase on P results in the formation of ordered structures, since the colloids come very close and start to pack. The structure formation was evidenced by a significant enhancement of the transmission at the focal point of the beam and confirmed by the diffraction pattern of the trapping region.

Surprisingly, the formed clear low refractive index channels remain long after LASER switching-off, as observed by microscopy. More specifically, the refractive index difference between the formed structure and the surrounding solution is fading out as time passes (after switching-off), however, refractive index variations can still be detected for minutes to hours after stopping the beam. Given that these solvent-rich channels could be formed even at very low polymer concentrations (as low as 1 % wt), which means not very viscous samples, the stability of the structures is quite remarkable.

Figure 4.11 shows microscope images of the optically induced 'holes', roughly 1 min after stopping the LASER beam ($P = 35 \text{ mW}$, writing time $\sim 10\text{-}11 \text{ min}$). The images were

acquired at the exit face of the square sample cell. Different beam sizes (a, c, e) were employed resulting in various channel diameters:

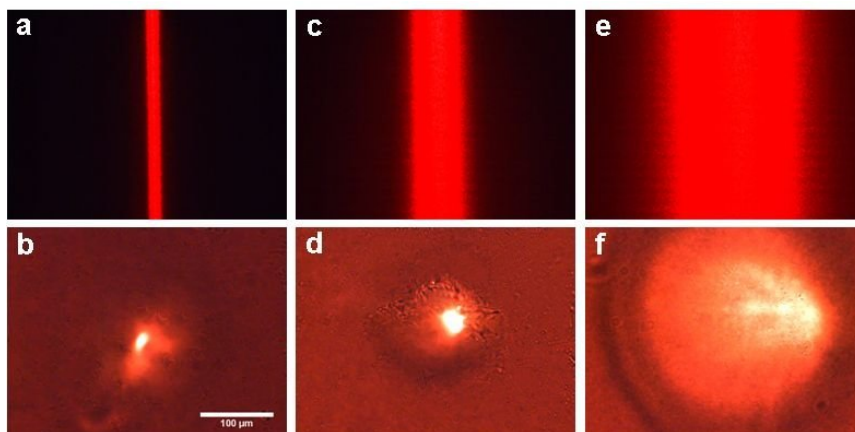


Figure 4.11: Optically induced 'holes' in IS4 / ethyl acetate solution ($c = 4.2\% \text{ wt} = 0.0377 \text{ g/ml}$). Different 'hole' diameters were achieved by varying the LASER beam size (shown on top). The power used was $P = 35 \text{ mW}$ ($\lambda = 660 \text{ nm}$) and the irradiation time $t = 10\text{-}11 \text{ min}$.

The channel diameter (b, d, f) directly relates to the beam size utilized. Moreover, the reduced concentration of the inner part of the channel results in the enhanced transmission of the microscope's white light, in contrast to the clearly reduced transmittance of the turbid surrounding solution.

4.3 Discussion

In this Chapter, the variety of different formations observed for different solvents was presented. LASER-induced local decrease in the polymer concentration was observed for the first time. The sign of the local variation of concentration (δn) is not defined by the refractive index difference between the macromolecules and the solvent (Δn), as was clearly evidenced by means of phase contrast microscopy, in a series of polydiene solutions (**Table 4.1**) in a variety of organic solvents of different refractive indices.

Interestingly, a similar behavior is observed for more complex solutions, such as micellar solutions of a diblock copolymer PI-PS. When dispersed in hexane (selective solvent

for PI), it responds to LASER irradiation by forming fiber-like patterns. The phenomenology is very similar to the homopolymers / hexane systems. On the contrary, solutions of the same copolymer in ethyl acetate (selective solvent for PS at room temperature) behave in the opposite way: solvent-rich channels are formed upon LASER irradiation.

The decoupling of Δn and δn leads to the possibility of obtaining all four possible combinations, as shown in **Figure 4.12**:

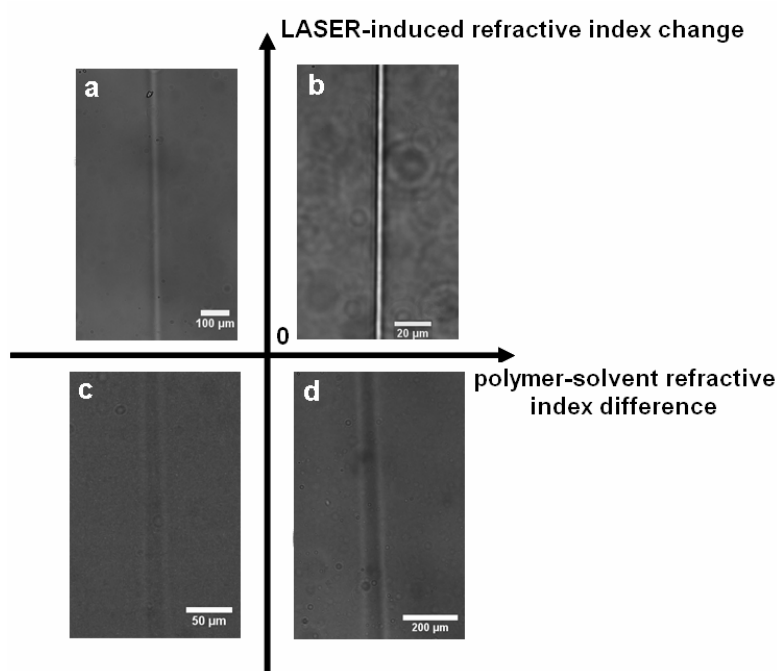


Figure 4.12: All possible combinations of solution optical contrast (Δn) and structure optical contrast (δn). a) PI / bromonaphthalene, $\Delta n < 0$, $\delta n > 0$, b) PI / decane, $\Delta n > 0$, $\delta n > 0$, c) PI / THF, $\Delta n > 0$, $\delta n < 0$, and d) PB / tetralin, $\Delta n < 0$, $\delta n < 0$.

The decoupling of the LASER-induced variation of the refractive index and the refractive index difference between the polymer and the solvent is best illustrated in **Figure 4.12**, where the x-axis corresponds to the optical contrast of the polymer solutions, while the y-axis represents the optical contrast of the LASER-induced patterns. The first quadrant (b), includes structures which possess a higher n than the surrounding solution, which are formed in solutions of polymers having higher n than the solvent. These formations have an

enhanced polymer concentration, since the high n component in the binary mixture is the polymer. All cases described in **Chapter 3** fall in this regime. Typical examples are polydienes dissolved in linear alkanes, irradiation of which results in fiber-like patterns of high contrast. The second quadrant (d) includes patterns which are formed in solutions of positive optical contrast and exhibit lower refractive index compared to the unpatterned surrounding solutions. In other words, the optical field results in structures having a reduced polymer concentration. Examples of this case are the polydienes/THF systems and the PI-PS/ethyl acetate solutions. The third quadrant (c) refers to solutions of negative contrast ($\Delta n < 0$), which respond to the LASER beam by locally increasing the polymer concentration. Thus, locally the index of refraction decreases. The only example of this case was the system PB / tetralin. Finally, the fourth quadrant (a) includes patterns of higher refractive index induced by LASER irradiation of solutions with $\Delta n < 0$. Examples in this case are polydienes dissolved in bromonaphthalene and chlorobenzene.

The coarse grained description of the light-polymer solution interaction in terms of polarizabilities (refractive indices), even though accurate for explaining light scattering, will not be able to capture the observed phenomenology. Therefore a more microscopic description of the polymer-solvent system will be required to describe the observed effects. The interactions between the solvent and the solute molecules will have to be taken into account at the microscopic level.

References

1. 'CRC Handbook of Chemistry and Physics'. CRC Press: 2009.
2. Lide, D. R., 'Handbook of Organic Solvents'. CRC Press: 1995.
3. Mountrichas, G., Mpiri, M., and Pispas, S. *Macromolecules* **2005**, 38, 940-947.
4. Liu, J., Dai, Q.-F., Meng, Z.-M., Huang, X.-G., Wu, L.-J., Guo, Q., Hu, W., Lan, S., Gopal, A. V., and Trofimov, V. A. *Appl. Phys. Lett.* **2008**, 92, 233108.
5. El-Ganainy, R., Christodoulides, D. N., Rotschild, C., and Segev, M. *Opt. Express* **2007**, 15, 10207-10218.
6. Dai, Q.-F., Liu, H.-Y., Liu, J., Wu, L.-J., Guo, Q., Hu, W., Yang, X.-B., Liu, S.-H., Lan, S., Gopal, A. V., and Trofimov, V. A. *Appl. Phys. Lett.* **2008**, 92, 153111.
7. Liu, J., Dai, Q.-F., Huang, X.-G., Wu, L.-J., Guo, Q., Wei H., Yang, X.-B., Lan, S., Gopal, A. V., and Trofimov, V. A. . *Opt. Lett.* **2008**, 33, 2617-2619.

CHAPTER 5

CONCLUDING REMARKS

A discussion concerning possible origins of the effect studied, and the remaining open questions are given in this Chapter. The conclusions made during this thesis are presented, and finally future perspectives are described.

5.1 On the origin of the light-concentration coupling

In this Section, possible origins of the observed light field-polydiene solutions coupling are discussed. The optical forces, the optical Kerr effect and thermal effects are considered, and as will be shown, cannot provide a satisfactory explanation for our observations.

5.1.1 Optical forces

One of the characteristics of a focused LASER beam is its capability of applying photon pressure to particles suspended in dielectric liquids. This phenomenon developed into the extremely useful techniques of LASER trapping, used in several branches of science.

For particles much smaller than the wavelength of the light (Rayleigh regime), the photon pressure exerted on a Rayleigh particle is expressed as follows:

$$F = \frac{1}{2} a \nabla \vec{E}^2 + a \frac{\partial}{\partial t} (\vec{E} \times \vec{B}) \quad (\text{Equation 5.1})$$

where \vec{E} and \vec{B} are the electric field strength and magnetic flux density, respectively, a is the polarizability of the particle. Under the dipole approximation, for a sphere suspended in a dielectric liquid, the polarizability is given by the Clausius-Mosotti relation (**Equation 2.6**). The first term in **Equation 5.1** is an electrostatic force acting on the dipole in the inhomogeneous electric field, and is called the gradient force (F_{grad}):

$$F_{grad} = -\frac{n_0}{2} a \nabla E^2 = -\frac{n_0^3 r^3}{2} \left(\frac{m^2 - 1}{m^2 - 2} \right) \nabla E^2 \quad (\text{Equation 5.2})$$

For particles of radius r higher index of refraction than that of the continuous medium ($n > n_0$), the polarizability is positive, resulting in a gradient force which attracts the particle to the high intensity region (focus). The second term is derived from the change in the direction of

the Poynting vector and is called scattering force (F_{scat}), which pushes the particle along the beam direction. F_{scat} is given by

$$F_{scat} = \frac{I_0}{c} \frac{128\pi^5 r^6}{3\lambda^4} \left(\frac{m^2 - 1}{m^2 + 2} \right)^2 n_0 \quad (\text{Equation 5.3})$$

where I_0 is the LASER intensity. For a particle to be optically trapped¹, F_{grad} has to be larger than F_{scat} , as depicted schematically in **Figure 5.1**:

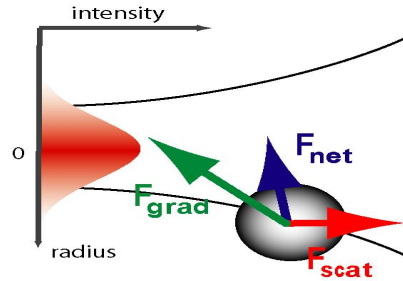


Figure 5.1: Schematic showing the optical forces acting on a particle suspended in a dielectric liquid.

Given the weak scattering of the semidilute polydiene solutions, and the small characteristic size (ξ), we expect very weak optical forces compared to the case of colloidal particles. Using

typical values of the blob size $\xi = 8\text{nm}$, the polarizability of the blob $a_{blob} = 5.77 \cdot 10^{-36} \frac{\text{Cm}^2}{\text{V}}$

(**Equation 2.6**) the refractive index $n_0 = 1.41$ and the squared electric field $E^2 = 3.68 \cdot 10^{11}$

$\frac{\text{V}^2}{\text{m}^2}$, the gradient force potential can be calculated for our system through the relation:

$$U_{grad} = \frac{1}{2} n_0 a_{blob} E^2 \quad (\text{Equation 5.4})$$

The result of the calculation is $U_{grad} = 1.50 \cdot 10^{-24} \text{ J}$. In order to have sufficient trapping,

U_{grad} has to exceed thermal energy kT . At room temperature, $kT = 4.05 \cdot 10^{-21} \text{ J}$. Therefore,

we see that the ratio $U_{grad}/kT = 3.7 \cdot 10^{-4}$, indicating clearly that optical gradient forces are extremely weak to support sufficient trapping in these polymer solutions.

5.1.2 Optical Kerr effect

The large polarizability anisotropy per repeating unit along the chain backbone could induce alignment of the macromolecules. However, the estimated monomer order parameter² is very low, in analogy to the insufficient trapping forces. In addition to this, no measurable birefringence was revealed during observations of the light-induced structures under cross polarizers.

5.1.3 Thermal effects

Molecules drift along temperature gradients, an effect called the Soret effect, or thermodiffusion. In an isotropic binary fluid mixture with nonuniform concentration and temperature, the mass flow \vec{j}_m of the one component contains both a contribution stemming from the concentration and one from the temperature gradient³:

$$\vec{j}_m = -\rho D \nabla c - \rho c(1-c) D_T \nabla T \quad \text{(Equation 5.5)}$$

where D is the collective diffusion coefficient, D_T the thermal diffusion coefficient, ρ the mass density, and c the concentration of the component. In a stationary state, $\vec{j}_m = 0$ and the Soret coefficient S_T is given by the ratio of D_T to D . S_T can be positive or negative. In the first case, solute molecules move towards the cold region, and when $S_T < 0$, motion of the solute towards the hot region occurs.

In order to check if thermodiffusion is related to the observed writing effect, the Soret coefficient for two solutions showing an opposite writing effect was measured. More specifically, two solutions of cis-1, 4 PI ($M_w = 1090$ kg / mol) in hexane and in THF at the same concentration ($c=5.02$ % wt) were examined. As mentioned in the previous Chapters,

application of LASER light to the former system leads to an enhanced polymer concentration in the irradiated region, while the opposite is true (reduced concentration) for the THF case. For the PI / hexane solution, it was found that $S_T = 0.27 \text{ K}^{-1}$, while for the PI / THF solution, $S_T = 0.046 \text{ K}^{-1}$. The fact that both systems exhibit positive Soret coefficients, means that PI in both cases moves to the cold region, in other words is expelled from the irradiated volume. This is contradictory to the enhanced polymer concentration that we observe during LASER irradiation. We may therefore conclude that thermodiffusion cannot explain our experimental observations.

Additionally, thermally induced phase separation is not expected in the polydiene solutions examined, since these systems are far from critical points. Moreover, application of a macroscopic gradient of T shows no observable differences in the observed effect.

5.1.4 Other possibilities

Except for optical forces and thermophoretic effects, chemical modification of the polymers due to LASER irradiation could be an issue. However, the minute absorption of the polymer and the solvent molecules in the visible region of the electromagnetic spectrum should exclude such a possibility. Moreover, if chemical crosslinking of the macromolecules upon irradiation occurs, the same should happen for the 1, 2 PI and PB. On the contrary, as mentioned in **Chapter 3**, solutions of 1, 2-polydienes exhibit a neutral behavior (i.e. no pattern formation) when irradiated. Furthermore, in early experiments, Sigel et al.⁴ illuminated a small volume of a PI / hexane solution ($c = 0.1 \text{ g / ml}$) by a red LASER beam ($\lambda = 647 \text{ nm}$, $P = 200 \text{ mW}$) for several hours, thus inducing extensive pattern formation. No detectable change in the narrow molecular weight distribution of the (anionically synthesized) PI was observed, indicating no chemical modification.

Preliminary experiments on the wavelength dependence of the phenomenon were carried out in a cis-1, 4 PI ($M_w = 1090 \text{ kg / mol}$) in decane solution ($c = 5.5 \text{ \% wt}$). Despite the limited amount of the qualitative data, it was clear that pattern formation is fast for red LASER beams ($\lambda = 647 \text{ nm}$, 650 nm , 660 nm and 671 nm), and a significant slow down was observed for shorter wavelength LASERs. For $\lambda = 532 \text{ nm}$ and $\lambda = 488 \text{ nm}$, the phenomenon is working but it clearly longer irradiation times are required. Surprisingly, irradiation of polydiene solutions with a near-infrared LASER beam ($\lambda = 830 \text{ nm}$) for several

hours ($P = 67 \text{ mW}$) does not lead to any observable changes in the sample properties. This strong wavelength dependence points towards a resonance effect.

5.2 Conclusions

This thesis was devoted to the study of the unexpected response of transparent semidilute polydiene solutions to an applied optical field in the visible region. The experimental investigation led to the establishment of a detailed phenomenology of the effect.

Through phase contrast microscopy, it was found that depending on the solvent used, polydiene solutions respond to the applied optical field by lowering or increasing the local polymer concentration inside the irradiated volume. The decoupling of the refractive index difference between the macromolecules and the solvent and the optical contrast of the formed structures leads to a variety of different patterns, such as high-contrast polymer-rich fibrillar structures or solvent-rich stripe-like formations of much lower contrast. A variety of polydiene-solvent couples was examined and a summary of the different pattern formations was presented.

The utilization of real-time phase contrast microscopy allowed for the quantification of the kinetics of the fibrillar pattern formations, which exhibit relatively high refractive index changes. An exponential-like early stage was revealed. The growth rate as a function of material parameters and irradiation conditions was investigated in detail. The growth rate is affected by the LASER power, the polymer molecular weight, the polymer microstructure and the refractive index difference between the polymer and the solvent. Polymer concentration seems to have no influence on the rate.

Reversibility of the writing process was found to depend on irradiation time. For short exposures, written structures of higher polymer concentration redissolved in the solutions, while prolonged irradiation resulted in insoluble structures.

Preliminary experiments clearly indicated the wavelength dependence of the writing process. The phenomenon is fast for red LASER beams ($\lambda = 633\text{-}671 \text{ nm}$), slow for green and blue LASER beams ($\lambda = 532 \text{ nm}$, $\lambda = 488 \text{ nm}$) and absent for higher wavelengths ($\lambda = 830 \text{ nm}$).

An analogy between light-induced fibrillar pattern formations and Optical Spatial Solitons and Modulation Instabilities (MI) was shown. Both (1+1)D and (2+1)D MI were evidenced as 1D and 2D arrays of filaments formed by using a cylindrical lens or by defocusing the LASER beam. Despite the elusive origin of the underlying nonlinearity, it was clearly shown that polydiene solutions offer an unexpected, simple and versatile system for non linear optics.

The writing effect is not limited only to homopolymer polydiene solutions, but also occurs in more complex macromolecular architectures. In order to open possibilities for 3D micropatterning, more complex micellar solutions of a diblock copolymer of PI-PS in two different selective solvents we employed. In particular, the astonishing concept of Self Induced Transparency was demonstrated. Dissolving PI-PS in a selective solvent for the isoprene block (i.e. hexane), results in solutions of reduced light transmission. LASER irradiation leads to a behavior very similar to the homopolymer / hexane case, where fibers of enhanced polymer concentration (and thus higher refractive index) are formed. Solutions of PI-PS in ethyl acetate (selective solvent for PS) exhibit more enhanced turbidity, even for relatively thin samples. Application of the optical field in this case leads to a rapid enhancement in the transmission of the samples, through a complex patterning process.

Despite the rich and clear phenomenology, the coupling between the optical field and the polydiene-solvent systems still remains unclear. Common effects, such as electrostriction, alignment and thermodiffusion fail to provide a satisfactory explanation for the observed behavior. The strong dependence of the effect on the solvent used and on the LASER wavelength indicates a microscopic resonant mechanism. Macroscopic descriptions in terms of refractive indices (polarizabilities) ignore the interactions of the solute with the solvent molecules at a microscopic level, and therefore seem to be too coarse grained to account for our experimental observations.

Polydiene solutions emerge as a unique, distinct and cheap material in the promising and quickly growing field of Soft Matter non linear optics. The richness of polymer chemistry, in conjunction with the specific physical properties of soft materials and the ability to manipulate their properties at will, definitely offer several perspectives for both fundamental and applied research.

5.3 Further work

In spite of establishing a clear phenomenology of the writing effect, further investigation is required in order to gain insight to the origin of the effect. Towards this direction, future work will include an investigation of polymer-solvent interactions as a function of LASER irradiation in dilute solutions. In particular, the second Virial coefficient (A_2) which indicates the solvent quality can be measured at different LASER powers and at different wavelengths, since the effect appears to be frequency dependent.

Another direction for future experiments is the utilization of polydiene solutions as platform for conducting non linear optics experiments. Interesting phenomena such as interactions between Optical Spatial Solitons can be experimentally studied.

Preliminary experiments have shown that solutions of polydienes are promising candidates as materials for lithography. The fact that prolonged irradiation leads to insoluble structures can be employed to pattern at will bulk solutions and films. **Figure 5.2** a-b shows Scanning Electron Microscopy images of an isolated fiber⁵. The structure was created by irradiating a thick film (200 μm) of a cis-1, 4 PB / decane solution and consequently rinsing with pure solvent. The irradiation conditions were similar to the ones described in **Chapter 2**.

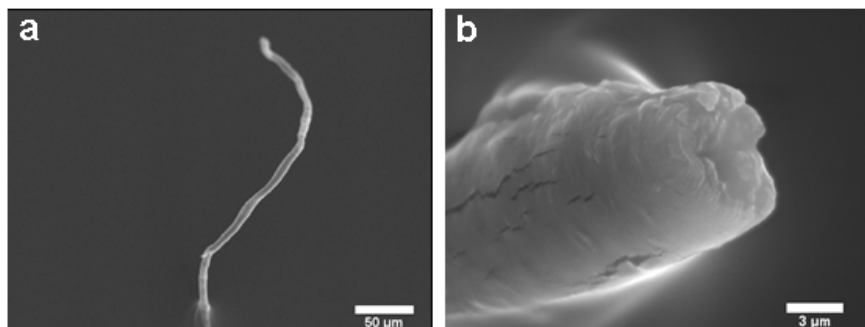


Figure 5.2: a) Scanning Electron Microscopy image of a fibrillar structure⁵. The structure has been formed by irradiation of a 200 μm thick film of cis-1, 4 PB / decane on a SiO_2 substrate solution and consequently isolated by rinsing with solvent, b) Magnified image of the fiber end.

As has been shown in **Chapter 4**, patterning can be extended to more complex systems, such as micellar solutions. The capability of encapsulating organic or inorganic substances with different properties in the core of self-assembled micelles along with the possibility to manipulate the micelles clearly offers several perspectives. For example, the formation of Au nanoparticles inside micelles that can be assembled by LASER irradiation could lead to controlled formation of microwires.

Another possibility offered by the polydiene solutions is that these samples can be used as a photosensitive material for designing and creating 2D or 3D structures by employing a two-photon polymerization method⁶. Generally, the method is based on two-photon absorption; when the beam of an ultrafast LASER is tightly focused on a volume of photosensitive material, the polymerization process can be initiated by two-photon absorption within the focal region. By moving the beam focus in a 3D manner through the material, 3D structures can be fabricated. **Figure 5.3** shows a square-shaped structure which was created in a solution of cis-1, 4 PI / decane solution⁷. The writing source used was a pulsed LASER ($P = 160$ mW, $\lambda = 800$ nm, pulse duration < 20 fs, repetition rate ~ 75 MHz), focused through a x20 objective to a spot with a diameter of $1.3 \mu\text{m}$.

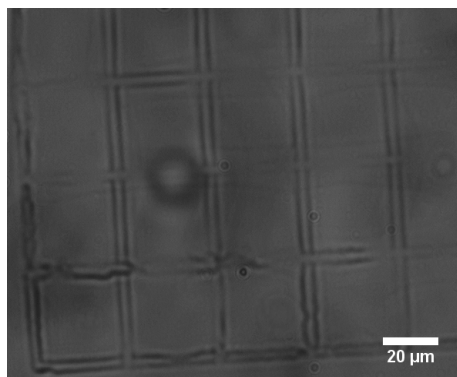


Figure 5.3: Square shaped structure created by two-photon polymerization in a cis-1, 4 PI / decane solution⁷.

From these preliminary results, it seems that polydiene solutions could be a new, cheap and available material for micro- and nano-manufacturing useful devices and structures.

Finally, experiments for the characterization of the written patterns are being continued. Additional Raman scattering as well as x-rays scattering experiments will be

performed, in order to see possible changes in the microstructures of the materials or ordering due to LASER irradiation.

References

1. Ashkin, A., Dziedzic, J. M., Smith, P. W. *Opt. Lett.* **1982**, 7, 276-278.
2. R. Sigel, G. F., N. Vainos, S. Pispas, N. Hadjichristidis. *Science* **2002**, 297, 67-69.
3. Rauch, J., and Köhler, W. *Phys. Rev. Lett.* **2002**, 88.
4. Sigel, R., Fytas, G., Vainos, N., Pispas, S., and Hadjichristidis, N. *Science* **2002**, 297, 67-69.
5. The Scanning Electron Microscopy images were kindly provided by L. Athanasekos from the collaborating group of Prof. N. Vainos at the National Hellenic Research Foundation in Athens.
6. Farsari, M., and Chichkov, B. N. *Nature Photon.* **2009**, 3, 450-452.
7. The two-photon polymerization experiments were carried out in collaboration with A. Gaidukeviciute in the lab of M. Farsari at the Institute of Electronic Structure and Lasers.

APPENDIX

STATIC AND DYNAMIC LIGHT SCATTERING

A brief description of Static and Dynamic Light Scattering is given in this Appendix.

Static and Dynamic Light Scattering

X-ray, neutron and light scattering techniques can be used for measuring various static and thermodynamic properties of materials such as molar mass, size, conformation, and interaction parameters. In addition to static properties, scattering can provide important information on the dynamics of condensed matter. In order to characterize the linear homopolymers used during this study, Static and Dynamic Light Scattering (SLS and DLS, respectively) experiments were conducted.

In a typical light scattering experiment, a LASER beam impinges in a transparent liquid sample and it is scattered at all directions. A photodetector, placed at the desired scattering angle θ , collects the scattered light. Polarizers and analyzers are used to define the polarizations of the incident and scattered light beams, respectively. A schematic representation of a typical light scattering setup¹ is shown in **Figure I.1**.

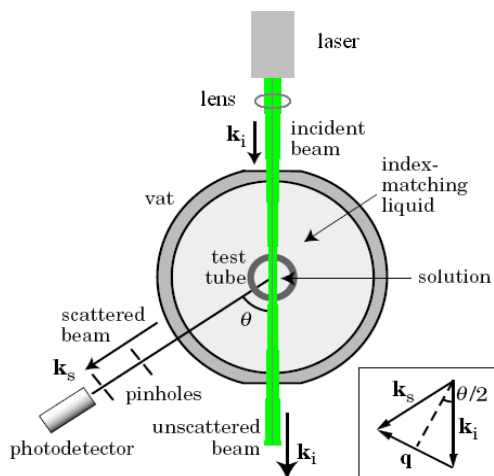


Figure I.1: Schematic illustration of a typical light scattering setup. A polarized LASER beam impinges in the tube that contains the sample, and is scattered at all directions. A photodetector collects the scattered light at a desired scattering angle θ . The inset shows the scattering wavevector \mathbf{q} , which is defined as the difference between the scattered and the incident beam, \mathbf{k}_s and \mathbf{k}_i , respectively.

For a given incident beam of wavelength λ and scattering angle θ , the scattered intensity is related with the spatial density distribution of the scatterers through the relationship

$$I(q) = \int \bar{\rho}(\vec{r} - \vec{r}') \bar{\rho}(\vec{r}') \exp(i\vec{q} \cdot \vec{r}) d^3r d^3r' \quad (\text{Equation I.1})$$

where

$$q = \frac{4\pi n}{\lambda} \sin\left(\frac{\theta}{2}\right) \quad (\text{Equation I.2})$$

is the scattering wavevector, n the refractive index of the medium, and $\bar{\rho}(\vec{r})$ describes the distribution of the scattering density. Virtually $\bar{\rho}(\vec{r})$ is the property of matter that interacts with the incoming electromagnetic waves. The scattered intensity consequently probes how a density fluctuation $\delta\rho(q)$ spontaneously arises and decays due to thermal motion of the molecules. In light scattering, $\bar{\rho}(\vec{r})$ is the distribution function of the refractive index (or the local polarizability)².

In a light-scattering experiment the quantity that is measured is the total scattered intensity $I(\vec{q}, t)$, which can be used to extract information about static (SLS), and dynamic properties (DLS) of the system probed at a length scale of $2\pi/q$. The instantaneous scattering intensity $I(\vec{q}, t)$ depends on the spatial arrangements of scattering centers (positions and conformations of molecules) at time t . As molecules move, changing their conformations and locations in space, the scattering intensity fluctuates in time². The value of the scattering intensity averaged over a long time interval t , is the static scattering intensity $I_{sc}(q)$:

$$I_{sc}(q) = \langle I_{sc}(q, 0) \rangle = \lim_{t \rightarrow \infty} \frac{1}{t} \int_0^t I_{sc}(q, t') dt' \quad (\text{Equation I.3})$$

The absolute scattering intensity for the polarized geometry, R_{VV} , is given by

$$R_{VV} = \frac{I_{sc}(q)R_{tol}}{I_{tol}(q)} \quad (\text{Equation 1.4})$$

where R_{tol} is the Rayleigh ratio for toluene, equal to $R_{tol} = 2.78 \cdot 10^{-5} \text{cm}^{-1}$ for $\lambda = 532 \text{ nm}$.

The weight averaged molecular weight M_w , and the radius of gyration R_g can be calculated through the relation

$$\frac{cH}{R_{VV}} = \frac{1}{M_w} \left(1 + 2A_2M_w c + \frac{q^2 R_g^2}{3} \right) \quad (\text{Equation 1.5})$$

where A_2 is the second Virial coefficient, and H is the optical constant

$$H = \frac{4\pi^2 n^2}{\lambda^4 N_A} \left(\frac{dn}{dc} \right)^2 \quad (\text{Equation 1.6})$$

with N_A being the Avogadro number and $\frac{dn}{dc}$ is the specific refractive index increment.

In a DLS experiment, the normalized intensity autocorrelation function, $G(q,t)$, is measured:

$$G(q,t) \equiv \frac{\langle I_s(q,0)I_s(q,t) \rangle}{\langle I_s(q,0) \rangle^2} \quad (\text{Equation 1.7})$$

Polarized geometry provides us information about the fluctuations of the concentration or the density of the material. The quantity related with the dynamic response of the system is the autocorrelation function of the scattered field $C(q,t)$. The two autocorrelation functions are related via Siegert's relation:

$$G(q,t) = 1 + f^* |C(q,t)|^2 \quad (\text{Equation 1.8})$$

where f^* is a spatial coherence factor that depends on the experimental setup, the scattered volume and the number of coherence areas viewed. When the dissolved molecules do not interact, $C(q,t)$ describes the decay of concentration fluctuations, due to mass diffusion:

$$C(q,t) = A \exp(-Dq^2t) \quad (\text{Equation 1.9})$$

where A is the amplitude of the correlation function and D is the diffusion coefficient.

References

1. Teraoka, I., *Polymer Solutions: An Introduction to Physical Properties*. John Wiley & Sons, Inc.: New York, 2002.
2. Berne, B. J., Pecora, R., *Dynamic Light Scattering*. Dover: New York, 2000.
3. Finnigan, J. A., Jacobs, D. J. *Chem. Phys. Lett.* **1970**, 6, 141-143.

Ευχαριστίες

Τελειώνοντας τη διαδακτορική μου διατριβή, θεωρώ χρέος μου να αναγνωρίσω την (άμεση ή έμμεση) συνεισφορά κάποιων ανθρώπων για την επίτευξη αυτού του στόχου και ακολούθως να τους ευχαριστήσω.

Αρχικά, θα ήθελα να ευχαριστήσω τον κ. Φυτά, ο οποίος μου έδωσε την ευκαιρία να ασχοληθώ με ένα θέμα εξαιρετικού ενδιαφέροντος. Επίσης, μέσα από τις συζητήσεις μας, είχα τη δυνατότητα όλα αυτά τα χρόνια να μάθω πολλά.

Ιδιαίτερα αισθάνομαι την ανάγκη να ευχαριστήσω τον Benoit L. για δύο λόγους. Αφενός γιατί ήταν δίπλα μου καθ' όλη τη διάρκεια της ερευνητικής μου εργασίας με πολλές ιδέες και ιδιαίτερο ενδιαφέρον, και αφετέρου διότι μέσα από τις συζητήσεις μας (επιστημονικές και μη, πάνω στο θέμα της διατριβής μου αλλά και γενικότερου ενδιαφέροντος) κατάφερε πάντα να δίνει κίνητρο σε μένα.

Ακόμα, θα ήθελα να πω ένα μεγάλο ευχαριστώ σε όλα τα μέλη της ομάδας Πολυμερών στο I.T.E., στα εργαστήρια της οποίας εκπόνησα το μεγαλύτερο μέρος της διατριβής μου. Ιδιαίτερα ευχαριστώ το Δρ. Μανώλη για τις σοφές συμβουλές του και τα 'κατά ρυπάς' πειράγματα του, τα οποία σε συνδυασμό με την παρουσία της Χριστίνας και του Κώστα δημιουργούσαν ένα απίστευτα ευχάριστο κλίμα στο εργαστήριο. Επίσης, η συμβολή του Παναγιώτη Β., της Ελένης Π., του Αντρέα Π. (μουσική επιμέλεια για τις δύσκολες ώρες) και των γειτόνων Νίκου Κ. (επί ώρες συνομιλητής) και Βασιλικούλας Μ. ήταν καθοριστική.

Επίσης, θα ήθελα να ευχαριστήσω τον κ. Butt, ο οποίος με δέχτηκε στο Max Planck Institute for Polymer Research στο Mainz, στα εργαστήρια του οποίου πέρασα τους τελευταίους 10 μήνες του διαδακτορικού μου. Επίσης, οφείλω να αναγνωρίσω την πολύτιμη και αναγκαία βοήθεια του Andreas, καθώς και τις χρήσιμες συμβουλές του Kaloian K. και του Werner S.. Φυσικά, δε μπορώ να ξεχάσω τον Sullivan V., τον Tiago R., την Karmena J., τον Akihiro S. και τα υπόλοιπα παιδιά για την ευχάριστη παρέα και τη στήριξη και φυσικά το Νίκο Γ. για την πολύτιμη βοήθειά του κυρίως τον πρώτο καιρό αλλά και γενικότερα στο Mainz.

Θα ήθελα να ευχαριστήσω το 'συνθέτη' και πολύ καλό φίλο Χρήστο Μ. για τη συνεργασία μας και τις ωραίες στιγμές που περνούσαμε όταν ερχόταν για πειράματα στην Κρήτη.

Κλείνοντας, οφείλω να ευχαριστήσω τα προγράμματα ΠΕΝΕΔ από τη Γενική Γραμματεία Έρευνας και Τεχνολογίας και το International Max Planck Research School για τη χρηματοδότηση.

Τέλος, αισθάνομαι την ανάγκη να ευχαριστήσω τους γονείς μου Γιώργο και Μαρία, καθώς και την αδερφή μου Νατάσσα για εκατομμύρια λόγους που δε χρειάζεται να αναφέρω εδώ.